UNIVERSITY OF GENOA
PHD PROGRAM IN BIOENGINEERING AND ROBOTICS

Development of engineered human-derived brain-on-a-chip models for electrophysiological recording

by

Muzzi Lorenzo

Thesis submitted for the degree of *Doctor of Philosophy* in Bioengineering and Robotics 34° cycle

Supervisors: prof. Sergio Martinoia
prof. Monica Frega

The head of the PhD Program: prof. Giorgio Cannata

Dibris

Department of Informatics, Bioengineering, Robotics and Systems Engineering

I hereby declare that except where specific reference is made to the work of others, the contents of this dissertation are original and have not been submitted in whole or in part for consideration for any other degree or qualification in this, or any other university. This dissertation is my own work and contains nothing which is the outcome of work done in collaboration with others, except as specified in the text.

April 2022

Abstract

The study of the central nervous system represents a great challenge in the field of neuroscience. For years, various techniques have been developed to study neuronal cells *in-vitro* as it is difficult to conduct *in-vivo* experiments due to ethical problems deriving from its anatomical location. Consequently, both *in-vivo* and *in-vitro* animal models have been used extensively to gain new insights into basic functioning principles of neuronal tissue and therapeutic approaches for brain diseases. Over time, we have seen that there is a poor correlation between the clinical diagnosis and the underlying pathological mechanisms. In fact, some symptoms that may occur in the patient are not replicated in the animal, making many promising approaches in animal studies not translatable in the clinic. With the advent of human-induced pluripotent stem cells (h-iPSC) several protocols for the generation of human-neuronal cells are becoming available for all laboratories. The importance of this technique lies in the opportunity to develop a human model derived directly from the patient: the patient's *in-vitro* cells will exhibit the same genetic and epigenetic modifications as the *in-vivo* cells. This has raised hopes for the generation of engineered brain models that can be coupled to sensors / actuators in order to better investigate their functional properties *in-vitro* (i.e. brain-on-a-chip). A reliable method for evaluating the functionality of neuronal cultures is the study of the spontaneous electrophysiological activity using microelectrode arrays (MEA). There are numerous studies in the literature that used h-iPSC on MEAs, showing the characterization of neuronal patterns of patient-derived cultures, demonstrating how this platform is valid for disease phenotyping, drug discovery and translational medicine. Although these models helped to shed light on fundamental biological mechanisms, the majority is based on two-dimensional neuronal cultures, which lack some key features to mimic *in-vivo* behavior. Three-dimensional h-iPSC-derived models possess a microenvironment, tissue architecture and potential to model network activity with greater complexity than two-dimensional models. Depending on the purpose of the study, we can choose different approaches to recreate 3D *in-vitro* brain, from those that aim to reproduce the trajectories of neurodevelopment (i.e. brain-organoids) to the use of synthetic materials that reproduce the functionalities of the extracellular matrix (ECM) (i.e. scaffold-based) (Chiaradia and Lancaster, 2020, Tang et al., 2006). Although h-iPSC-derived brain models summarize many aspects of network function in the human brain, they are subject to variability and still do not perfectly mimic behavior *in-vivo*. Therefore, to reach the full potential of this model we need improvements in differentiation methods and bioengineering, making these models engineered and reproducible. The aim of this PhD thesis was to implement different 3D neuronal culture generation methodologies that can be integrated on MEA devices to offer robust engineered platforms for functional studies.

Thesis Structure

This thesis shows the experimental path I followed during these 3 years of PhD.

Chapter 1 is introductory and aims to offer to the reader an overview of the various topics that I had to master before starting to design the experiments.

Chapter 2 is about the first experimental phase which took place during the first year and a half of the PhD. I was guested for 2 months at the Clinical Neurophysiology group (CNPH) at the University of Twente (Enschede, NL). During that time, I learned to work directly with human-induced pluripotent stem cells (h-iPSCs) cultures and in particular, I learned the differentiation protocol proposed by Frega et al., in 2017. Once back in Italy I was able to reproduce the h-iPSCs technology also in our laboratories and I started designing the experiments and adapting the protocols to make it more easily compatible with the creation of 3D structures neuronal network. In this chapter I show and discuss the first results obtained on two-dimensional cultures in order to evaluate if the modifications to the protocol produced healthy and functional cultures.

The collaboration with Bio3DMatrix (Genoa, Italy) led to Chapter 3 (that is an extension of the Chapter 2), once we tested the functionality of the cultures generated with the adapted protocol, we successfully used them to test the effects of the chitosan used as an adhesion factor.

Chapter 4 describes the first method to generate 3D model on MEA that I experimented during my thesis. It proposes a modular approach in which chitosan microbeads covered with cells are used as the basic unit to build the 3D network. Results from our laboratory have already been showed but with primary animal cultures. Therefore, this work represents the first adaptation for h-iPSCs-derived cultures.

Chapter 5 describes the first results obtained from the generation of 3D networks encapsulated in a thermogel that mimics the properties of the ECM. These experiments arise from the strong collaboration with the startup Bio3DMatrix which is giving life to a new formulation of chitosan-based thermogel, able to actively support long-term neuronal growth. In particular, we show how the gel guarantees a correct and healthy development of a 3D network by immunofluorescence pictures and also evaluating the functional aspect by detecting spontaneous electrophysiological activity.

Chapter 6 shows the generation of 3D neuronal networks without the use of synthetic scaffolds. Thanks to the adaptation of the rapid differentiation protocol described in Chapter 2, I was able to generate spheroidal cultures composed of already differentiated cells, which we will define as neurospheroids. I then evaluated the functionality of these spheroids using different MEA devices. I used MEA60 and MEA60 3D but thanks to the collaboration with 3Brain I also had the latest generation C-MOS HD-MEA devices available which allowed a more accurate analysis of these samples.

Thesis Aims

Studies of neuronal electrophysiological activity on simplified and more controlled *in-vitro* models are a fundamental step towards understanding the functioning of brain tissue. Many laboratories adopted microelectrode arrays (MEAs) technology to understand how cellular composition, connectivity, genetic and epigenetic expression correlate with the functional electrical activity expressed by *in-vitro* neuronal models (Vassallo et al., 2017, Pelkonen et al., 2021, McCready et al., 2022, Mossink et al., 2021b). MEAs applicability ranges from drug / toxicological screening (Shafer, 2019, Vassallo et al., 2017) to the characterization of various neuronal disorders (Keller and Frega, 2019, McCready et al., 2022, Mossink et al., 2021b). With the introduction of human-induced pluripotent stem cells (h-iPSCs) differentiation protocols, human-derived neuronal models could be created, potentially making the *in-vitro* approach more reliable and representative of *in-vivo* conditions. This allows to generate and study neuronal cells carrying the precise genetic information of the donor in a non-invasive way easing translation of results to clinic and limiting the use of animal experimentation (Song et al., 2018, Liu et al., 2013). Although these models are widely accepted, most are based on monolayer cultures of neurons. The fact of culturing the cells only in one plane is certainly an effective simplification for many purposes, yet the *in-vitro* results are not always congruent with those *in-vivo* (Napoli and Obeid, 2016). In the literature we find different approaches to generate 3D neuronal networks each with its advantages and disadvantages but, few of these used MEA to study the electrophysiological activity arising from these networks. My PhD was therefore focused on the research of methodologies that allow to generate 3D neuronal cultures on MEA devices in order to guarantee the characterization of their spontaneous electrophysiological activity over time. I focused on three approaches that offer different degrees of designability based on the scientific question you choose to model *in-vitro*.

Table of contents

CHAPTER 1

I. INTRODUCTION

Brief history of neuronal cell cultures

During the second half of the nineteenth century a heated scientific debate developed, well known to today's neuroscientists. Several scientists were attempting to study the cytoarchitecture of the nervous system, the staining techniques and samples used by neuroanatomists at the time were similar, but their interpretations diverged in two antagonistic schools of thought that attempt to explain the architecture and development of the brain: the reticular theory and the doctrine of neurons.

The reticular theory was introduced in 1871 by the German anatomist Josef von Gerlach who argued that the nervous system is not composed of discrete cells, but that its fibrous ("reticular") structure is syncytial. This theory was strongly supported by an Italian physician and pathologist Camillo Golgi who in 1873 invented an optical microscopy technique (the silver-chrome impregnation later called the Golgi's method) which allowed the neurons and its organelles to be colored black, thus allowing the body and processes to be highlighted.

The doctrine of neurons, on the other hand, was based on the experimental observations made by the Swiss anatomist and embryologist Wilhelm His who argued that the brain was composed of single cells, that nerve fibers grew from those cells and, above all, that they were discontinuous (Louis and Stapf, 2001). One of the major proponents of this theory was the Spanish physician histologist and neuroscientist Santiago Ramon y Cajal, who immediately adopted Golgi's technique and perfected it, allowing him to produce detailed representations of the structure of the brain. From these analysis (1888 - 1892) he deduced that the doctrine of neurons must be the right theory. More than that, Cajal was able to describe the growth cone in detail and theorized that its function was related to chemotaxis (Ramón and Cajal, 1890).

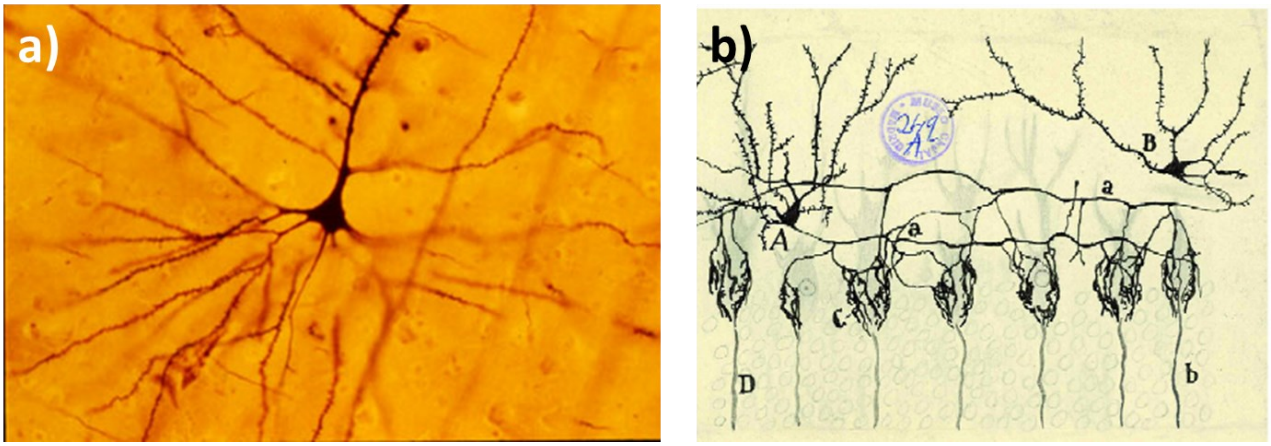

Figure 1.1 a) A neocortical human pyramidal neuron stained by the Golgi technique. Note the apical dendrite extending vertically above the soma and the numerous basal dendrites radiating laterally from the base of the cell body. Photo by Bob Jacobs, Laboratory of Quantitative Neuromorphology Department of Psychology Colorado College https://www.coloradocollege.edu/basics/contact/directory/people/jacobs_bob.html. b) Transverse section of a cerebellar lamella, where A and B are stellate (basket) cells of the molecular layer, whose axons (a) produce terminal nets around the Purkinje cells (D). Is a reproductions of Cajal's original drawings from the "Cajal Legacy " (Instituto Cajal, Madrid).

Nowadays we would have had no doubts, the doctrine of neurons should have prevailed quickly. Yet for the technologies of the time the limit remained the analysis of the fixed tissues. For example, it was impossible to stain and see synapses microscopically (made possible in the 1950s with the electron microscope (Gray, 1959, Yuste, 2015). Thus, although the staining techniques and the samples used by the scientists of the different factions were almost identical, different interpretations arose (Harrison, 1910). The scientific debate continued until 1910 when the biologist and anatomist Ross Granville Harrison was able to dynamically observe the elongation of the axon from the cell soma, seeing the growth cone in action, thus experimentally confirming the hypothesis of Cajal. Harrison was a contemporary of Cajal and immediately understood the limitations of the histological techniques of that time. He consequently developed his own methodology to answer the question of neurite growth, combining methods used in bacteriology and embryology (Harrison, 1910). He devised the technique called 'hanging drop' which allows the long-term cultivation of embryonic tissue by ensuring repeated and protracted observation through a standard microscope, thus creating a valid method for observing tissue development without directly interfering with the cells. In his experiment he isolated the neural tube from a frog embryo and cultured the pieces in a drop of lymph (coagulated blood serum, practically a predecessor of current culture media) thus creating the first *in-vitro* model for the study of neuronal development. The hanging drop technique was rapidly used by several scientists for other mammalian cell types for disease research and was thus perfected to improve the long-term viability of cells, making neuronal culture more accessible and useful to researchers of time (Banker and Goslin, 1988, Millet and Gillette, 2012). In particular, the protocols

for isolating and culturing brain tissue from rodents were optimized and standardized (Banker and Cowan, 1977, McCarthy and de Vellis, 1980, Thomas, 1985, Brewer and Cotman, 1989), developing formulations of serum-free media, defined chemically and commercially available (Brewer et al., 1993, Bardy et al., 2015), thus ensuring the possibility of using the technique in different laboratories. Although technical improvements have led to better growth, long-term survival and reproducibility, neurons are not proliferating cells and consequently a continuous source of animals is needed. Therefore, in order to have human neuronal models, it would be necessary to take the nervous tissue directly from patients and this can only happen in very rare circumstances. For this reason, starting from the 1970s, cell lines are generated from rodents and human tumors: These cells are modified to be able to be propagated indefinitely in culture. Some of these lines include cells such as SH-SY5Y, NT2 or PC-12 which, when expanded *in-vitro*, can be differentiated into neuron-like cells (Gordon and Amini, 2021). Unfortunately, the usefulness of these cell lines for modeling human disease is extremely limited, as they are derived from few patients. Furthermore, the cells differentiated from these lines only express characteristics similar to those of semi-mature neurons and there is no control over the specificity of these derived cells. On the other hand, primary neurons obtained from rodents and grown in culture proved to be crucial for the initial study of brain tissues. It has been discovered that from the embryonic or postnatal rodent brain it is possible to obtain thin slices or a large number of vital and functional neurons from specific regions, maintaining the ability to develop and mature *in-vitro* (Yamamoto, 1972). Another advantage in using rodents primary cells in the possibility to obtain and validate behavioral models *in-vivo* to test similar human phenotypes. Especially with mice it is easier to generate transgenic disease models especially for monogenic disorders. For these reasons rodents are still an acceptable source for neuronal cells, and have constituted most of the state of the art for neurotoxicity studies of drugs, chemicals and for modeling neurological disorders *in-vitro* (Keller and Frega, 2019, Feber, 2019).

Over the years, however, it has been realized that the translatability of the results in the human clinical field is strongly influenced by the difference in species. Although rodent brains can approximate normal or pathological human processes, their genomic divergence, shorter development times and reduced complexity mean that some diseases cannot be fully replicated or at worst in toto (Ardhanareeswaran et al., 2017). It is also extremely difficult to extrapolate from rodent to human phenotypes and it has been seen that sporadic human diseases generally cannot be replicated in laboratory animals (Han et al., 2011). More specifically, there are significant differences at the cellular level, as in the case of astrocytes (a specific subtype of glial cell present in the brain) which in humans have significantly greater dimensions and complexity, clearly denoting an evolutionary gap (Oberheim et al., 2009). Rodent neurons also demonstrated a different type of development at the

network level, reaching maturity very quickly, thus questioning the possibility of correctly replicating human neuronal networks (Napoli and Obeid, 2016). Consequently, a propensity to limit the use of animal models has been motivated in the biomedical field, to concentrate energies on the development of methodologies and techniques that allow the use of human derived cells usable for diagnostic tests, drug discovery or more predictive and accurate *in-vitro* models.

Electrophysiology and MEA devices

Harrison's (Harrison, 1910) initial methodology was quickly adopted for other mammalian cell types. This technique has been continuously refined to improve the long-term viability of mammalian neurons in culture and different protocols have been developed to optimize and standardize cell isolation. Therefore, starting from that study, the mammalian cerebral cortex was studied *in-vitro* in the form of dissociated monolayer cultures and acute and organotypic slices from animals, in particular rodents. Dissociated cultures are mainly used to study the basic physiological functioning of various types of neurons, synapses and astrocytes by simplifying typical brain structure *in-vivo*. Neurons *in-vitro* retain morphological, pharmacological and electrical properties of cortical networks *in-vivo*. In particular, it has been observed that after a few days in culture the neurons begin to connect with each other with functionally active synapses, forming a random network and showing spontaneous electrophysiological activity that changes during development (Van Pelt et al., 2004). Starting from the second week in culture, the 'spikes' (single supra-threshold signals representing the electrical activity of one or more neurons), tend to group in 'bursts' (sequences of closely spaced spikes), and give rise to an activity that persists throughout the life of the network and represents its stage of maturity (Marom and Shahaf, 2002). This behavior is evident both in very simple systems, such as the leech or lamprey, and in dissociated cultures of hippocampal or cortical neurons from mammals. These changes depend on the maturation of the network and reflect modifications in synaptic efficacy, a behavior recognized as the cellular basis of learning, memory and plasticity during development (Chiappalone et al., 2006). For these reasons accessing and studying neuronal electrophysiological activity is crucial for understanding and evaluating functionality in neurons. Neuronal electrophysiological activity can be measured with different approaches. The first important distinction to be made concerns intracellular and extracellular measurement techniques. Among the intracellular techniques, the classic patch-clamp technique, introduced in 1976 by the two German scholars Neher and Sakmann (Neher et al., 1978), stands out. This technique allows to directly measure the electrical activity of neurons by blocking a small portion of cell membrane with the tip of a micropipette, allowing to detect the intracellular signals of single cells. It is a very precise method that provides direct access to the fundamental components of signal propagation, such as large-

amplitude, single-neuron action potentials and also sub-threshold synaptic and ion-channel signals. However, this technique is invasive and time-consuming as the electrodes must be individually micro-positioned in the target cell. Furthermore, electrical activity cannot be repeatedly monitored in the same neurons during development due to a loss of cell viability after a few hours. As an alternative to intracellular methods, it is possible to record the electrical activity of electrogenic cells and tissues (e.g. central and peripheral neurons, heart cells and muscle cells) by means of substrate-integrated micro-electrodes arrays (MEA). These devices allow to measure the extracellular activity of several cells at the same time in a non-invasive way. They are suitable for repeated and prolonged measurements of the same culture. The disadvantage of this technique is related to the loss of sub-threshold signals and the amplitude of the detected signal is smaller. However, it is a promising technique that is widely used for long-term monitoring and detailed analysis of the *in-vitro* dynamics of neural models.

MEAs were first introduced in 1972 by Thomas et al. (Thomas Jr et al., 1972). They proposed a device with approximately 30 microelectrodes integrated on a glass substrate for recording the activity of cultured chick cardiomyocytes. Five years later G. Gross and his collaborators (Gross et al., 1977) recorded the activity from an isolated snail ganglion placed over these electrodes. In 1980 Pine was able to record the activity of a 3-week-long neuronal network (derived from rat neurons) using an MEA with 32 gold electrodes (Pine, 1980). These three characteristic studies marked the beginning of *in-vitro* network electrophysiology using MEAs. These devices have been adopted for an increasing number of researches and have undergone significant improvements in the following years (Potter, 2001, Stett et al., 2003), thanks to the development of lithographic techniques and the semiconductor industry which has led to a gradual increase in performance and adaptability. There is great variability in MEA technology, but they can be classified according to some specifications such as active or passive devices, number of electrodes, designs, shapes or materials, number of compartments. All devices have in common that they consist of several electrodes integrated in a planar substrate suitable for cell and tissue culture (Obien et al., 2015). Neural activity can be recorded by all electrodes simultaneously and one or more electrodes can be used for electrical stimulation. In this way, MEAs allow both the stimulation and the non-invasive registration of the electrophysiological activity exhibited allowing to carry out repeated and prolonged measurements of the same culture. Typical MEAs consist of a well-plate in which a matrix of extracellular microelectrodes is integrated at the bottom. The choice of materials to be used is crucial since they must be biocompatible and humidity-resistant for prolonged periods of time (MEAs are stored inside the incubator during the development of the culture). The diameter of each electrode ranges from 10 to 30 µm and the electrodes are often arranged in a grid covering approximately 0.2-2 mm^2. The

opposite end of each electrode extends to the periphery of the chip and makes contact with an external amplifier, which passes electrical signals for further conversion, filtering, , storage and analysis of data.

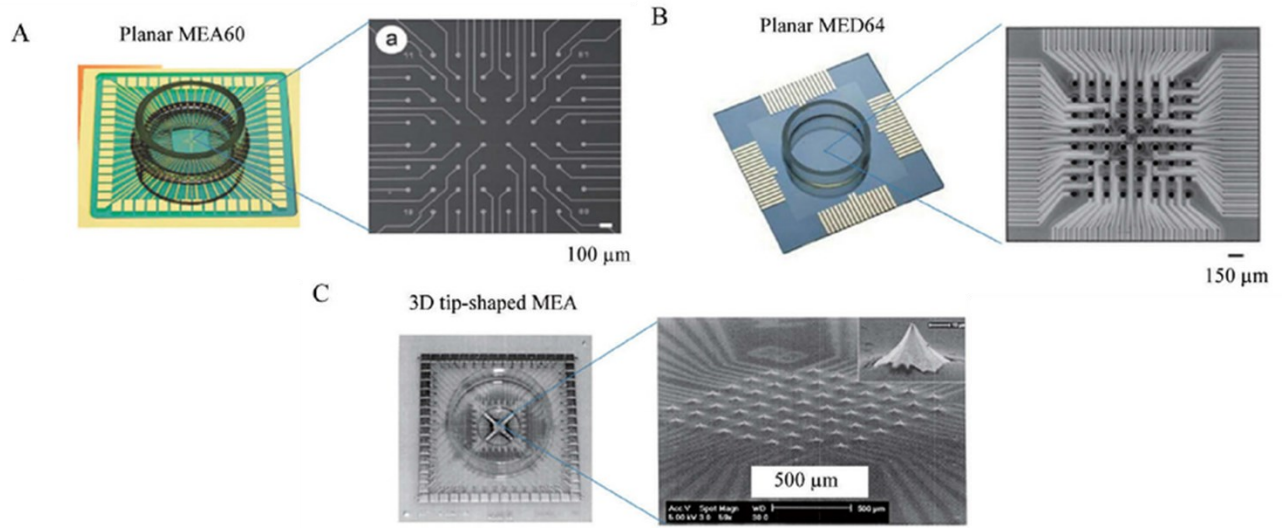

Figure 1.2 Three types of standard multi-microelectrode arrays (MEAs). A) The planar MEA60 biochip. Left, an overview of the MEA60 chamber; right, design of MEA60 showing that the recording field is composed of 60 microelectrodes connected to strip conductors. B) The planar multi-electrode dish 64 (MED64) biochip. Left, overview; right, design of MED64 showing that the recording field is composed of 64 microelectrodes connected to strip conductors. C) The 3-dimensional (3-D) tip-protruding MEA biochip. Left, overview; right, design of 3D MEA photographed under a scanning electron microscope showing that the recording field is composed of 60 tip-protruding microelectrodes connected to strip conductors;. Scale bars: A 100 µm; B 150 µm. Images adapted from Liu, Ming-Gang, et al. "Use of multi-electrode array recordings in studies of network synaptic plasticity in both time and space." Neuroscience bulletin 28.4 (2012): 409-422.

The extracellular activity recorded by the MEAs is composed of the collective contribution of many cells rather than single-neurons. This is typically due to the low number of microelectrodes embedded in the substrate (few tens of microelectrodes) and to their relatively large spatial separation (hundreds of micrometers). Until the early 2000s, little improvement was made to increase the spatial resolution of these devices, mostly because thin-film technology limited the increase of the number and density of substrate-integrated electrode sites. However, during the past decade, systems with higher resolution became available to study neuronal functional activity and effect of chemical manipulations with unprecedented sensitivity and spatio-temporal resolution. We definitely moved from a few units of electrodes (80s) to arrays of tens of units (90s) up to the current high resolution (HD-MEA) with more than 1000 electrodes, on the same device (10s). The advantage of having MEAs with high spatial resolution is the possibility of improving the performance of the neuronal signal analysis, looking for the origin of the various neuronal dynamics such as Burst and synchronous network activity; a high-resolution MEA therefore allows you to have a view of both the overall activity of the entire network and the activity of individual neurons. A relevant problem parallel to the increased spatial resolution of MEAs is the difficulty in handling the enormous amount

of electrophysiological data (i.e. a 10-minute recording with a 4096 electrode MEA and sampling rate of 20 kHz is approximately 90 GB in size). A new generation of high-density active MEA was first presented in 2001 (Berdondini et al., 2001) and has taken over the last decade (Jones et al., 2011). These devices are defined as 'active' MEAs, because they are made with CMOS (complementary metal-oxide-semiconductor) technology, and each microelectrode has an embedded amplifier following the Active Pixel Sensors (APS) technology. The advantage in integrating active electronic components on the same substrate as the actual electrodes lies in the possibility of increasing the number of electrodes, and their density. Furthermore, the co-integration allows to amplify the signals with an optimal quality thanks to minimal capacitance and parasitic resistances (Jones et al., 2011). The potential of this architecture also lies in its modularity and scalability, allowing the creation of MEAs of different size and resolution based on the needs and purposes of the measurements. A peculiar feature of these MEAs lies in the management of the large amount of data generated by the measurements. In fact, the signals of each channel are not acquired and displayed as single voltage traces (as conventionally done in electrophysiology), but the data are acquired and managed as image sequences. Rapid acquisition of extracellular electrophysiological signals is performed as a sequence of frames by encoding extracellular voltage signals as pixel data, using a false color map, this allows for video observation of overall network activity and local activity on the data base of a single pixel. Raw data from a single micro-electrode is reconstructed by combining single pixel data from sequential frames. The high sampling frequency, with which the signal is acquired, allows the monitoring of both rapid Spike activity and slow oscillations, thus guaranteeing in addition to a good spatial resolution, given by the large number and density of electrodes, also an excellent temporal resolution. In this thesis we used both passive and active and 3D MEA to perform measurements of the electrical activity of h-iPSC derived neuron networks.

Analysis of electrophysiological data

MEA devices allow recording of neural signals, which are then analyzed to monitor / characterize the electrophysiological activity of neuronal network. By neuronal signal we mean the temporal and spatial variation of the neuron's membrane potential recorded extracellularly. When a neuron is not excited by surrounding cells, it is at rest and it has a resting membrane potential, typically of the order of -70 mV (Hodgkin and Huxley, 1952). This value depends on the types of ion channels that are open and the concentrations of different ions in the intracellular and extracellular fluids during the resting state. In neurons, K+ and organic anions are typically found at a higher concentration within the cell than outside, whereas Na+ and Cl- are typically found in higher concentrations outside the cell. This difference in concentrations provides a concentration gradient for ions to flow down when

their respective channels are open. Hence, K+ ions would be moving out of the cells, while Na+ and Cl- ions would be moving into the cell. These concentration gradients are maintained by the action of the Na+/K+ ATPase via active transport, which in turn allows the membrane potential to be maintained. Consequently, we define action potential (AP) a rapid rise and subsequent fall in voltage or membrane potential across a cellular membrane with a characteristic pattern and it constitutes the elementary unit associated with the transmission of neuronal signals. The AP is defined as an "all or nothing" response because the action potential is triggered only when the neuron receives a depolarizing stimulus high enough to move the membrane potential to reach a threshold potential (-55 mV). The excitatory stimulus that comes from other neurons connected to it causes positively charged ions to flow into the cell body. If the cell body gets positive enough to reach the threshold potential, the opening of voltage-gated sodium channels will be triggered and v , the action potential will be generated and sent to another neuron. The generation of the AP is allowed thanks to the coordinated activation / inactivation of different families of voltage-dependent ion channels (of Na^+ / K^+ / Ca^{2+}). The first phase of the AP is called depolarization in which voltage-gated sodium channels at the part of the axon closest to the cell body activate, thanks to the recently depolarized cell body. This lets positively charged sodium ions flow into the negatively charged axon and depolarize the surrounding axon. We can think of the channels opening like dominoes falling - once one channel opens and lets positive ions in, it sets the stage for the channels down the axon to do the same thing. The second phase is the repolarization and starts when the inactivation gates of the sodium channels close, stopping the inward rush of positive ions. At the same time, the voltage-gated potassium channels open. There is much more potassium inside the cell than out, so when these channels open, more potassium exits than comes in. This means the cell loses positively charged ions and returns back toward its resting state. As the action potential passes through, potassium channels stay open a little bit longer, and continue to let positive ions exit the neuron. This means that the cell temporarily hyperpolarizes or gets even more negative than its resting state. As the potassium channels close, the sodium-potassium pump works to reestablish the resting state. Every spike is followed by a refractory period that determines the maximum frequency at which a single neuron can send action potentials. We can distinguish two types of refractory period. The absolute refractory period occurs once the sodium channels close after an AP and then enter an inactive state during which they cannot be reopened, regardless of the membrane potential. The relative refractory period which occurs when sodium channels slowly come out of the inactivation. During this period the neurons can be excited with stimuli stronger than the one normally needed to initiate an AP. Early on in the relative refractory period, the strength of the stimulus required is very high. Gradually, it becomes smaller throughout the relative refractory period as more sodium channels recover from the inactivation stage.

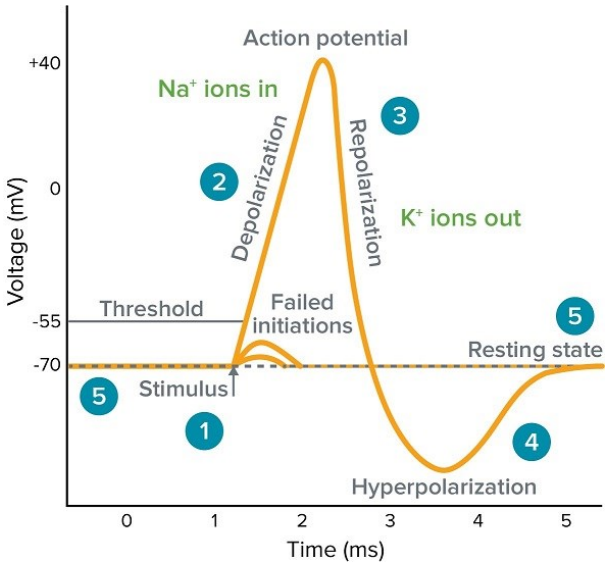

Figure 1.3. Schematic representation of the main phase of an action potential. 1) Stimulus starts the rapid change in voltage or action potential. In patch-clamp mode, sufficient current must be administered to the cell in order to raise the voltage above the threshold voltage to start membrane depolarization. 2) Depolarization is caused by a rapid rise in membrane potential opening of sodium channels in the cellular membrane, resulting in a large influx of sodium ions. 3) Membrane Repolarization results from rapid sodium channel inactivation as well as a large efflux of potassium ions resulting from activated potassium channels. 4) Hyperpolarization is a lowered membrane potential caused by the efflux of potassium ions and closing of the potassium channels. 5) Resting state is when membrane potential returns to the resting voltage that occurred before the stimulus occurred. Image taken from *https://www.moleculardevices.com/applications/patch-clamp-electrophysiology/what-action-potential*

While the basic characteristics of an action potential are common to the various types of excitable cells, its shape can change from cell to cell and reflects the functions that that signal must perform to support cellular activity. Furthermore, the magnitude of the action potential is independent of the magnitude of the stimulus; the variation of the nervous information is therefore obtained, not by modifying the amplitude of the action potential, but by modifying the frequency with which the action potentials arise (Hodgkin and Huxley, 1990). Different network dynamics can be identified thanks to the different modulation of the AP frequency in the various neurons of the network. Typically, when we refer to the signal emitted by a neuron we mean the temporal sequence of the APs, also called Spike Train. In fact, given the "all or nothing" concept of the nerve impulse, each peak is considered indistinguishable from the others produced by the same neuron, if not for the instant in time at which it occurs, unique for each Spike, measurable with a high degree precision (Lama et al., 2018). The time interval between two spikes is called Inter Spike Interval (ISI), the variation of this parameter indicates a change in the dynamic state of the neuronal signal. During a Spike Train, at the single channel level, it often occurs that there are periods during which the Spike frequency is relatively high interspersed with periods of quiescence in which the spike frequency is very low, this phenomenon is called Burst (Bologna et al., 2010a).Typically, a Burst is considered when there are a certain number of Spikes, usually at least 3, having an ISI lower than a certain time interval (of the

order of 100 ms). The time interval between two Bursts is identified by the acronym IBI (Inter Burst Interval). From a biophysical point of view, the onset of this dynamic state is attributable to different aspects and neurons with different morphology reach this state in different ways (Turnbull et al., 2005). Bursting phenomena are caused by the interaction of membrane conductance's with fast dynamics (Na + channels) which generate Spikes and slower mechanisms (Ca2 + channels), which control when they occur; based on the morphology of the neuron and therefore on where the ion channels are located, different biophysical mechanisms occur which trigger the Bursts (Krahe and Gabbiani, 2004). The Bursting dynamic has an important role in the transmission of information between neurons. In particular, it seems that high frequency Spikes can improve the reliability in transmission, where "unreliable synapses" occur and in specific situations they would improve transmission of sensory information *in-vivo*. If more Spikes occur within a short period of time, the accumulation of Ca2 + in the presynaptic terminal causes the release of more transmitter ensuring a stronger postsynaptic response, therefore bursts can be transmitted across the synapse more reliably than isolated peaks. Bursts appear to play a primary role in synaptic plasticity, in fact it has been shown that in some cases single bursts are sufficient to produce Long Term Potentiation / Depression (LTP / LTP) (Lisman, 1997). Bursting behavior is one of the most important properties for evaluating the dynamics of electrical activity during the development of neuronal networks.

By observing at the same time Spike Train of a certain number of neurons connected to each other (therefore forming part of a network), it can be verified that at specific instants of time, for a variable duration, many neurons emit action potentials in a synchronous manner, these events are called in the literature with the name of Network Burst (NB). A NB is a very complex dynamic state that occurs spontaneously and involves the entire neuronal population; periods of depolarization of the entire network are followed by periods where activity is relatively low. Due to its complex dynamics, studies using electrophysiological data deriving from MEAs have proposed algorithms based on different approaches to correctly detect them. In particular, Van Pelt et al rely on moments of high network activity evoked by synchronous activation of multiple electrodes (i.e. synchronicity among spikes) (Van Pelt et al., 2004, Chiappalone et al., 2006). Bologna et al others uses the same method but restricts the detection only when the high activity originates from bursts on different electrodes (i.e. synchronicity among bursts)(Bologna et al., 2010b). Where NBs originate from is not yet known with certainty, but the most quoted theory is that there are isolated populations of oscillatory neurons (30-40 neurons), which by spontaneously synchronizing generate very regular network bursting phenomena (Fardet et al., 2018). In dissociated cultures the network burst resembles the sleep spindles of the cerebral cortex *in-vivo*, as well as the epileptic activity (Wagenaar et al., 2005b). The persistence of this activity is linked to the lack of input from other parts of the brain. Synchronized

activity between neurons occurs in many areas of the brain and is believed to be relevant to information processing, including sensory processing, cognition, and sleep. Spontaneous activity is also a common feature of all developing brains; plays a role in the ontogenesis of the neuronal network.

Neurons do not work alone but are inter-connected in a network and participate collectively in multiple functions (Nicolelis, 1997). It is therefore important to understand the complex interaction, i.e. the connectivity, between single neurons, small neural networks and large populations. This allows us to investigate the way in which information is represented and stored by the central nervous system. There are three types of connectivity: structural, functional and effective connectivity. The first represents the set of anatomical connections that bind neurons at a given instant. It can range in size from local circuits to inter-area routes. It generally does not vary over short periods of time (between seconds and minutes), while it varies dynamically during development or learning (between hours and days). Functional connectivity is based on the cause / effect relationship and exists between two neurons if it is possible to predict the activity of one based on the activity of another. Finally, the actual connectivity is experimentally obtained in response to a series of perturbations, it requires a causal relationship between two neurons; it does not study the effects on other units among themselves. To estimate the functional-effective connectivity of *in-vitro* networks, there are two different strategies: the first one relies on the direct analysis of the acquired sequence of voltage values from each recording electrode (i.e., the time series). The other approach deals with point processes (e.g., spike trains). Statistical analysis of spike train data was pioneered by Perkel (Gerstein and Perkel, 1969) and followed by more than four decades of methodology development in this area (Brown et al., 2004). Analytically, cross-correlation based methods remain the main statistics for evaluating interactions among the elements in a neuronal network and produce a weighted assessment of the connections strength. Weak and non-significant connections may tend to obscure the relevant network topology constituted by strong and significant links, and therefore are often discarded by applying an absolute, or a proportional weighted threshold (Friston, 2009). Correlation based techniques include: independent components analysis and various measures of synchrony, smoothed ratio of spiking activity (Ventura et al., 2005), cross-correlation and cross-correlogram (Brosch and Schreiner, 1999, Salinas and Sejnowski, 2001), correlation coefficient ref (Bedenbaugh and Gerstein, 1997), partial-correlation (Poli et al., 2015). Cross-Correlation (CC) measures the frequency at which one particular neuron or electrode fires (“target”) as a function of time, relative to the firing of an event in another network (“reference”). Recently was introduced a new CCH-based algorithm able to infer functional-effective excitatory-inhibitory links called Filtered Normalized Cross-Correlation Histogram (Pastore et al.).

2D in-vitro model of neuronal network

The study of in situ brain disorders in humans is hampered by ethical problems concerning direct access to tissue, therefore animal models have been used extensively to gain new insights into possible therapies. Unfortunately, there is a poor correlation between the clinical diagnosis and the underlying pathological mechanisms, and this complicates the design of appropriate animal models. Not only that, but some symptoms that may occur in the patient are not replicated in the animal, making many promising approaches in animal studies not translatable in the clinic (van der Worp et al., 2010). For this reason, a possible solution lies in the use of *in-vitro* models of brain disorders. The peculiarity of *in-vitro* models is the high experimental freedom, they can be designed to mimic a specific mechanism within a disorder. Conversely, they usually fail to show all other symptoms clinically associated with the disorder as well, therefore, these aspects can sometimes suggest solutions that are not translatable in the human clinic. Indeed, there are drugs that have worked well in *in-vitro* models but have not been able to cross the blood-brain barrier or even cause problems in systems that have not been included in the model (de Lange et al., 2017). Nevertheless, *in-vitro* models remain widely used proving that the relevant mechanisms of the disorder can be isolated i*n-vitro* and possible treatment to patients can be derived. Consequently, *in-vitro* models of brain disorders focus on dysfunction at the cellular or synaptic level combining electrophysiological analysis of the so formed networks. The most promising *in-vitro* models of brain disorders include epilepsy, stroke and memory-related disorders. They serve as models for studying the pathophysiology of the disease, identifying new biomarkers, options for mechanism-based treatment or screening for high-throughput drugs. Cultures of dissociated neurons on MEAs offer easy access to many neuronal cells, as the cultures remain viable for several months. After plating, neurons forms dendrites, axons and new synapses. After approximately 3 weeks *in-vitro*, the cultures show stable firing patterns, demonstrating mature development and here they are ready for experimentation. Lacking the classic three-dimensional spatial organization, the cells adhere only in one plane and consequently the morphology of the cells is similar but not equal to *in-vivo*. This exemplification made these models particularly useful for studying the basic physiological functioning of various types of neurons, synapses and astrocytes. In 1989 a work demonstrated that the cultures of dissociated hippocampal neurons showed epileptic-like events when treated with other concentrations of Mg2 + and with a glutamate receptor antagonist (Furshpan and Potter, 1989) suggesting a use of these models to study the pathological mechanisms related to excitability disorders. The observation that networks of dissociated cortical or hippocampal neurons develop activity patterns that are dominated by synchronous bursts that show remarkable resemblance to interictal spikes (Ramakers

et al., 1990) has been confirmed in numerous later studies, see, e.g., (Chiappalone et al., 2007, Eckmann et al., 2008, Pasquale et al., 2008, Van Pelt et al., 2004). To show seizure-like activity the cultures require additional treatment using glutamate agonists (Kiese et al., 2017) or GABA antagonists such as bicuculin (Colombi et al., 2013). In particular in Colombi et al studied the effect of anti-epileptic drugs valproate and carbamazepine on both control and bicuculline-treated neuronal networks finding significance differences in the effects of the drugs on both networks. Alternatively, primary cultures obtained from genetically modified mice can induce / reproduce seizure activities (McSweeney et al., 2016) or for example cause sleep-related partial epilepsy. These cultures have been shown to become hyperexcitable and to represent a chronic model of spontaneous epileptiform activity *in-vitro* that does not require pre-treatment with seizure drugs (Gullo et al., 2014). In particular Gullo et al 2014 demonstrated that the effect of carbamazepine on the epileptic network was stronger than its effect on a control network that had shorter duration bursts. In the field of cerebral stroke there have been several studies that used primary cultures of dissociated neurons to model the peripheral area of the region affected by stroke, the so-called penumbra (Hofmeijer et al., 2014, Stoyanova et al., 2016, le Feber et al., 2016, Muzzi et al., 2019). Here the tissue is not necrotic as in the central stroke area, and we are interested in understanding what are the mechanisms that guide the recovery of the damaged area in a remedial way. Experimental results confirmed that synaptic failure occurs rapidly after the induction of hypoxia (Hofmeijer et al., 2014, le Feber et al., 2016). This is at least in part due to presynaptic mechanisms, including adenosine-mediated mechanisms (Khazipov et al., 1995, Sun et al., 2002), impeded phosphorylation of presynaptic proteins (Bolay et al., 2002), and impeded endocytosis and exocytosis of synaptic vesicles (Fedorovich et al., 2017). Consequently, were proposed model that tested prevention strategies to increase the chances of recovery of cells subjected to periods of hypoxia. During my master thesis I implemented an optogenetic closed-loop stimulation protocol in an *in-vitro* model of the penumbra. We showed that the electrophysiological activity is essential for the survival of neurons and to increase the chances of recovery, a certain minimum level of activity must be maintained during the onset of hypoxia (Muzzi et al., 2021b). Regarding memory disorders (i.e. Alzheimer disease), the decrease in activity in primary hippocampal mouse cultures was found to be due to synaptic dysfunction. This is because the addition of Aβ amiloyd to cultures of dissociated mouse hippocampal neurons on MEAs rapidly reduced their firing rate (Kuperstein et al., 2010), without significant cell death at low concentrations (Varghese et al., 2010). More recently, also Charkhkar *et al.* added amyloid-β 1-42 (Aβ42) directly to cortical neurons harvested from embrionic mouse, finding a significant reduction of network spiking on MEA. Additionally, they demonstrated that NMDA and

AMPA/kainite receptors play a role in the the effects of Aβ42 on neuronal activity *in-vitro* (Charkhkar et al., 2015).

Recent work suggests that the sensitivity to detect early changes occurring after the addition of amyloid oligomers to the medium of *in-vitro* electrophysiological recordings may be further enhanced by the use of high-density electrode arrays (Amin et al., 2017).

In this chapter, we presented some results from different brain disorder models to illustrate the power of MEA-based brain disorder models. Despite the advantages highlighted so far, these models have limitations that need to be removed to make these models more efficient. For example, in the case of the penumbra models, the oxygen levels used to simulate hypoxia (and also normoxia) are very different from those *in-vivo*. The interpretation of the organization of the culture in synchronous network activity is also debated. They can reflect the hyperexcitability of input-less networks, but they can also play a role in information processing (Kepecs and Lisman, 2003, Singer, 1993), or in increasing the reliability of communication between neurons and avoiding synaptic transmission failure (Chen et al., 2009). Another fundamental aspect is related to memory and how it works, in particular how we manage to retrieve information saved in long-term memory. The discovery of this mechanism would certainly broaden the use of MEAs models and would represent an important step forward in memory research. A common limitation concerns the cellular composition (fraction of inhibitory / excitatory neurons; relationship astrocytes: neurons, etc.) which always remains linked to the initial dissection tissue, the two-dimensional spatial organization that cells assume *in-vitro* and the origin of the cells. Although by isolating slices of the brain the spatial organization is preserved, it is very difficult to make this type of tissue survive for a long time and in any case, it cannot be obtained by humans. The advent of human induced pluripotent stem cells and the continuous development of differentiation protocols offer new horizons for *in-vitro* modeling on MEAs. This would create the possibility to generate human models completely engineered from the point of view of cellular composition and structure. This will provide a very solid platform for the development of new brain disorder models, particularly in combination with newly developed tools to design specific structures.

Human-induced pluripotent stem cells and neural differentiation

Stem cells can be classified according to their differentiation potential or according to their origin. As for the differentiation potential, stem cells can be divided into totipotent, pluripotent, multipotent, oligopotent and unipotent. While based on their origin, relative to different periods of the life of an organism or to artificial derivations, stem cells can be divided into embryonic, fetal, adult, reprogrammed and tumor. The stem cell par excellence is the zygote, which derives from the

fertilization process that takes place between the two gametes, the sperm and the oocyte. The zygote, and the cells that derive from it by segmentation up to the 8-cell stage, are totipotent cells. These are cells capable of giving rise to all the cells of an individual, including the extra-embryonic tissues that support the development of the organism. Pluripotent cells are one step below totipotent cells. This category includes embryonic cells that originate in subsequent development processes. These cells are capable of generating all the cells of a living being with the exception of the supporting extraembryonic tissues. They are found in the internal cell mass of the blastocyst up to the 4-5th day after fertilization. Embryonic stem cells (ESCs) are artificially derived from the inner cell mass of the blastocyst which is destroyed for their derivation and cultured for the generation of stable stem cell lines. Multipotent cells derive from embryonic cells during the formation processes of the three embryonic sheets and support, during the organogenic phase, the formation of the tissues and organs in which they reside. Multipotent cells remain in post-natal life, they reside in adult tissues where they are able to generate different lines of differentiation. Examples of this process are hematopoietic stem cells (HSCs) capable of differentiating into all cell populations circulating in the blood, and mesenchymal stem cells (MSCs) capable of originating all connective tissues such as bone, cartilage, adipose tissue, muscle and vases. Oligopotent and unipotent cells have an increasingly restricted capacity for specialization and can differentiate into few or single cytotypes such as nerve stem cells (NSCs), capable of forming neurons and supporting cells present in the nervous system, and, such as stem cells epithelial cells (KSCs), capable of committing themselves to the specialized cells that make up the outermost layers of our skin. The clinical use of embryonic stem cells is currently severely limited by ethical issues and immunocompatibility problems. Furthermore, studies conducted on animal models with ESCs have shown an uncontrolled growth of these cells which led to the development of tumors. Instead, there are several clinical applications of adult stem cells in the field of regenerative medicine. These cells are in fact studied in medical research with the aim of being able to replace any diseased tissue or organ in the body, recreating it in the laboratory. Currently, adult hematopoietic stem cells are used in the clinic to treat different types of leukemia and lymphoma and to treat some inherited and acquired blood diseases. They have the advantage that they can be extracted from adult individuals and are easily controlled. However, they are limited by a small amount and poor versatility. Corneal stem cells, on the other hand, have been used since 1997 to regenerate the epithelium of the cornea, which is transplanted into patients with cornea damaged by disease, infection or trauma. Skin stem cells are also used. Thanks to their ability to grow the skin on transplantable media, they are essential for treating victims of severe burns. Stem cells are also used for toxicology applications, for the study of drugs and as an *in-vitro* model for genetic pathologies.

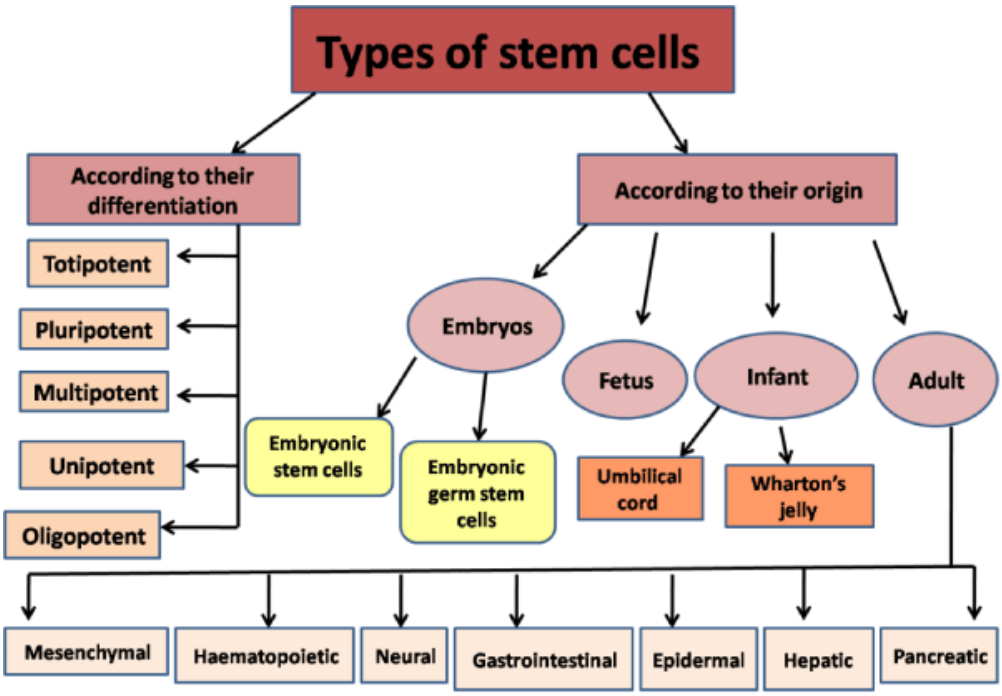

Figure 1.4. Schematic representation of different types of stem cells.

In recent years, Yamanaka's discovery (Takahashi and Yamanaka, 2006), of bringing adult somatic cells back to a stage of induced pluripotency (iPSCs), has revolutionized the evaluation of the mechanisms underlying the development of human pathologies. The potential of these cells is that they can differentiate *in-vitro* into any desired cell type, which has initiated the study of different differentiation protocols of iPSCs into neurons *in-vitro*. The importance of this technique lies in the opportunity to develop a human model derived directly from the patient: the patient's *in-vitro* cells will exhibit the same genetic and epigenetic modifications as the *in-vivo* cells. The availability of these lines and the patient's medical history can be very informative for the development of research at the clinical level, which can lead to the development of precision medicine. In addition to providing a possible cellular model of pathology, human-iPSCs (h-iPSCs) could also represent an excellent model for the discovery of new drugs capable of slowing or blocking a pathology. Compared to primary cultures, which derive from tissues composed of multiple cell types, Yamanaka's discovery introduces the further advantage of building a model with only the desired cell components, and therefore of being able to recognize the contribution of the different cells in culture. In general, the technique proposed by Yamanaka consists in reprogramming, through the expression of transcription factors (such as SOX-2, octamer 4, kruppel-like factor 4 and c-MYX), adult somatic cells that are induced to a stage of pluripotency. The release of the reprogramming factors occurs using retroviral and lentiviral vectors, but non-viral methods that use plasmids instead of viruses have also been tested (Paspala et al., 2011).

For a long time, it was believed that neurons lost the ability to proliferate during the early stages of development and that the adult brain completely lacked specialized cell types capable of providing for the addition and / or replacement of neuronal cells during the course of life. Altman's pioneering works of 1965 (Altman and Das, 1965) and numerous subsequent studies have instead demonstrated the presence of neural stem cells (NSCs) and the continuous generation of new neurons in the central nervous system of adult mammals (Gage, 2000). It is a life-long event, due to the neurogenesis process new neurons are generated in the subventricular zone of the lateral ventricles and in the dentate gyrus of the hippocampus. Neural stem cells are multipotent self-renewing cells capable of generating neurons, astrocytes and oligodendrocytes in the nervous system (Taupin and Gage, 2002). The use of NSCs in research allows to recreate *in-vitro* the developmental events of the nervous system offering the possibility to study the effects of characteristics on "self-renewal", on proliferation, on the addressing towards a specific neural fate and the differentiation of multipotent cells (Cacci et al., 2017). Furthermore, the possibility of isolating NSCs from different brain areas constitutes an important system for studying the effects of specific molecules on cell types from specialized areas. These cells therefore constitute an important tool for the derivation of appropriate cell models for the study of pathological processes, an alternative to the engineering of genetically modified or transformed lines. NSCs have been isolated and characterized from various regions of the adult central nervous system (CNS) from biopsies and postmortem tissues. In several studies, NSCs derived from adult tissue have been transplanted into animal models and studied as a functional graft, and their potential use for possible cell therapy has been highlighted (Graziadei and Monti Graziadei, 1980).

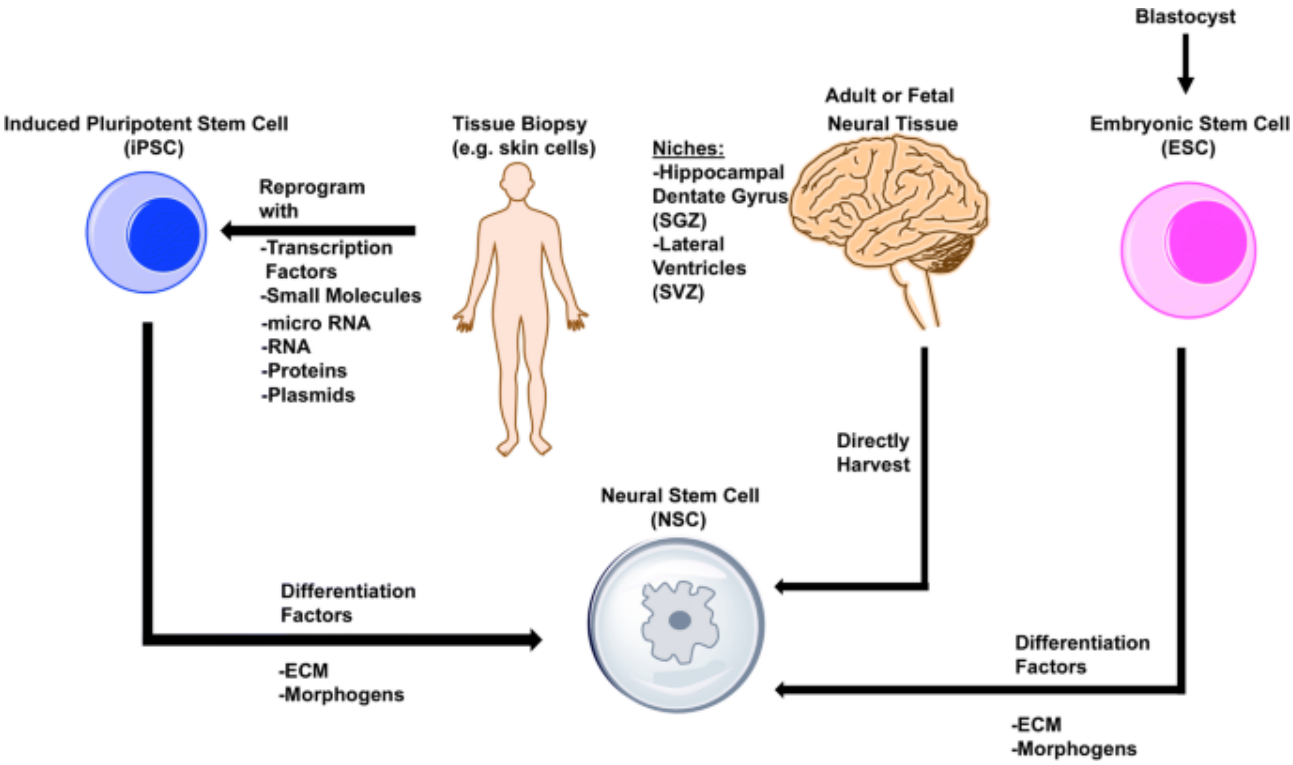

Figure 1.5. Schematic diagram of NSC generation via multiple methods. NSCs can be extracted directly from neurogenic niches, including the subgranular zone (SGZ) of the hippocampal dentate gyrus and subventricular zone (SVZ) of the lateral ventricles, from adult or fetal neural tissue and expanded in vitro. NSCs can be reprogrammed from patient-derived induced pluripotent stem cells by using combinations of specific transcription factors, small molecules, microRNAs, plasmids, and other morphogens. In addition, NSCs can be generated from blastocyst-derived embryonic stem cells by using specific combinations of differentiation factors, such as morphogens and extracellular matrix (ECM) proteins. Picture from Boese, Austin C., et al. "Neural stem cell therapy for subacute and chronic ischemic stroke." Stem cell research & therapy 9.1 (2018): 1-17.

Human-derived neuronal networks on MEA

The first recording of hESC-derived neurons occurred in 2009 (Heikkila et al., 2009) where neurons were pre-differentiated into floating 3D spheroidal structures, then mechanically dissociated and plated on MEA (Heikkila et al). The results showed that the type of activity was comparable to those obtained from neuronal networks derived from mouse embryonic stem cells (mESC) (Illes et al., 2007). In fact, the networks showed spontaneous activation with the onset of synchronous network activity, and they also responded to pharmacological treatment. Subsequently, the same differentiation protocol was successfully applied to h-iPSCs, producing electrophysiologically active neurons on standard MEA (Toivonen et al., 2013) and also on CMOS-MEA (Amin et al., 2016). It was from this last work that the importance of adhesion factors in 2D MEA models emerged, in fact the neuronal networks grown on CMOS-MEA coated with poly-dl-ornithine (PDLO) showed a greater activation, compared to the polyethyleneimine coating. (PEI), which is often favored in standard MEAs. Not only that, but it has been seen how important it is to insert proteins contained in

the extracellular matrix (ECM), such as laminin. In particular the human recombinants contained in chain 5 are optimal for neuronal networks derived from hPSC on MEA (Hyysalo et al., 2017). These first studies of 2D human neuronal cultures of MEA have established the first tricks to be successful in recording action potentials and have shown the potential in the study of neuronal function. The most common 2D neuronal differentiation methods are based on two essential steps. The first step is the induction of differentiation into neuro precursors cell (NPCs), often achieved through small molecule inhibitors of the activin / nodal and bone morphogenic protein (BMP) pathways (so-called dual-SMAD inhibition). The second step is the proliferation of NPCs and the subsequent differentiation into more specialized neuronal cells by adding medium containing various supplements including usually brain derivative neurotropic factor (BDNF) and Glial cell-derived neurotrophic factor (GDNF). Several studies have shown electrophysiological results deriving from these cultures with slightly variable parameters for example, the burst rate after 45-56 days in culture (Hyvärinen et al., 2019a, Hyvärinen et al., 2019b). These differences are partly attributable to the inherent variability of the differentiation protocols that generate mixed populations of neuronal cells with slightly variable rates. Thanks to immunohistological analysis and to the neuromodulation it was possible to identify the presence of functional glutamatergic and GABAergic neurons as well as astrocytes (Hyvärinen et al., 2019b). Another work that used dual-SMAD inhibition shows that 1.3% of the neurons in the culture were cholinergic, with 6.7% of the neurons GABAergic and the rest deemed glutamatergic (Shimba et al., 2019). We can note that the percentage of inhibitory neurons is considerably lower compared with the percentage in the cortex *in-vivo* which is around 20% (Peyrache et al., 2012, Markram et al., 2004). There have been developed protocols that aimed at generating only homogeneous populations of mature neurons that show network activity in just a few weeks. An example is that of Pang et al (Pang et al., 2011). And Zhang et al. (Zhang et al., 2013) who first proposed an approach to generate cortical excitatory neurons from h-iPSCs by overexpressing the mouse transcription factor neurogenin-2 (*NgN2*) via lentiviral infection. Consequently, in 2017 Frega et al. (Frega et al., 2017) implemented the protocol thanks to a genetic modification, going to generate a stable line of h-iPSCs that could overexpress *NgN2* thanks to a tetracycline transactivator (rtTA), in order to induce the differentiation in excitatory cortical neurons of the 2/3 layer by adding doxycycline in the medium (Frega et al., 2017). The results showed functional and mature networks after only 23 days of culture with a fraction greater than 95% of MAP2 positive neurons. Not only that, but results from patch clamps showed that these neurons only receive post-synaptic excitatory potentials, further evidence that these are mainly glutamatergic. Another protocol aimed at the production of homogeneous populations is that focused on the lentiviral overexpression of the transcription factors of the mouse distal homeobox 2 (Dlx2) and the transcription factor bHLH of the

achete-scute family 1 (*Ascl1*) for the generation of GABAergic cortical neurons (Yang et al., 2017). This differentiation has been shown to induce GABAergic neurons which plated on MEAs with glutamatergic neurons produced electrophysiological activity after 5 weeks, with single electrode firing frequencies of about 3Hz and synchronized network activity at about 3-4 bursts per minute (Mossink et al., 2021a). Although some *in-vivo* results suggest that inhibitory neurons rarely produce bursts, it is impossible to say whether the *in-vivo* recordings actually sampled the GABAergic populations due to the lack of any type of molecular analysis (Peyrache et al., 2012). Furthermore, it is possible that the nature of neuronal networks *in-vitro*, due to the lack of inputs, induces cells to produce burst events (Mossink et al., 2021a). The disadvantage of differentiation methods for homogeneous populations lies in the fact that they are very simplistic models and often the so generated cells have a short life if not inserted in a co-culture with supporting cells (for example with astrocytes). However, the speed, efficacy and repeatability from cell line to cell line of the methods (Mossink et al., 2021b) highlight their feasibility in mechanistic and pharmacological studies of human neuronal networks, not only but hoping to have specific differentiation protocols available for each neural cell type, new horizons will open up to produce highly engineered *in-vitro* models.

Targeted Cell Type	Time to Tuj1/ MAP2$^+$ Cells	Time to Functional Synapses	Yield of Neurons	Neuronal Purity	Neuron Subtype Purity	Reference
Neurons	~6 weeks	12 weeks	ND	15–79%*	Mixed	Hu et al., 2010
NPCs	4–5 weeks	ND	ND	ND	Mixed	Zhang et al., 2001
Neurons	4 weeks	7 weeks	ND	89 ± 3%*	Mixed	Johnson et al., 2007
NPCs	~3 weeks	ND	ND	82%*	Mixed	Chambers et al., 2009
NPCs	~3–4 weeks	ND	ND	ND	Mixed	Elkabetz et al., 2008
Nociceptive sensory neurons	~2 weeks	ND	ND	>75%*	>60% **	Chambers et al., 2012
Midbrain dopamine neurons	~3–4 weeks	>7 weeks	ND	ND	60%–80%**	Kriks et al., 2011
NPCs	4 weeks	ND	ND	40–70%*	mixed	Koch et al., 2009
Cortical excitatory neurons	~3–4 weeks	>8 weeks	ND	40% *	<20%**	Espuny-Camacho et al., 2013
Neurons	4 weeks	~5 weeks with glia coculture	ND	70–80%*	mixed	Wu et al., 2007
Inhibitory forebrain neurons	~3–4 weeks	~6 weeks	ND	~70% **	80%**	Maroof et al., 2013
Inhibitory forebrain neurons	~3–4 weeks	8 weeks with glia coculture	ND	92% **	76%**	Nicholas et al., 2013
Neurons	~3–4 weeks	~4–5 weeks	ND	90% **	mixed	Israel et al., 2012
Excitatory neurons	~1 week	2 weeks	~100%**	100%**	~100%***	this study

*Based on 1 marker expression, ** based on multiple markers, ***based on functional data. All time periods listed are from the undiff state; ND: not determined.

Table 1.1. Comparison of the rapid iN Cell generation method presented in (Zhang et al., 2013) with previously reported methods of generating neurons from ESCs/iPSCs. Table taken from the article (Zhang et al., 2013)

However, we must consider that although the neuronal cultures derived from hPSC are functional, they are still far from mimicking the complexity of the human brain. Several studies have shown that the microenvironment of the culture is very important and influences the regulation of neurogenesis

as well as the survival of the culture (Zhang et al., 2013, Tang et al., 2019). Not only that, but it has also been shown that differentiating neural stem cells respond to the stiffness and elasticity of the surrounding scaffold by producing different ratios of glia and neurons (Asheghali et al., 2020). The previously mentioned models are all based on two-dimensional cultures, where cells interact with each other but only in one plane and the relevant interactions between cells and ECM are missing (Centeno et al., 2018). The other limitation is linked to the excessive timing to generate 'functionally mature' cells, which is also due to the vague definition as the criteria for defining an *in-vitro* neuronal network 'mature' vary between studies. One criterion is based on the observation of inhibitory neurons, when GABA is able to produce inhibitory responses then one can think of maturity, as in the early stages of development, GABA is excitatory. The onset of synchronous network events is also considered, (i.e. network burst) as they are associated with the decrease in excitatory GABA responses (Mäkinen et al., 2018). To give greater clarity to this onset of maturity, Odawara et al. cultivated commercial neurons derived from hPSCs on MEAs for about a year. Their results show that GABA took more than 230 days to produce inhibitory responses (Odawara et al., 2016).Luckily, Other studies already mentioned that used forced expression of transcription factor in h-iPSCs showed GABAergic inhibitory response from DIV28 (Yang et al., 2017) and at DIV42 (Mossink et al., 2021a) in Mossink.

There are examples in the literature that use hPSC and MEA-derived neuronal networks to model the underlying physiology of different events. As previously mentioned, there have been studies that have studied the effects of ischemic stroke on animal models. The use of cultures derived from h-iPSCs has confirmed many results and hypoxic conditions (10% air, 90% N2) have been found to reduce discharge rates and disrupt functional connectivity of human neuronal networks while recovery depends on the duration of the hypoxia (Monteiro et al., 2021), moreover, a 2019 paper proposed a model for mimicking sleep-wake states in dopaminergic neurons (Yokoi et al., 2019). During the 12-hour waking phases, serotonin was administered into the medium and this increased at the frequency of the network burst. A sleep state was then modeled with electrically stimulated glutamatergic neurons at 1Hz for 15min every 75min. It was observed how this stimulation reduced the activation and increased the synchronization of the bursts in the 15min following the stimulation, which recalls the patterns of neuronal activity induced by sleep *in-vivo* (Csercsa et al., 2010, Staba et al., 2002). Although the results are very promising, the model still lacks fundamental elements, such as the presence of astrocytes or ECM. In fact, with the astrocytic support it has been seen that the synchronous activity of the network on MEA increases (Tukker et al., 2018, Kayama et al., 2018). It seems that it is not enough to use mediums conditioned by astrocytes, as they only cause transient increases in neuronal activity, but do not affect synchrony (Lang and Rosenbluth,

2003). In addition to physiological models there are also studies using hPSC-derived neuronal cultures in the context of pathological conditions. As already described in the previous chapters, the primary cultures of neuronal networks on MEA lend themselves to the modeling of epileptic and convulsive events in which the application of clinically used antiepileptic drugs have been able to suppress (Odawara et al., 2018). Indeed, the study of parameters extracted from MEAs such as discharge rate, burst rate, bursting properties and synchronization provide appropriate readings for the toxicological analysis of human neuronal networks (Odawara et al., 2014, Nimtz et al., 2020, Ylä-Outinen et al., 2010, Kasteel and Westerink, 2017). The use of human-derived neurons allowed to demonstrate how there can be a noticeable difference in the effect caused from the same drugs on neurons obtained from different species. For example, it was demonstrate that methoxyetamine in rat cortical neurons has an effect that is approximately 10 times smaller compared to that in human iCell neurons (Hondebrink et al., 2017). Other studies, on the other hand, have compared the effects of TTX and amphetamine but did not find particular differences between rat cortical neurons and iPSCs-derived neurons (Kasteel and Westerink, 2017, Tukker et al., 2018). The comparisons between animal and neurons derived from h-iPSCs are still a bit risky as the differences could reflect maturation differences due to the different differentiation implemented. A huge advantage in using human iPSCs on MEAs is that the cultures will have exactly the same genetic heritage as the donor and therefore are more representative for polygenic disorders than knockout or knockdown models. Several lines of h-iPSCs derived from patients with neurodevelopmental problems have already been produced. Studies are trying to characterize the electrophysiological phenotype expressed by the neurons derived from these lines, succeeding in some cases in shedding more light on the biological mechanisms underlying the disease. For example, Wainger et al 2014 demonstrated that motorneurons derived from patient with amyotrophic lateral sclerosis (ALS) are more active than motorneurons derived from control iPSCs. They also created an isogenic line derived from an ASL patient in which they corrected the disease using genetic techniques and noted that the hyperexcitability of these cultures is again comparable to control samples (Wainger et al., 2014). Not only that, but it was possible to see the onset of the electrophysiological phenotype after only 28 DIV and only after 24 DIV of differentiation. This is very important as ASL patients can remain asymptomatic even for years. Another recent study exploited glutamatergic populations of neurons on MEA to evaluate the electrophysiological activity derived from patients suffering from Kleefstra syndrome, a neurodevelopmental disorder associated with the haploinsufficiency of the EHMT1 gene. Patient-derived cultures showed a decrease in bursting rate with longer mean durations and increased temporal irregularity (Frega et al., 2019). In mouse models with EHMT1 insufficiency the neuronal cultures have similar impairment behaviors due to an increase in NMDA

receptors function. Consequently, they applied pharmacological suppression of NMDA receptors in patient-derived neuronal network observing a recovery of the electrophysiological activity (Frega et al., 2019).This confirms the potential in the joint use of h-iPSC-derived cultures on MEAs to reveal network dysfunctions that are relevant in neurodevelopment and neurodegenerative diseases.

3D in-vitro model for electrophysiological recordings

As anticipated in previous chapters, *in-vitro* cell culture systems have mainly been developed on a planar substrate and therefore do not reproduce different aspects of normal brain development due to the lack of a 3D microenvironment and a 3D brain tissue architecture (Mason and Price, 2016). Hence the need to study *in-vitro* 3D conformations as they would allow a more feasible and truthful study of cell-ECM interactions, cell differentiation, cell-cell connections and properties of the electrophysiological network (Centeno et al., 2018, Jackson and Lu, 2016). In addition, these models mimic the fundamental biological processes related to pathogen invasion and drug treatment observed *in-vivo* (Jackson and Lu, 2016). Several approaches have been developed to create *in-vitro* 3D tissues each with pros and cons to be taken into consideration when designing an experiment. The main methodologies are divided into scaffold-based and scaffold-free

Scaffold-based technique tries to mimic properties of the ECM by using materials allowing cells growth and exchange of nutrients with the external environment (i.e. biopolymers (Lavik et al., 2002) (Lavik et al 2002), agarose (Kunze et al., 2011), collagen (Fan et al., 2017), chitosan hydrogel and gel-like substances (Alizadeh et al., 2019). It has been shown that the use of these materials induces the spontaneous formation of 3D networks with arborizations in the 3D space, improving cellular development and better representing the *in-vivo* condition (Willerth and Sakiyama-Elbert, 2007, Kunze et al., 2011). Although the methods used are very versatile, systematic electrophysiological recordings from these 3D neuronal networks have been presented only in few cases (Fan et al., 2017, Tedesco et al., 2018, Trujillo et al., 2019, Arnaldi et al., 2021, Shin et al., 2021). A disadvantage in the use of biopolymers and gels can be addressed in the relative position of neurons that are randomly sparse in the 3D scaffold making the connection between the cellular processes and the electrodes unlikely (Smith et al., 2015). Alternatively, a new experimental paradigm was proposed the first time in 2008 (Pautot et al., 2008) in which silica microbeads were used as scaffold to support 3D neuronal growth. The innovative idea derives from the possibility of being able to consider the microbeads as single units and lays the foundations for a modular approach to the construction of 3D networks. Taking inspiration from the work of Pautot (Pautot et al., 2008), Frega et al. showed that rodent hippocampal neurons can be plated in 5-8 interconnected layers on MEA using glass microspheres as 3D scaffolds (Frega et al., 2014). Interestingly, the 3D culture of microspheres also increased the

duration and reduced the count of synchronized explosions compared to the 2D culture, indicating greater excitability of the network. More recently, chitosan microbeads have been used as scaffold for 3D rodent neuronal networks (Tedesco et al., 2018) and it has been shown that such networks coupled to MEAs exhibited activities similar to the *in-vivo* situation. Chitosan is a linear cationic polysaccharide derived from the deacetylation of chitin, the major component of the exoskeleton of invertebrates and of cell wall of fungi (Dash et al., 2011). Its biocompatibility, biodegradability, antimicrobial activity and structural similarity with glycosaminoglycans, naturally present in the mammalian ECM, have made chitosan one of the most used biopolymers in tissue engineering (Islam et al., 2020). Recently, it was demonstrated (Di Lisa et al., 2020) that chitosan by itself is also able to sustain primary neuronal cell adhesion and growth, allowing the formation of functional neuronal networks, without the need of pretreating with adhesion molecules, such as synthetic polypeptides. Moreover, chitosan microbeads, obtained by phase-inversion reaction, have been demonstrated to have internal micro-porosities that allow not only the exchange of nutrients but also the growth of neuronal arborizations and mechanical properties similar to the *in-vivo* brain (Tedesco et al., 2018). Furthermore, the use of microbeads as scaffolds allows not only a better control of the structure (i.e. volume of the structure), but can also permit the insertion of functional elements, capable of controlling/regulating cell growth (Custódio et al., 2015, Arnaldi et al., 2020a, Arnaldi et al., 2020b). In summary, hydrogels and other 3D scaffolds enabled the cultivation of human brain models in a controlled 3D environment that also supports MEA recordings of network activity (Soscia et al., 2020, Smith et al., 2017). Furthermore, the intrinsic ability of stem cells to assemble into organized groups of cells within a hydrogel in the presence of suitable exogenous factors has paved the way for self-organizing tissue organoids (Yin et al., 2016).

The scaffold-free methods do not use synthetic materials to support cell growth, but simply rely on the ability of cells to make connections with each other and to self-organize into spheroidal shapes. Numerous studies aim at the realization of 3D neuronal tissues in order to obtain an *in-vitro* model that try to recapitulate the *in-vivo* condition (Langer et al., 1995, Tang et al., 2006). A very popular approach is to generate the so-called brain-organoids, structures derived from stem cells capable of self-organizing into a 3D aggregates that resembles a human embryonic brain (Jo et al., 2016, Lancaster et al., 2013, Mariani et al., 2012, Pasca et al., 2015, Qian et al., 2016a). To date, several protocols are proposed that allow these organoids to be guided into more specialized and representative structures of certain brain regions, such as the cortex, hippocampus and midbrain(Jo et al., 2016, Mariani et al., 2015, Pasca et al., 2015, Sakaguchi et al., 2015, Yoon et al., 2019). Here different approaches are adopted to favor the onset of these 3D structures, from the use of spinner vessel bioreactors (Terrasso et al., 2015, Jing and Jian-Xiong, 2011, Fair et al., 2020), matrices of

round bottom wells and / or non-adherent (Jorfi et al., 2018, Kato-Negishi et al., 2010, Boutin et al., 2018, Mukai et al., 2016), micromolding and/or microfluidics, cell aggregates on adherent substrates (Rybachuk et al., 2019, Lecomte et al., 2020, Izsak et al., 2019), hanging drop (Lee et al., 2012, Tung et al., 2011, Ganguli et al., 2021). Each of these methodologies has disadvantages and advantages depending on the final purpose for which the experiment was designed. For example, the creation of cellular aggregates on a substrate is easy but it is difficult to control the final position and the final volume of the structure. The use of round or non-adherent wells allows to obtain one sample per wells and to be able to generate spheroidal structures in parallel, reducing the variability between sample (Durens et al., 2020). The use of bioreactors or rotating plates allow to create structures that will probably look more like an *in-vivo* situation, thanks to the perfusion of the medium these constructs will tend not to adhere and preserve a 3D structure, however the integration of special tools inside the incubator is not always easy and could lead to problems during the development of the culture. Brain organoids are considered a model for the early and middle stages of embryonic development. Electrophysiological results and calcium imaging analysis revealed that functional neuronal properties and synaptic transmission show a tendency for organoids to mature with age (Qian et al., 2016b); they do not always show spontaneous synchronous network activity, or even activation, but they begin to show these characteristics only after several weeks or months in culture, indicating their progressive maturation (Quadrato et al., 2017, Kathuria et al., 2020a, Fair et al., 2020).We find confirmation in a study on organotypic slices of human fetal cortex in which no action potentials were detected in patch-clamp analyzes until gestational week (GW) 23, where neurons in the deeper layers were found spontaneously active (Zhong et al., 2018). A recent work has analyzed the electrophysiological properties of a cortical organoid to try to draw parallelism with the development of the human brain (Trujillo et al., 2019). They followed the electrophysiological development of this organoid on MEA over the course of 10 months. Cortical organoids showed a consistent increase in electrical activity, with mean spiking rates reaching ~ 17 Hz and burst rates ~ 15 per minute starting to exhibit highly synchronous and stereotyped network activity at 2 months. At 6 months, oscillatory activity showed a cross-frequency coupling between delta and gamma oscillations, a communication signature of the functional neuronal network (Voytek et al., 2015). In order to compare the activity with an *in-vivo* situation, Trujillo et al used an EEG dataset from preterm infants. The authors noted developmental similarities between the two datasets, and a regression model based on preterm infant EEG characteristics was able to predict the developmental trajectory of LFP activity in organoids with a very strong correlation from week 25. The coupling of neural oscillations and the developmental trajectory of electrophysiological activity has provided some of the strongest evidence that these organoids can shape the complex network activity of the developing human brain. Another

work (Mansour et al., 2018) generated organoids derived from hPSC and then grafted them into the mouse brain and recorded the electrophysiological activity via MEA. The results show that the organoids are integrated and vascularized, this is very important as it guarantees their survival. The electrophysiological data revealed an increase in electrically active sites and in the number of active neurons in each site from 50 to 155 days after implantation with evocation of response to environmental stimuli (Mansour et al., 2018). These results indicate that maturation of electrophysiological activity also occurs in grafted organoids, but further analyzes will be required to assess whether the *in-vivo* environment improves functional organoid maturation compared to an *in-vitro* environment. Organoids have also been used to model brain pathologies as well as physiology, but few works have used MEA to track pathological changes derived from electrophysiological activity. Recent work used cortical organoids to test the effects of methadone on neurodevelopment, showing that it causes neuronal growth interruption and a dose-dependent (transient or permanent) reduction in activation in a cortical organoid model of MEA (Yao et al., 2020). Other works have used these structures derived from hPSCs to model bipolar disorder (Kathuria et al., 2020b), schizophrenia (Kathuria et al., 2020a) and alzheimer disease (Ghatak et al., 2020). In these cases, functional analysis using MEA helped to better describe the pathological mechanisms behind these diseases. Although there are some recent studies using organoids and MEAs in the study of brain disorders, they could be applied more widely to model human neuronal network pathology.

While brain organoids have helped solve essential problems, they still have several limitations that need to be overcome. In fact, All these approaches start from the aggregation of stem or progenitor cells, and then induce cell specialization when a 3D architecture has already been achieved. Therefore, the first limitation concerns the vascularization of these structures, in fact they do not have any and the main problem lies in the fact that diffusion allows oxygen and nutrients to penetrate less than 1 mm into the tissue, cell viability in deep parts of 3D models can be a problem and organoids tend to develop a necrotic core (Qian et al., 2019). H-iPSC-derived epithelial cells have been shown to form vessels into brain organoids (Pham et al., 2018, Wörsdörfer et al., 2019, Cakir et al., 2019). The vascularized organoids were not reported to display accumulation of necrotic cells (Pham et al., 2018), supposedly because the medium can reach deep inside the organoid. As we have already explained in the previous paragraphs, a solution would be to cut the organoid to obtain slices and this can have different pros and cons depending on the application. Similar to classic organotypic cultures, the slices can also be maintained on membranes in air – liquid interfaces, which removes the need for repeating the slicing (Giandomenico et al., 2019, Szebényi et al., 2021). The membrane-grown slices can be transferred to MEA where they display firing and synchronized bursts. Another limitation consists in guiding the cellular organization in differentiation. For example, reproducing cortical

structure is otherwise challenging, since while organoids may develop rudimentary architecture and cortical layer markers, they still lack the fine architecture of all six layers of the cortex and the complex interregional neuronal circuits (Qian et al., 2019). Although these protocols can generate different cell types specialized for specific regions, they generally have long timescales and therefore not easy to manage experimentally. Similar to 2D models, slow and low maturation can be a limitation in 3D models and hPSC-derived organoids. For example, stable production of oligodendrocytes with adequate organization of the cortical layer can take more than 100 days (Marton et al., 2019) (Qian et al., 2020). To overcome these problems, new protocols are emerging aimed at producing homogeneous populations in faster times (i.e. stable lines *NgN2* and *Ascl1*) and it has been seen how an adaptation of the dual-SMAD inhibition protocol has produced functional neuronal networks (ie network burst) with oligodendrocytes in less than 60 days (Izsak et al., 2019). Considering that it takes more than 70 days to develop oligodendrocyte precursor cells in the human embryo (Barateiro et al., 2016) and up to 180 days to develop synaptic activity (Zhong et al., 2018), the protocol represents a significant advance in 3D differentiation methods (Izsak et al., 2019).

A further limitation is still the technology for the MEA like devices, as most commercially available systems are designed for 2D cultures and have planar electrodes on a substrate. Several studies have used 3D cultures on planar MEAs (Trujillo et al., 2019, Mayer et al., 2018, Hofrichter et al., 2017, Ylä-Outinen et al., 2010, Smith et al., 2017, Izsak et al., 2019, Monzel et al., 2017, Kathuria et al., 2020a, Muzzi et al., 2021b) but although the approach is valid and can provide insight into the network activity of the culture, it does not take full advantage of having a 3D model as the related data to the electrophysiological activity is sampled only from the planar substrate where the electrodes are present. Some researchers circumvent the problem by slicing their own organoids and plating the slices obtained on the MEAs. Unfortunately, this expedient does not solve the limitation of the 2D as in any case the slice is recorded by means of planar electrodes and most of 3D structure is lost in the slicing procedure. Furthermore, although MEAs that have 3D electrodes are already commercially available, these were specifically designed for the study of brain slices, as the electrodes penetrate into the thickness of the tissue, avoiding the superficial layer of dead or damaged cells. It should be noticed that, in any case, the recording takes place only in a single plane as all the electrodes have the same height (Spanu et al., 2020, Giandomenico et al., 2019, Szebényi et al., 2021). A new approach to simultaneously obtaining the electrical activity of 3D cell cultures from different 2D planes is to use a true 3D MEA (Lam et al., 2021). Since *in-vivo* 2D MEAs have previously been used for organoid registration (Quadrato et al., 2017), it is conceivable that *in-vivo* 3D MEAs (Yao et al., 2006) can also be repurposed for organoids and other *in-vitro* 3D models. The approach could provide comparable data between *in-vivo* and *in-vitro* models, but the *in-vitro* application of MEA *in-vivo*

may require the construction of difficult micromanipulation setups (Quadrato et al., 2017). To our knowledge, Soscia et al. published the first work of a successful registration of human neurons in 3D culture with an *in-vitro* MEA in which the electrodes are dispersed in 3D space rather than in a single 2D plane (Soscia et al., 2020) . Furthermore, in 2021 Shin et al. reported an alternative 3D MEA setup in which the electrode shanks could be lowered into the sample from above using a micromanipulator (Shin et al., 2021).

In summary, organoid models currently do not fully recap the functionality of the adult human brain. However, new technologies, such as vascularization (Pham et al., 2018, Wörsdörfer et al., 2019, Schwartz et al., 2015, Cakir et al., 2019) and various bioengineering methodologies (Trujillo et al., 2019, Mayer et al., 2018, Hofrichter et al., 2017, Ylä-Outinen et al., 2010, Smith et al., 2017, Izsak et al., 2019, Monzel et al., 2017, Kathuria et al., 2020a, Muzzi et al., 2021b) , are undergoing intensive development and it is hoped that, in the future, they will overcome current limitations.

CHAPTER 2

II. 2D ENGINEERED MODEL FROM H-iPSC

After studying the state of the art and learned how to work with h-iPSCs, the first experiments were focused on understanding how to make a protocol for the generation of 2D network suitable for the generation of 3D cultures. Data presented were not published.

Concept and rationale

With the advancements in h-iPSC technology and neuronal differentiation protocols (Ohnuki et al., 2009), investigations on neuronal network properties in health and disease became possible in a model system that more closely resembles the human brain. Nowadays, h-iPSCs derived neuronal networks grown onto MEAs represent a widely accepted model system (Mossink et al., 2021b) (Mossink et al 2021a) with applicability ranging from the study of information transmission (Shew et al., 2011) and biological mechanisms (i.e. plasticity, memory loss) (Accardi et al., 2016), to the characterization of neurological disorders (Russo et al., 2018, Frega et al., 2019, Monteiro et al., 2021) and toxicological screening (Ylä-Outinen et al., 2010). The majority of these models are two-dimensional (2D), with limitations in representing and mimicking the complex features of a region of brain tissue (Duval et al., 2017). The goal of this series of experiments was to optimize the rapid differentiation protocol proposed by Frega et al 2017 (Frega et al., 2017) in order to make it more suitable for the creation of three-dimensional engineered models. The original protocol plates the positive h-iPSCs rtTa / *NgN2* line directly on the MEAs to induce differentiation into excitatory cortical neurons by adding doxycycline. Three days after the start of differentiation, rat cortical astrocytes are added to support the correct development and maturation of the differentiating neurons and to ensure their long-term survival. However, plating the h-iPSCs directly on the MEAs reduces the control on the final cell density as h-iPSCs do not immediately lose their pluripotency and a significant proliferation is noted within the first 3 days of differentiation. The astrocytic support cannot be immediately inserted into the culture and consequently the protocol is not suitable for the generation of 3D constructs.

In this chapter, I show an adaptation of the protocol that allows for greater control over the parameters of the culture, such as cell density and cell ratio. In particular, instead of directly plating the h-iPSCs on the final substrate, I pre-differentiated them into multiwell plates. Once the cells showed first neuronal characteristics and loss of proliferative capacity, we collected and mixed them with different rates of neurons and astrocytes; 1: 0.5 1: 1 and 1: 2. Then, once the cultures were plated, we recorded the spontaneous activity of these at DIV 24-28-30-32-35-42 and we evaluated their development and maturation in relation to the number of astrocytes in culture. The results showed that the modification

to the protocol does not affect the viability of the neurons obtained and that the creation of networks with the same number of excitatory cortical neurons and rat astrocytes favors a maturation in line with the trends reported in the literature.

Material and Methods

h-iPSCs and differentiation protocol

I used an already characterized rtTa/*NgN2* positive h-iPSC line kindly provided by Frega et al (Frega et al., 2017) in frozen vials (Passage 10). Cells were obtained from reprogrammed human fibroblasts from a healthy donor that stable express the transcription factor Neurogenin2 (*NgN2*) thanks to Tetracycline-Controlled Transcriptional Activation. For maintaining the pluripotency, Matrigel (Corning) is used to coat the substrate of the 6 well plate and E8 flex (Thermo Fisher Scientific), supplemented with puromycin and G418, is used as medium. Cells were incubated at 36˚C/5% CO2. Medium was refreshed every 2-3 days and cells were splitted twice per week using ReLeSR (Stem Cell Technologies).
Three days prior to the experiments, h-iPSCs were single cell plated and medium was supplemented with Doxycycline in order to start the differentiation, I will refer to this day as day after differentiation 0 (DAD0) (Figure 2.1). The day after, medium is replaced with DMEM F12. On DAD3, early stage induced neurons (iN) are ready to be detached with Accutase and to be used in experiment.

Rat astrocytes

To obtain astrocytic feeder, brain cortices were collected from E18 Sprague-Dawley rat embryos (Charles River). Briefly, cortices were enzymatically dissociated and single-cell suspension was then plated in T-75 flasks. Cells were propagated once 80% of confluence was reached and frozen after the first passage. More detail can be found (Aprile et al., 2019). Cells were shipped in frozen vials. Astrocytes were thawed and seeded in T-75 flask with DMEM high glucose (Invitrogen, Thermo Fisher Scientific) supplemented with 10% fetal bovine serum (FBS, Sigma Aldrich) and 1% pen/strep. Cells were kept in incubator to grow and proliferate. After 7–10 d, astrocytes reached confluence and were split in two flasks using trypsin-EDTA 0.05% (Thermo Fisher Scientific). Cells were finally maintained in incubator and used in the following 14 d when confluence is reached again.

MEA devices and data acquisition

We used MEA60 from MultiChannel System (MCS) to record the network activity of the different neuronal networks. These devices present 60 electrodes (TiN/SiN, 30 μm electrode diameter, 200 μm spaced) arranged in an 8 × 8 square grid without the four corners. The electrophysiological activity

was acquired with the 2100 System (MEA 2100-System, MCS) and signals were sampled at 10 kHz. One day before cell seeding, MEAs were washed and sterilized in the oven (120 ◦C for 2 h). The day before plating the cells, we coated the electrode area with a solution of DPBS containing 50µg/ml Poly-L-ornithine and 10µg/ml laminin. Devices were then stored at 4°C overnight. During the recording, sterility was maintained using an autoclavable cap on top of the MEA chamber while normal conditions were maintained by pre-heating the head stage at 37 ◦C and by delivering humidified air with 5.5% CO2 over the MEA thanks to a plastic box placed on top of the recording system. Recordings lasted 15 min and data were analyzed offline using MATLAB (The Mathworks) scripts. Raw data were first subjected to high-pass filtering (cutoff frequency = 200 Hz) then to spike detection and finally analyzed as point processes. For each channel, noise was estimated by dividing the whole recording in 60 s bins and the noise with the lowest standard deviation was chosen among the bins.

Neuronal differentiation

We directly induced the differentiation of h-iPSCs into excitatory cortical Layer 2/3 neurons by overexpressing the neuronal determinant Neurogenin 2 (*NgN2*) factor upon doxycycline treatment (Frega et al., 2017). Figure 2.1 *a* summarizes the main steps to create neuronal network on MEA from h-iPSCs. Cells were detached from a well after reaching confluence (6×10^6 cells) using ReleSR (Stem Cell Technologies) and were redistributed equally as single cells in E8F medium with 4 µg ml−1 Doxycycline (Sigma Aldrich) on two wells of a 6-wells plate. We will refer to this step as day after differentiation (DAD) 0 (figure 2.1 a— DAD0). The day after, the medium was entirely replaced with DMEM/F12 (ThermoFisher Scientific) supplemented with 100x N2-supplement (Thermo Fisher Scientific), MEM non-essential amino acid solution 100x (Sigma Aldrich), 10 ng ml−1 human- NT-3 (BioConnect), 10 ng ml−1 human-BDNF (BioConnect), 4 µg ml−1 Doxycycline and 1% pen/strep (figure 2.1 a)—DAD1). Cells will proliferate and reach confluence in both wells therefore, during DAD2 (figure 2.1 a—DAD2) medium needs to be replaced only if cells death/detachment is observed. On DAD3, the medium was changed in Neurobasal (Thermo Fisher Scientific) supplemented with B-27 supplement (Thermo Fisher Scientific), GlutaMAX (Thermo Fisher Scientific), human-BDNF, human- NT-3, 4 µg ml−1 doxycycline and 1% pen/strep. From now on we will refer to this medium composition as ‘complete medium’. At this day (DAD3/DIV0), early stage induced neurons (iN) were detached from the well and were used in combination with rA, previously stored in a flask in the incubator, to create the 2D neuronal networks (figure 2.1 a—DAD3/DIV0). In particular, iN and rA were detached by using Accutase (Sigma Aldrich) and trypsin-EDTA 0.05% respectively and, were collected in two separate 15 ml Falcon tubes (Corning) (figure 2.1 c). We then

proceed in generating three different cells solutions containing neurons and astrocytes in three different ratio, 1:0.5, 1:1, 1:2 and having the same concentration of cells of 800 000 cells ml^{-1} . Consequently, we seeded a 60 µl drop of solution containing 50 000 cells in the active electrodes area of the MEAs to achieve a final cell density of ~2500 cells mm^{-2} (figures 2.1 c–e). After the monolayer deposition, we left the MEAs in the incubator for 3 h to allow cells adhesion. Therefore, 1ml of complete medium was added to avoid evaporation during the night. The next day (DIV1), the entire medium was replaced with complete medium supplemented with Ara-C (2 µM, Sigma Aldrich) (figure 2.1 a—DIV1). MEAs were then stored in the incubator and checked daily. At DIV3, 50% of the remaining medium was removed and new complete medium was added. From this DIV on, half of the medium was changed every two days and from DIV 7, complete medium was supplemented with 2.5% of FBS (figure 2.1 a—DIV7).

Immunofluorescence

Sample were washed with sterile PBS solution and fixed in 4% para-formaldehyde (PFA, Sigma-Aldrich) solution for 15 min at room temperature. Then we used 0.2% of Triton X-100 (Thermo Fisher Scientific) for 10 min to permeabilize the cells and non-specific binding antibodies were blocked by adding to the sample a blocking buffer solution (BBS, composed of 5% normal goat serum (Sigma Aldrich), 1% bovine serum albumin (Sigma Aldrich, 0.2% Triton X-100 in phosphate-buffered saline) for 45 min. Primary antibodies were diluted in BBS and left overnight.

Data analysis

We implemented Precise Time Spike Detection algorithm as detailed (Maccione et al., 2009). Spike were extracted if the peak was five times higher than the noise's standard deviation and the peak-to-peak amplitude was six times the noise's standard deviation, considering 1 ms of Peak Lifetime and refractory period. For the analysis we considered as active electrodes the ones that showed at least 0.1 spikes s−1. For each recording we quantified the array wide firing rate (AWFR) by dividing the recording in 100 ms bin and counting all the spikes detected in each bin, the mean firing rate (MFR) as the sum of all spikes recorded in one electrode divided by the recording time, averaged across only active electrodes. Inter spike interval (ISI) was obtained for each active electrode and calculated in bin of 10 ms for 10 s as probability to have an event after a certain amount of time.

Burst detection algorithm was applied to each channel. We considered burst as a series of at least five spikes in which the ISI among them was not longer than 100 ms. Therefore, we quantified the array wide firing burst and the mean burst rate as we described for the spikes analysis. Inter burst interval (IBI) was obtained as the ISI but considering the time between the end of a burst and the start of the

next one. Burst duration (BD) was obtained by calculating the duration (ms) of each burst. We evaluated the percentage of random spikes (PRS) as the total number of spikes in the culture that does not belong to a burst.

We defined network burst (NB) as synchronous burst activity among channels. We detected a NB whenever we observed bursts in 20% of the active channel with an IBI $\leqslant$ 100 ms (Bologna et al., 2010b).

Statistical analysis

We used rank-sum MATLAB function to perform non parametrical Mann–Whitney U-test since data do not follow a normal distribution. Significance differences were considered when $p < 0.05$.

Results

In Figure 2.1 I show the variation of the protocol that allowed to obtain human neuronal network with different rates of astrocytes. Instead of plating single cell h-iPCS directly on MEA treated with standard adhesion factors, we started the differentiation on multi-well plates coated with Matrigel. During first days in culture there is a notable increase in the number of cells which ends about 3 days after differentiation. Furthermore, at DAD3 the cells still do not show excessively long and interconnected extensions and consequently I choose to detach early stages during this day. In this way we have the possibility of being able to detach neurons and collect them in a solution that can be used in combination with other cell types, or even be cryopreserved for future experiments. The cultures were morphologically healthy, and we proceeded with the analysis of the electrophysiological signal.

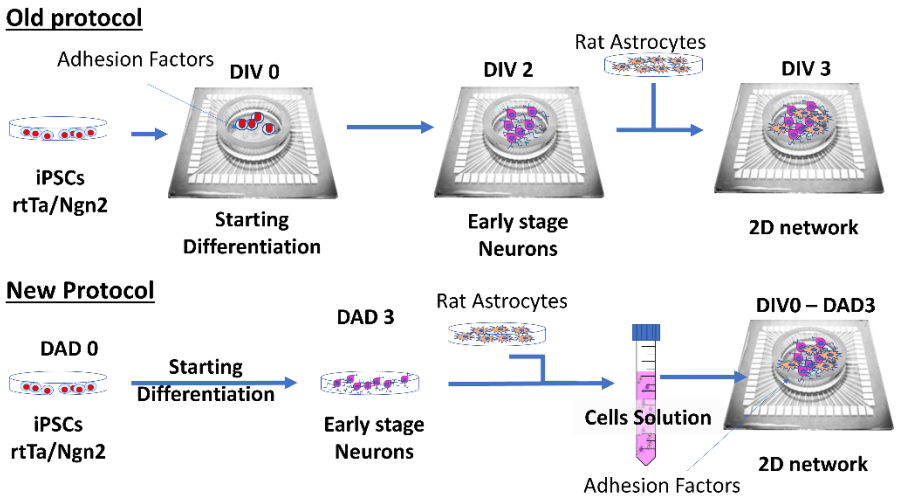

Figure 2.1. Overview of the adaptation of the differentiation protocol. The old protocol directly plate the iPSCs on the final substrate and then the differentiation start. The adapted protocol start the differentiation in well plate and only 3 day after differentiation (DAD) neurons are detached and plated together with astrocytes to the final substrate (i.e. MEA).

In order to evaluate the correct functional development of the neuronal network, we monitored the development of the electrophysiological activity of the cultures over time. In particular, we recorded activity for 20 minutes at DIV24-28-30-32-35-42. In general, the results show that the cultures increase their total spontaneous activity. For all three different cultures rates, the number of active electrodes increases over time in parallel with the single electrode firing properties (Figure 2.2 a-c). Taking into consideration the random percentage of spikes (PRS), it can be seen that all cultures tend to change their activity from a predominantly random (i.e., single spikes) to bursting.

Although all three cultures show similar dynamics, the analysis of the coefficients of variation at DIV 42 shows how the cultures with 1: 1 ratio of neurons to astrocytes exhibit activity with lower variability.

Cultures increase their mean bursting rate (MBR) during development until DIV 32 and after the rate remained almost unchanged except for the 1:0,5 samples (Figure 2.2 c). The mean burst duration (MBD) oscillates around 400 ms for the entire observation period in all 3 conditions (Figure 2.2 d). Although we noted sporadic network bursts in samples at DIV 24 and DIV 28, we have the net occurrence of these events from DIV 30 only in 1: 1 and 1: 0.5 ratio cultures. The cultures that had double the number of astrocytes showed network bursts only from the DIV 35 with events of an average duration of about 1s, greater than the duration detected in the other two experimental conditions (Figure 2.2 g). Parallel to a decrease in PRS we have detected an increase in the percentage bursting channel (PBC) which confirms the tendency of the cultures to exhibit spontaneous activity preferably in the form of a burst (Figure 2.2 h).

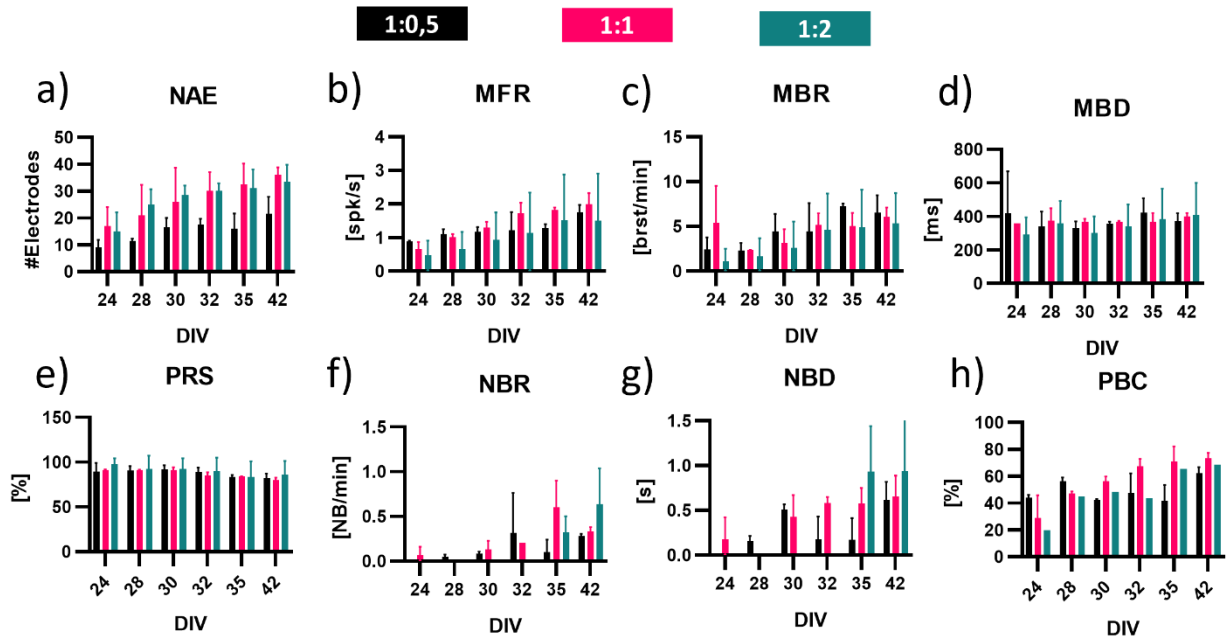

Figure 2.2 Evaluation of the spontaneous electrical activity during development. a) Number of active electrodes (NAE) considered as electrodes with firing rate >0,1 spks/s. b) Mean firing rate (MFR) evaluated as the mean firing rate across active electrodes. c) Mean bursting rate (MBR) evaluated as bursting rate across bursting electrodes (i.e. electrodes with bursting rate > 0,1brst/min). d) Mean burst duration (MBD) evaluated across all the burst in culture. e) Percentual random spikes (PRS) represent the percentage of spikes that are fired and not detected as part of a burst. f) Network burst rate (NBR) show the mean NBR detected within samples and the g) Network burst duration (NBD) represents the mean duration of NB in the cultures. h) Percentual bursting channels (PBC) represent the percentual of bursting channels respect to the active channels averaged across cultures. Bars represent mean across cultures on MEAs (n=2 for each condition) error bars represent standard deviation.

We evaluate the evolution of bursts in cultures by representing each bursting electrode in a plane where the *y* coordinates represent MBD at that electrode and *x* the number of detected bursts. From figure 2.3 *a,b,c* it can be seen how in all three cultures the bursts occupy similar planes in space to similar DIVs, however we can notice a broader spectrum of burst considering the 1:1 culture. This is then confirmed if we consider the Burst duration histogram (BDH) of the cultures at DIV 42 (Figure 2.3 f). The BDH shows the probability of having a burst with a particular duration in a culture, and we can see that in 1:1 culture burst are generated with duration lower than 100 ms while, in the other conditions this was not observed. However, we did not noticed any particular differences in the Inter Spike Interval (ISI) and Inter burst interval (IBI) at DIV42 but, by looking at the evaluation of the coefficient of variation (CV) at DIV 42 we can see that the cultures seeded at 1:2 ratio obtained the biggest variation.

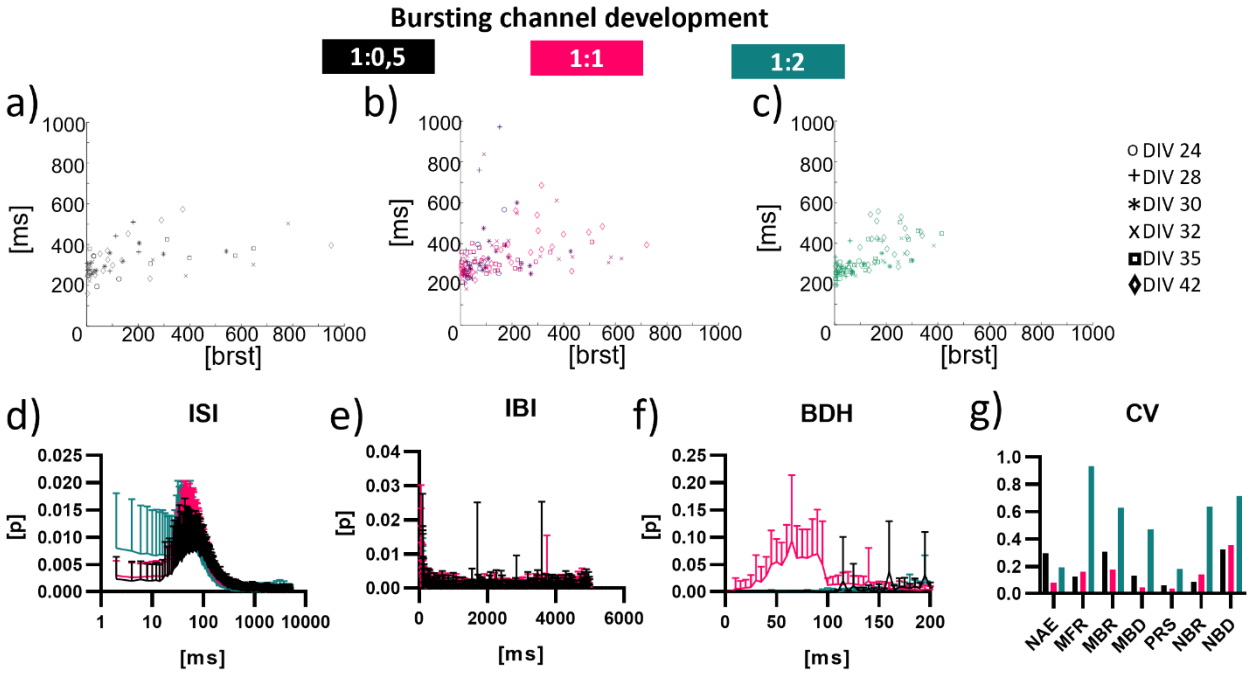

Figure 2.3. a-c) Represent the bursting channel development of a culture (n=1) during the development respectively of **a)** 1:0,5 ratio, **b)** 1:1 ratio, **c)** 1:2. Each point represents an active channel in a precise DIV expressed in the legend. **d)** Inter spike interval (ISI) showing the probability of having a subsequent spike after a certain latency expressed in the x axis. **e)** Inter burst interval (IBI) represent the same probability regard burst evaluated as the ISI. **f)** Burst duration histogram (BDH) represent the probability distribution of burst duration in cultures condition. **g)** Coefficient of Variation (CV) evaluated at DIV 42 of the spontaneous index showed in figure 2.2. Graph **d-g)** are evaluated at DIV42 in which point represent mean and standard deviation is used as error.

Discussion

The modification to the protocol consisted in avoiding the seeding of h-iPSCs on the final substrate. By doing so, we had the opportunity to add astrocytic support (necessary for the long-term survival of neurons) from DIV 0, making the protocol also suitable for the construction of 3D structures. I analyzed the activity of three types of cultures that differ from each other by ratio neuron: astrocytes, in particular I used ratio 1: 0.5, 1: 1 and 1: 2. This type of approach allowed me to verify whether the generated cultures were able to develop in a 'healthy' way despite the changes to the protocol. The results show that all conditions evolve as per the literature, in fact the cultures are spontaneously active since DIV 24 (Frega et al., 2017) with already a good number of active channels. we found a gradual increase in active electrodes in parallel with an increase in firing properties during development. In all 3 conditions we have seen the onset of single-electrode and network-level bursting phenomena, over time finding an organization of activities that prefers firing of burst events over single spikes. It is known from the literature that network burst activity is a typical behavior of the developing brain and plays an important role in establishing appropriate synaptic connections. However, in *in-vitro* systems this dynamic is more marked as the networks lack the natural input-

output pathways of the brain *in-vivo* (Wagenaar et al., 2005a). All the cultures show a rich network burst activity characterized by a sharp increase in the bursting rate. This confirms that despite the adaptation of the protocol, the cultures are healthy and functional throughout the observation period (Chiappalone et al., 2007, Frega et al., 2017). However, the analysis of spontaneous activity also revealed some differences between the different culture ratio, thus suggesting that we were able to obtain an effective control on the density and final ratio of the culture. In particular, we note how 1: 1 cultures tend to be more 'stable'. We can see this from the analysis of the CVs of the different parameters but also from a more linear growth of the firing parameters and without too many jumps. Not only that, but from the BDH (Figure 2.3 f) we see how at DIV 42 the cultures with a 1: 1 ratio are able to produce a wider range of bursts, especially in the 10-100ms range, index of a correct synaptic maturation that is able to generate fast spikes in succession (Wagenaar et al., 2006). Astrocytes play a key role for neurons as they support their growth and ensure their long-term functionality. These results show a relationship between spontaneous activity and the portion of astrocytes supporting the neurons, supporting the idea of having improved the protocol by being able to better manage the number of astrocytes and neurons in culture (Muzzi et al., 2021b).

In conclusion, these first results show that the modification to the differentiation protocol produces healthy and functional networks over time and we manage to have greater control over the final number of cells and the composition of the network (Muzzi et al., 2021b). With these first results I started to become familiar with the world of h-iPSCs derived cell cultures and I used MEAs and neuronal networks to test an innovative adhesion factor. The results are reported in the following chapter.

CHAPTER 3

III. CHITOSAN AS ADHESION FACTOR FOR NEURONAL NETWORKS

All the data and images are adapted from the article *On the Way Back from 3D to 2D: Chitosan Promotes the Adhesion and the Development of Functional Neuronal Networks* currently under revision to *Biomaterials* journal

I this work I directly contributed in generating cultured neuronal network on MEA and coverslips and I recorded and analyzed the electrophysiological data from both rat and human-derived network. All the other results are shown to offer a complete view of the study.

Concept and rationale

Most *in-vitro* functional and morphological studies in the developing nervous system have been performed using traditional monolayer culture developed onto supports modified by extracellular matrix components (laminin, fibronectin, etc.) and synthetic biopolymers (poly-ornithine and poly-lysine), which are expressed at stages critical for neuronal differentiation in situ and are functional in neurite outgrowth *in-vitro* acting as adhesion proteins.

In this study, we present Chitosan (CHI) as an alternative adhesion material. The role of cell-to-substratum adhesion in the initiation, elongation and branching of neuritic processes, synaptogenesis and electrophysiological behavior was investigated. Cells from embryonic Sprague-Dawley rats and neurons differentiated from h-iPSCs (iNeurons) were cultured on chitosan and poly-ornithine-coated surfaces. This study analyzes development of both cell populations, focusing specifically on early developmental stages through 72 hr after cell seeding. The number of neurites, the growth of major/minor processes and the growth rate were similar on both substrates for both cell populations. Chitosan and the traditional adhesion factors (poly-ornithine e laminin) affect neurites outgrowth in manner dependent on the culture time; in particular, chitosan promotes neuronal polarity in both cell cultures. These results indicate that, chitosan could be considered as a valid alternative adhesion factor.

Materials and Method

Culture supports bioactivation

Poly-L-ornithine (PLO, P4957), laminin (LAM, L2020, from Engelbreth-Holm-Swarm murine sarcoma basement membrane), ethanol and acetic acid were purchased from Sigma-Aldrich. Chitosan (low molecular weight, High DDA 88.3%, B-85-471692, from chionoecetes opilio - Snow Crab) was purchased from Chitolytyc.

Chitosan solutions were prepared at concentrations of 0.1, 1% w/v in 0.1M acetic acid. PLO and LAM were used at a concentration of 50 μg/ml and 10 μg/ml in ddH_2O respectively. Culture supports were bioactivated by chitosan solution casting; traditional adhesion factors were used as a control: PLO/LAM. Solution of 1% CHI was autoclaved at 120 °C for 20 min before usage.

For the morphological characterization, CHI, and PLO/LAM solutions were pipetted onto the culture supports (Ø18mm coverslip and Ø35mm petri dishes), following the standard protocol (Dotti et al., 1988) and incubated overnight at 37°C. The excess of adhesion solutions was removed, supports were then washed twice with sterile ddH_2O and finally normalized in cell culture medium. For the induced neurons (iNeurons), after PLO deposition, LAM solution was pipetted on the supports and incubated for 2 hours at 37 °C.

Cell plating

Low density cultures were prepared for adhesion assay, plating efficiency and neurite outgrowth. Specifically, cells were plated at cell density of 28-30 cells/mm^2 in the presence of astrocyte conditioned medium. Neurons were plated on coverslips and incubated in Minimum Essential Medium (MEM; Invitrogen) supplemented with 10% Fetal Bovine Serum (FBS, Sigma-Aldrich).

h-iPSCs derived neurons culture

h-iPSCs were generated by lentiviral transduction from fibroblast taken from a healthy donor. Therefore, cell line was edited using two lentivirus to confer overexpression of the transcription factor Neurogenin 2 (*NgN2*) upon tetracycline reverse transcriptional activator (rtTa). Cell were kindly provided by Frega et all., 2017 and were received in frozen vials. Full protocol regarding generation and maintaince of the rtTa/*NgN2* positive cell line can be found in (Frega et al., 2017). Differentiation into neuron started by supplementing 4ug/ml Doxycycline (Sigma Aldrich) into the medium, defining the step as Day After Differentiation 0 (DAD 0). In detail, a confluent well of h-iPSCs were detached using ReLeSR and cells were seeded single cells in two 6-well pre coated with Matrigel solution (Corning, 1:30 in cold DMEM). Cells were cultured using Essential 8 Flex Medium (Thermo Fisher

Scientific) supplemented with 1% pen/strep, 50ug/ml G418, 0.5 ug/ml puromycin and 4ug/ml Doxycycline. On DAD 1, medium was changed using DMEM/F12 (Gibco) supplemented with N2-supplement 100x (dilution 1:100, Thermo Fisher, Invitrogen), MEM non-essential amino acid solution 100x (Gibco), 1% pen/strep, 10ug/ml human BDNF (Bio-Connect), 10ug/ml human NT-3 (BioConnect) and 4ug/ml doxycycline. At DAD 3, cells will stop to proliferate, and they can be considered as an early stage of neurons, suitable for experiments. Therefore, neurons were detached using 1ml Accutase per well and collected in a 15ml tube with Neurobasal medium (Thermo Fisher Scientific) supplemented with 1% pen/strep, B-27 (dilution 1:50, Thermo Fisher Scientific), Glutamax (dilution 1:100, Thermo Fisher Scientific), 10ug/ml human BDNF, 10ug/ml human NT-3 and 4ug/ml doxycycline (we will refer to this supplemented medium as Neurobasal-iN). After centrifugation (1200 rpm, 5 min), supernatant was discarded, and cells were resuspended in 2ml Neurobasal-iN. Neurons are now ready to be counted and used in co-culture with astrocytes in a 1:1 ratio.

Astrocytes cultures

Frozen cortical rat Astrocytes (rA) were received in frozen vials. Cortices were isolated from dissection of E18 rat, and non-astrocytic cells were removed thanks to 6h of orbital shaking after plating. More detail can be found in (Aprile et al., 2019). Cells were then frozen when confluence was reached in T-75 flasks. After rapid thawing, astrocytes were seeded in T-75 flask with DMEM High Glucose supplemented with 10% FBS and 1% pen/strep. Flasks were left in the incubator at 37°C at 5% CO2 and the medium was refreshed every 3 days for 7-10 days. Astrocytes needs to be passaged at least one time before using them in co-culture with neurons and the day of plating the need to be confluent. The plating day, astrocytes were mixed with iN (1:1) in Neurobasal-iN.

Morphometry and statistical evaluation

Only cells without contact with other cells were evaluated in according to a classification table suggested by Dotti et al. (Dotti et al., 1988). Cell stages as stage 1, a cell without neurites; stage 2, a cell with some neurites that are not labeled by axonal markers, suggesting no axonal differentiation at this stage; stage 3, a cell with an axon; stage 4, growth of dendrites and stage 5, mature cell. Different parameters were extracted: the number of neurites per cell, the total neurite length per cell, the length of major neurites per cell, the total length of all minor neurites per cell, and neuronal spreading. Neurites were defined as a process extending more than 10µm from the neuronal soma and with a length of at least one cell body diameter. Major neurites were defined as those neurites with the highest length after the computerized measurement of all neurites of a cell, specifically that

were at least 10-20 µm longer than any other neurite of the cell. An axon was defined as a neurite labeled by axonal markers, such antitau-1antibody or Ankirin-G. The polarity index was defined as the average length of major neurites divided by the average length of all minor neurites per cell. ImageJ and NeuronJ were used to analyze, trace and measure the neuritic processes.

In each experiment, an inverted IX-51 Olympus microscope equipped with a DP70 digital camera coupled with CPlan 10 N.A. 0.25 PhC objective was used to acquire contrast phase images. For each condition, 25 cells were acquired and analyzed for the morphometric study. ImageJ with NeuronJ plugin have been used to analyze, trace and measure neuritic processes. All graphs comprise data derived from three experiments. The significance of differences between experimental and control values were analyzed by statistical methods. Statistical analysis was performed using the non-parametric Mann-Whitney U test, and statistical differences were defined as $p < 0.05$ (*) and $p < 0.01$ (**).

Immunocytochemistry:

Cells were fixed with 4% paraformaldehyde in phosphate buffer solution (PBS), pH 7.4 for 30 min at room temperature. Permeabilization was achieved with PBS containing 0.5% Triton-X100 for 15 min at room temperature and non-specific binding of antibodies was blocked with an incubation of 45 min in a blocking buffer solution consisted of PBS, 0.3% BSA (bovine serum albumin, Sigma) and 0.5% FBS. Cultures were incubated with primary antibody diluted in PBS Blocking buffer for 2 hours at room temperature or incubated at 4°C overnight in a humidified atmosphere. Cultures were rinsed three times with PBS and finally exposed to the secondary antibodies. Differentiation is the establishment of the two distinct classes of neuronal processes, axons and dendrites. MAP-2 (1:500, dendritic microtubule-associated protein), TAU 2 (1:200, axon microtubule-associated protein), Akirin G (1:200, axon initial segment) and Dapi (1:10000, nuclei) were used to study their localization during early stages of axonal and dendritic development. To verify the presence of glial cells in the culture, we fixed and exposed to the marker GFAP (1:1000, glial fibrillary acidic protein). Cultures were finally exposed to the secondary antibodies: Alexa Fluor 488 and Alexa Fluor 549 Goat anti mouse or Goat anti rabbit, diluted 1:700 and 1:1000 (Invitrogen Life Technologies S. Donato Milanese). An Olympus BX-51 upright microscope was used for immunofluorescence evaluation of the biological samples and the image acquisition was done with a Hamamatsu Orca ER II digital cooled CCD camera driven by Image ProPlus software (Media Cybernetic).

MEA recording and analysis:

Standard MEA-60 (MultiChannel System) were used to record the electrophysiological activity of neuronal network. Devices were composed of 60 planar microelectrodes (TiN/SiN, 30 μm electrode diameter, 200 μm spaced) arranged over an 8 x 8 square grid (except the corners). Electrophysiological activity was recorded at different stages during development (DIV 21-28-35-42) and signal was acquired with the 2100 System (MEA 2100-System, MCS) sampled at 10kHz. A constant slow flow of humidified gas (air supplemented 5.5% CO2) was constantly delivered on the cultures and temperature was maintained at 37°C during recording to maintain incubator-like conditions.

Data and Statistical analysis:

Data analysis was carried using custom Matlab script. Precise timing spike detection (PTSD) was implemented (Maccione et al., 2009) and used with a threshold set to 6 times the standard deviation of the noise evaluated from each channel. To characterize the electrophysiological activity, we extracted some first order statistics. In particular, mean firing rate (MFR), (i.e., number of spikes per second of each channel) was evaluated and only active electrodes (MFR>0,1 spks/s) were considered into the analysis. Burst detection analysis was performed, defining a burst as a series of minimum 3 spikes that were fired no more than 50ms apart. Therefore, we defined the mean bursting rate (MBR), as the number of burst fired per minute in a channel,and the mean bursting duration (MBD), as the mean duration of burst for each channel.. Network bursts (NB) were defined as synchrounous bursting activation among different channels. Therefore, similar to the Burst detection, we defined a NB whenever we detect a series of burst fired from at least 25% of the active electrodes and spaced no more than 100ms. We then evaluated the Percentual of Random Spikes (PRS) as the number of spikes not fired in a burst divided by the total number of detected spikes, defining the percentual of spikes that are singularly fired. Statistical analysis was performed using the non-parametric Mann-Whitney U test, and statistical differences were defined as $p < 0.05$ (*).

Results

Choice of chitosan source

In order to validate the best chitosan for our experiments, we tested different chitosans obtained from different sources listed in table 1. In fact, depending on the purification process, chitosan has different degrees of deacetylation, which has been seen to be an important parameter that affects on cell adhesion.

index	Source	DD
1	Crab	91.5%
2	Crab	88.3%
3	Mushroom	90.1%
4	Mushroom	98.0%
5	Lactate(acetic-acid)	/
6	Lactate(Water)	/

Table 3.1. List of chitosan source and their deacetylation degree (DD) tested on iNeurons

So for each type of chitosan we tested two different concentrations, 0.1% and 1% w / v.. Figure 3.1 shows the appearance of the cultures on the different CHI after 4 days in culture.

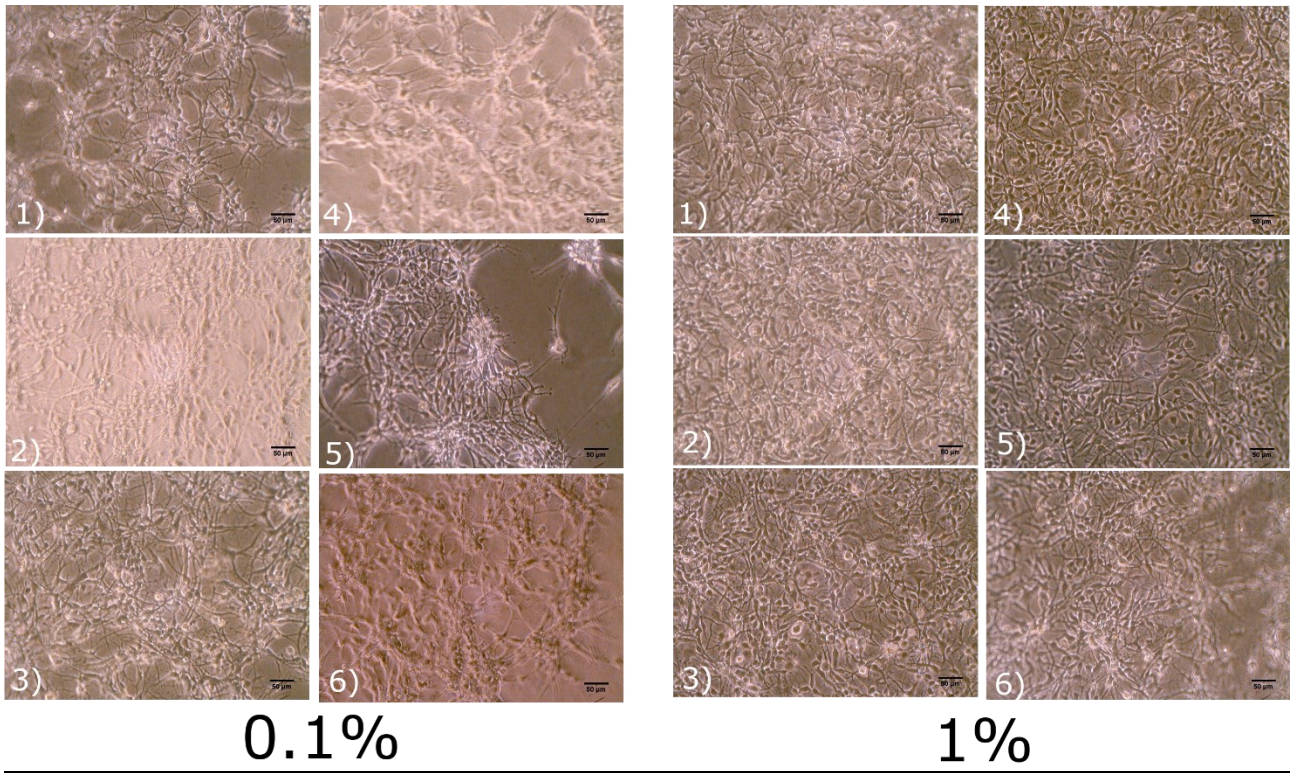

Figure 3.1 Comparison between cultures treated with different types of chitosan. Number in each corner represent the type of chitosan used as stated in Table1. Images were acquired at DIV7 with a 20x magnification. Scale bar indicates 50um.

As it is possible to observe from the images in Figure 3.1, all CHIs at lower concentration led to the formation of holes in the cultures and the detachment of some parts of it. On the other hand, at a concentration of 1%, we obtained more homogeneous and healthy cultures. After that, all the experiments were carried out using crab-derived chitosan because, although the degree of deacetylation was lower, it achieved excellent results at both concentrations tested.

Morphological characterization of 2D cultures

Individual cells in low-density cultures were selected and observed at 4, 24, 48 and 72 hours after cell seeding onto chitosan and standard coatings. The cell number was quantified at each selected time to observe the initial culture maturation. To investigate the polar growth (asymmetric growth of axonal versus dendritic compartments) the longest neurite (major neurite) was measured for each a given cell. iNeurons were cultured onto both chitosan and standard coatings in order to evaluate and compare the following main parameters: number of neurites per cell, average neurites length per cell, length of major neurite, total length of minor neurites per cells, at different maturation times (Figure 3.2 b). The number of neurites per cell increased during the whole culture period; at 4h after cell seeding, most cells were in stage 1 of Banker model and this behavior was observed to be similar between chitosan and standard coatings (Figure 3.2 a).

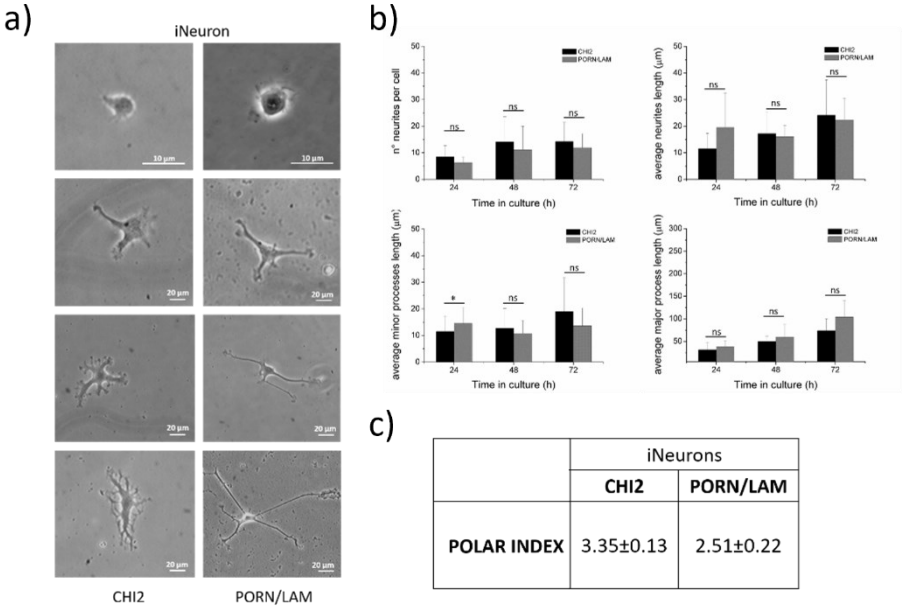

	iNeurons	
	CHI2	**PORN/LAM**
POLAR INDEX	3.35±0.13	2.51±0.22

Figure 3.2 Stages of neuronal development: optical images of **a)** iNeurons at 4, 24, 48, 72 hours on CHI, and PLO/LAM coatings. Coating influence on number of neurites and neurites lengths of **b)** iNeurons over time, * $p < 0.05$, ** $p < 0.01$. **c)** Table of polarity index obtained by dividing the length of major neurite by the total length of all minor neurites per cell.

On both coatings, the number of neurites increased steadily until 24h. In particular, the number of neurites increased during time in culture, showing lower values on PLO/LAM than on CHI coating (Figure 3.2 c). These results indicate that chitosan, and PLO/LAM coatings affected neurite outgrowth in a manner dependent on the culture time. No differences were observed in average length of neurites on chitosan or standard coatings. The neurite average length increasing was observed for both chitosan and standard coatings. At 24h, neurite average length on CHI was lower than the control (CHI: 11.55 ± 5.58 µm and PLO/LAM: 19.48 ± 12.92µm). At 48 h, the neurite average length was around 17.27 ± 8.05 µm on CHI and around 16.12 ± 4.21 µm on PLO/LAM coatings. At 72h, cells

seeded on CHI coating developed neuritic processes with a length around 24.19 ± 13.24 μm, similar to neurites developed on PLO/LAM coating, with an average length around 22.36 ± 5.04 μm. iNeurons, seeded on CHI coating, developed minor neuritic processes with an average length that increased over time, showing higher values than the control. Moreover, on PLO/LAM coating, a decrease from 14.54 ± 5.92 μm to 10.73 ±4.91 μm was observed between 24 and 48 h in culture. The major process on CHI coating showed an average length lower than PLO/LAM coating. After 24h, the major process showed a length around 31.23 ± 15.56 μm on CHI coating and 38.41 ± 12.92 on control; at 48h, on CHI coating the average length was around 49.61 ± 12.13 μm while on PLO/LAM coating it was 59.66 ± 28.94 μm. Finally, at 72 h, the major neurites adhered on control and CHI coatings reached an average length around 103.17 ± 36.8 μm and 73.87 ± 26.1 μm, respectively. Thus, CHI favored the growth of minor neurites over the growth of major neurites. On both chitosan and control coatings, sometimes it wasn't observed an axon clearly longer than other neurites. From the collected results, it is possible to affirm that CHI, compared to standard PLO adhesion factor, induced a temporary decrease of the total neurite lengths, favoring the growth of major neurites over the growth of minor neurites, and therefore promoting neuronal polarity at later stages of neuritogenesis. These results were already observed for other extracellular matrix components (tenascin, laminin, fibronectin, cell adhesion molecule Ll, lectin concanavalin A (ConA)), where the decrease in total neurite length was due to an arrest of growth of minor neurites, but major neurites grew faster than on PLO used as control (Lochter and Schachner, 1993).

Finally, the polarity index was calculated (Figure 3.2. c). After 24 h of culture, the polarity index was about 3.35 μm/h on CHI coatings and about 2.51 μm/h on control. The results indicated that CHI and PLO/LAM coatings promoted similar neurite outgrowth and neuronal polarization.

Moreover, in order to confirm the obtained, neuronal polarization was investigated by immunofluorescence. Polarization occurs when the two classes of neuronal processes, axons and dendrites, can be clearly distinct. Microtubule-associated proteins (MAPs) might be considered prime candidates to regulate the spatial control of microtubule function during neuronal development. To identify the major neurites as axons and the minor neurites as dendrites, the proteins MAP-2 and TAU were used. Before neuronal polarization, MAP-2 and TAU are not differentially distributed, and both of them are present in the axonal and in the minor processes. In mature neurons, MAP-2 is preferentially localized in dendrites, whereas TAU is preferentially localized in axons. Therefore, cultures were stained for MAP-2 and TAU to study their localization during early stages of axonal and dendritic development. After 24 hours *in-vitro* and iNeurons were labeled for MAP-2 and Ankirin G to localize the axon initial segment. Figure 3.3 shows neuron development onto CHI and PLO/LAM coatings, in according with Banker's. Despite the double staining, during the first stages in culture

(4-24 h), processes were still immature, and it was difficult to differentiate neuritic processes between axons or dendrites, due to the overlap of the markers. At 72 h, axons and dendrites were well-differentiated, and the distribution of MAP-2 and TAU was found to be quite different. Finally, after 3 days *in-vitro* in culture, it can be observed that neurons, grown on both CHI and PLO coatings, showed distinct major and minor processes, with major processes longer than 80 µm, consistent with the data provided by Banker.

a)

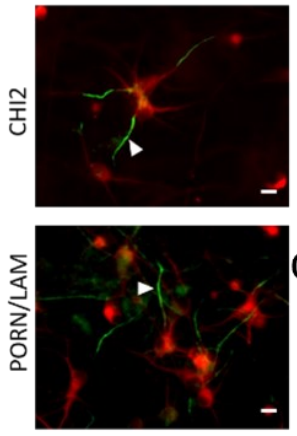

b)

iNeurons	[24÷48 h]	[48÷72 h]
CHI2	0.76 µm/h	1.24 µm/h
PORN-LAM	1.02 µm/h	1,77 µm/h

c)

iNeurons	[24÷ 48 h]	[48÷72 h]
CHI2	0.18 µm/h	0.22 µm/h
PORN-LAM	-0.22 µm/h	0.14 µm/h

Figure 3.3. **a)** iNeurons developed on CHI2 and PLO/LAM coatings, stained for AnkG (green) and TAU (red) at 72 h *in-vitro*. Scale bar: 10 µm. Table of average growth rate of major **b)** and minor **c)** neuritic processes of iNeurons expressed in µm/h.

For iNeurons, the average growth rate of major processes extended on CHI coating is slightly lower than on PLO/LAM coating, during the different development stages. Between 24-48 h, the average growth rate of minor processes was higher on CHI2 than on standard coatings, where it was possible to observe a retraction (-0,22 µm/h). Between 48-72 h, CHI2 induced a faster elongation than PLO/LAM coating.

These results suggest that no increase of growth rate was observed on both type of coatings, and axonal growth resulted slower on CHI2 than on PLO/LAM coatings.

Further characterizations by immunofluorescence techniques were carried out to compare iNeurons co-cultured with astrocyte glial fraction, grown on both chitosan and traditional coatings. To this purpose, cell cultures were fixed with 4% PFA at 21 DIVs and labeled by using MAP-2 as specific cytoskeletal component for neurons, and the glial fibrillary acidic protein GFAP as specific cytoskeletal component for astrocytes (Figure 3.4).

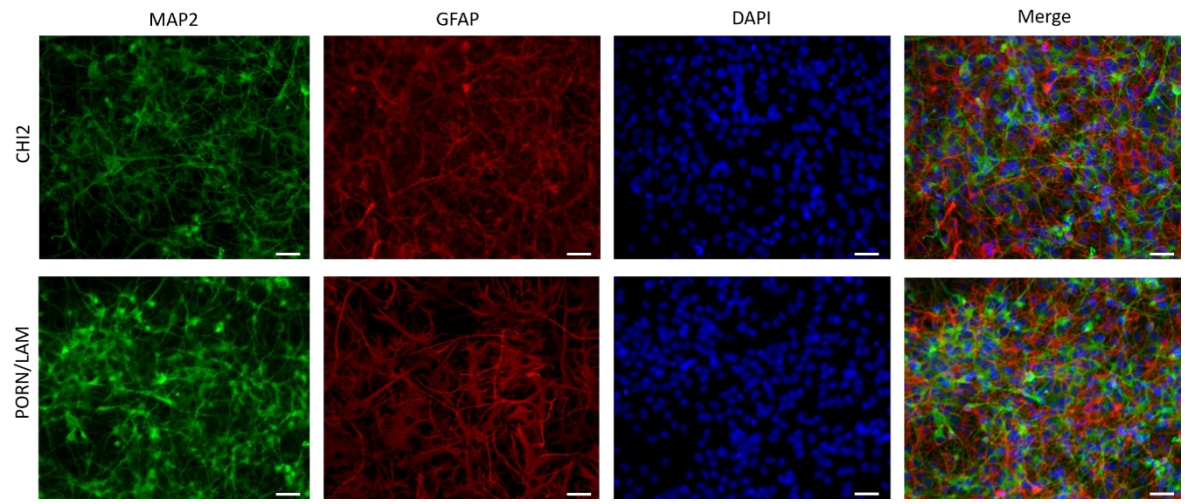

Figure 3.4. Optical images of 2D neuronal cultures stained for MAP-2 (green), GFAP (red) and DAPI (blue) at DIV 21: iNeuronal culture onto CHI2 and PLO/LAM coatings. Scale bar: 20 µm.

Cells showed a homogeneous distribution and the formation of a dense network. Neuronal morphologies revealed no differences between chitosan and traditional coatings.

Meanwhile, glial cells present a remarkably different morphology depending on the coating. In fact, on traditional adhesion coatings, PLO/LAM (Figure 3.4), GFAP positive cells were found as a flat monolayer. On the contrary, glial cells grown on chitosan coatings exhibit a thin morphology and numerous processes extended in a non-directed manner. Moreover, a further difference was observed: on CHI coating, MAP-2 positive cells were located predominantly on the top of the glial monolayer, while on PLO/LAM coatings, neuronal cells were mixed and immersed in the glial ones (Figure 3.4). In addition, the detection of structurally intact synapses was carried out by VGLUT and PSD95 immunostaining (Figure 3.5 a). The colocalization of VGLUT and PSD95-positive puncta (yellow dots) indicates that a synapse was formed (Pyka et al., 2011). Generally, the overall expression of synaptic puncta increased with time in all experiments, reflecting a progressive and adequate maturation of the cultures. As first step, the emergence of synaptic puncta over time was monitored roughly, to identify an appropriate time point for further analysis. During the first week of culture, synapse development was almost absent everywhere. Then, an increase in the number of co-localizations and robust synaptogenesis were observed after 14 days on both coatings, passing from about 0,10 to 0,5 synapse/10 µm (Figure 3.4 b) and increasing again at DIV21. We did not find significance difference between standard and chitosan coatings.

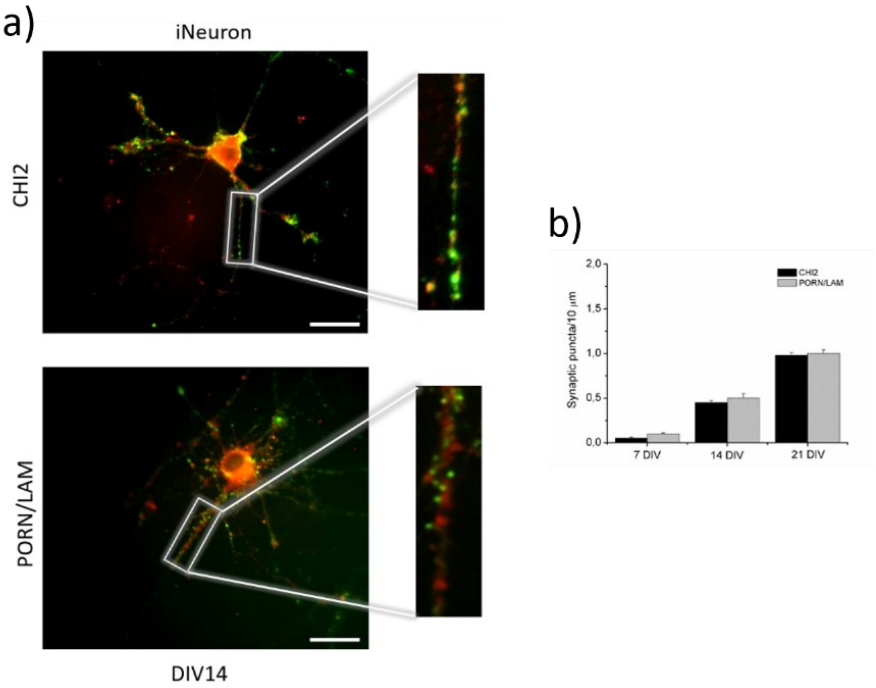

Figure 3.5 Optical images of **a)** iNeurons 2D cultures, stained for VGLUT1 (green) and PSD-95 (red), at DIV 14, scale bar: 20 µm. **b)** Quantification of synaptic puncta in iNeurons at DIV 7, 14 and 21.

Functional characterization of 2D networks

To evaluate functionality of the networks, MEA60 were used as substrate for neuronal culture. N= 7 MEA were coated with chitosan solution and n=7 MEA were coated with PLO/LAM solution. Consequently, we generated neuronal networks using separately iNeurons and primary neurons from rodent. We used 10 MEAs for cultures with iNeurons (N = 5 for each type of coating) and 4 MEAs for primary cultures (N = 2 for each type of coating). A culture with iNeurons on MEA treated with PLO / LAM detached after 10 days in culture. We recorded cultures with iNeurons at regular one-week time intervals starting from DIV21 through DIV42. Figure 3.7 shows 4 samples during the last registration. From the rasterplots of the cultures with iNeurons (Figure 3.7. a,b) the general activation phases of the network (Network Burst) can be observed very well from the darker vertical bands that arise in the graph. In primary cultures, this feature cannot be appreciated given the high frequency of these events. We therefore wanted to show 3 seconds of raw activity taken from an active electrode during a NB in these cultures (Figure 3.6 c-h). While it does not appear to be any major difference with respect to iNeurons cultures, you may notice a small difference in the signals of rodent crulture which appear to have more irregular bursting activity when laid on

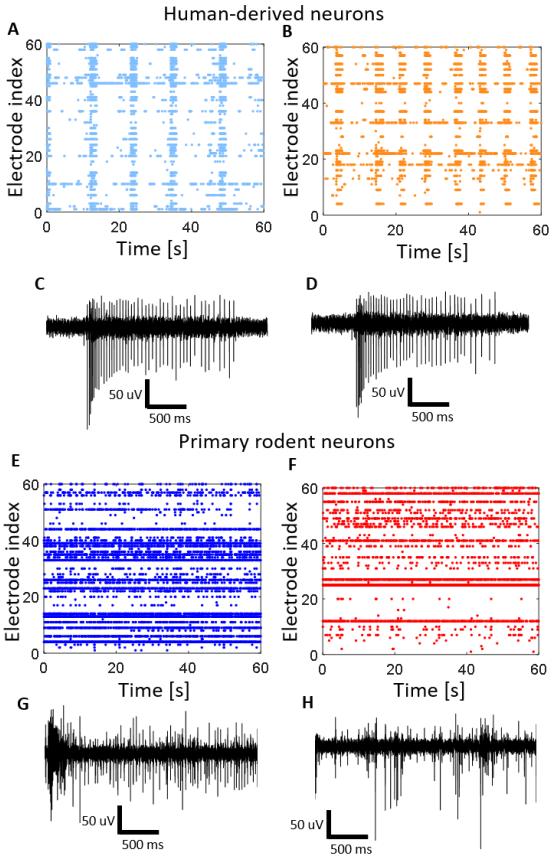

Figure 3.6. Qualitative analysis of the electrophysiological activity of cultured neural network at DIV 42 **(A-D)** and at DIV 26 **(E-H)**. **A,B,E,F)** Rasterplots showing 1 minute of spontaneous activity. Each colored dot represents a detected spikes at the given electrode. **C,D,G,H)** Raw signals extracted from an active electrode, showing 3 seconds of spontaneous activity.

Electrophysiological analysis shows how cultures increase their total activity over time and how this changes in a more mature network dynamic. During the first 21 days the activity is predominantly random, in fact about 85% of the spikes do not belong to bursts (Figure 3.6 f). The single electrode average properties slowly increase over the time with the increase of the active electrodes (Figure 3.6 a-b-c-d). At the network level, the network bursts are already present since DIV21 even if not in all the samples, and increase in frequency with the progress of the cultures (Figure 3.6 e). Comparing the mean values derived from the two different experimental conditions, no significant differences are observed, except for the number of active electrodes which, from DIV 28, is significantly higher in the cultures adhered to CHI (Figure 3.6 a).

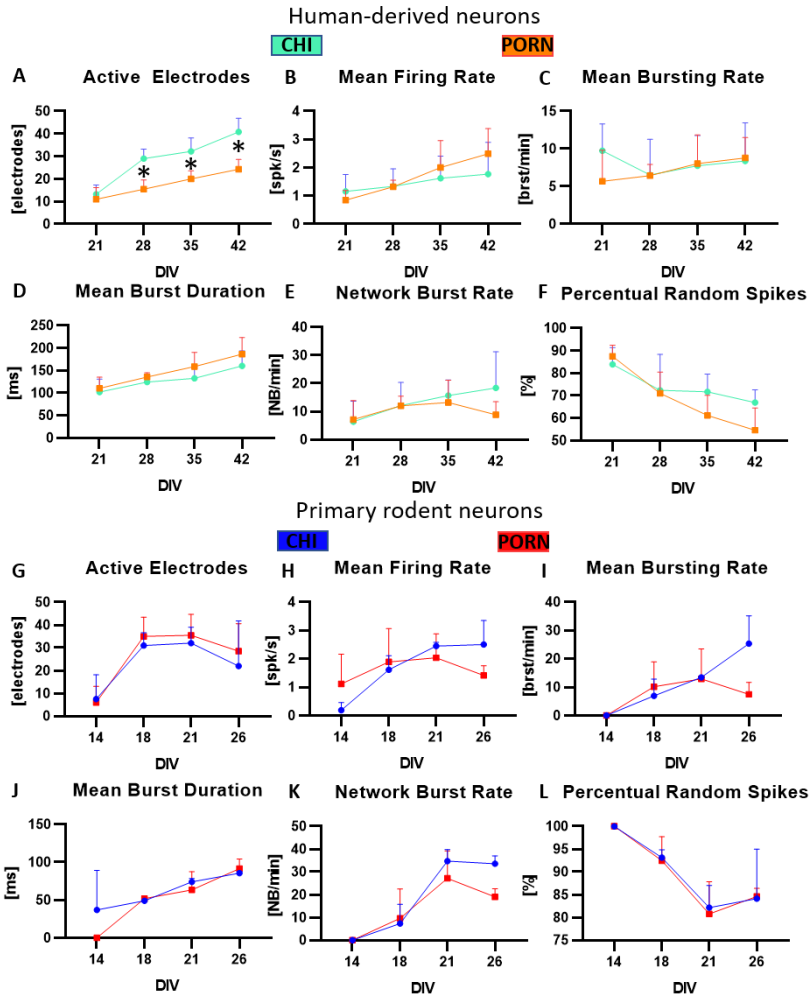

Figure 3.7 Functional evaluation of neuronal network obtained from **A-F)** iNeurons and **G-K)** rodent on CHI and PLO/LAM coatings at different Days *In-vitro* (DIV) during development. We quantified the **A,G)** number of active electrodes, **B,H)** mean firing rate, **C,I)** mean bursting rate, **D,J)** mean burst duration, **E,K)** network burst rate, **F,L)** Percentual of random spikes. Points and errors bars represent respectively mean and standard error. Asterisk indicate significance difference with $p<0.05$

However, we do not find the same significant difference in primary rat cultures, where the active electrodes are almost identical in the two coating conditions. Comparing the activity of primary cultures between the different coatings used, no significant differences can be seen in any of the parameters we took into consideration. Cultures tend to organize their network activity in bursts, going from 100% PRS to about 85% at DIV26. Unlike iNeurons cultures, the firing properties appear to reach a plateau phase towards DIV21 (Figure 3.6 g-l). This is significant of the shorter life span of primary culture and also indicates a difference in age and therefore in the maturation of network activity. Although there are no significant differences, it is clear from the graphs that the cells on CHI develop higher firings and above all, they seem to stabilize, even in the long term on rodents. From figure 3.6 h,i,k) it can be seen how at DIV26 the culture on CHI tends to have a higher activity to that recorded at DIV21, suggesting a longer conservation of the network on the MEA device.

Discussion

In this work, chitosan has been introduced as an alternative adhesion factor used to support neuronal cultures. The standard methods for the functionalization of supports used for 2D neuronal cultures are based on the use of poly-lysine and PLO, which generally have a high cost compare to CHI (Younes and Rinaudo, 2015). These macromolecules containing amino groups, are frequently used as coating materials for *in-vitro* neuronal cultures: the electrostatic attraction between the positive charges of the NR3+ amino groups and the negatively charged neuronal membranes was suggested as an indispensable factor for stable neuronal adhesion and proper network development (Tedesco et al., 2018, Muzzi et al., 2021a, Arnaldi et al., 2021, Younes and Rinaudo, 2015, Mu et al., 2019). Chitosan can behave as a poly-cation under acidic conditions (pH<6), due to the protonation of the free amino groups along its chains, similarly to the abovementioned standard macromolecules.

In synthesis, morphological features during the early developmental stages of both rat neurons and iNeurons, were similar between chitosan and the traditional adhesion factors tested in this work (PLO/LAM). During rat neurons development, chitosan favored the growth of major neurites over the growth of minor neurites and therefore increased neuronal polarity at later stages of neuritogenesis. These results were similar to data provided by Banker (Dotti et al., 1988). As regards iNeurons, it was difficult to observe a complete maturation during the early developmental stages comparing to rat neurons, because as it was observed already in literature, these cells require a longer time to mature (Ohara et al., 2015). Nevertheless, the morphological studies indicated that CHI coatings favored the growth of minor neurites over the growth of major neurites, suggesting that axonal differentiation of iNeurons occurs at slower rate, as it was observed on the control coatings (Ohara et al., 2015). These assumptions are reinforced by the functional analysis of the electrophysiological signal. In fact, there are no significant differences in the development activity of cultures with iNeurons apart from the high number of active electrodes. The same is true for rat cultures, in which, however, there is a tendency of the parameters to arrive at a plateau phase. We can certainly conclude that chitosan can be used as a valid adhesion factor for neuronal cultures and we can speculate that it promotes better cell development *in-vitro* given the significant number of extra active electrodes in iNeurons cultures and the tendency to have more stable firings. over time in primary cultures.

To our knowledge, this is the first work reporting the ability of pure chitosan to support both primary and h-iPSC neuronal cells attachment and functional neuronal network development. This represents a valuable contribution in the search for low-cost biomimetic culture systems, which can have important applications in neuropharmacology, toxicology, and regenerative medicine. Finally, as mentioned before, chitosan can be easily shaped both in 2D and 3D form.

The use of the same biomaterial as main component of 2D and 3D models offers the possibility to overcome possible chemical or physical artifacts when comparing the behavior of cells grown in both different dimensional *in-vitro* models.

Conclusion

In this chapter we have shown that by adapting the differentiation protocol to allow the generation of 3D neuronal network we were able to obtain healthy and functional 2D cultures.. We have also been able to achieve greater versatility as it is now possible to generate cultures by plating neurons and astrocytes togheter in specific rat defined a priori by the user. The study of the electrophysiological activity related to cultures that have been designed with different numbers of cultured astrocytes showed differences that suggest the use of 1: 1 ratio cultures for *in-vitro* models. Consequently, we used these cultures to test an innovative adhesion factor. From the analysis of immunofluorescent images and through the tracing of axonal differentiation it was seen that the neurons are healthy and the results are comparable with neurons grown on coatings considered standard. the electrophysiological properties of the network evolve as per the literature confirming that CHI can be successfully used as coating for *in-vitro* neuronal network.

As a consequence of these results we have started to test different methodologies to produce 3D neuronal networks on MEA.

CHAPTER 4

IV. RAPID GENERATION OF FUNCTIONAL ENGINEERED 3D HUMAN NEURONAL ASSEMBLIES: NETWORK DYNAMICS EVALUATED BY MEA

All the data and images are taken from the published article *Muzzi, L., Di Lisa, D., Arnaldi, P., Aprile, D., Pastorino, L., Martinoia, S., & Frega, M. (2021). Rapid generation of functional engineered 3D human neuronal assemblies: network dynamics evaluated by micro-electrodes arrays. Journal of Neural Engineering, 18(6), 066030.*

The first experiments aimed on building a 3D network focused on the modular approach, where a basic element is used to assemble the whole network. Results exploiting this techniques were already presented by our lab using firstly silica microbeads (Frega et al) and more recently chitosan microbeads (Tedesco et al). The cells were obtained from cortical rat dissection therefore, I dedicated my self to replicate the model using h-iPSCs. Although this type of approach does not allow to recreate morphologies similar to *in-vivo*, it is particularly interesting from an engineering point of view. In fact, we could create very particular neuronal networks by having full control over various parameters chosen a priori by the user such as the size of the beads, the number of cells attached to each and the total number of beads. Furthermore, the approach would also allow to functionalize the individual beads (i.e. addition of gold nano particles / barium titanate nanoparticles) offering the possibility of localized network modulation. Results have already been presented in our laboratory using this technique with glass beads and chitosan beads, but the cells origin ways from primary rat cultures

Concept and rationale

Although recent advances, Lab-on-a-chip technology has a yet limited impact on *in-vitro* human brain models (Williamson et al., 2013). The field is truly moving towards precision medicine, but only recently 3D neuronal networks have been used as platforms for investigating brain (dys)functions and complementing *in-vivo* animal studies (Langer et al., 1995, Tang et al., 2006). Some of these rely on the generation of organoids, structures that try to recapitulate features of early human neurodevelopment, including the generation, proliferation, and differentiation of neural progenitors into neurons and glial cells and the complex interactions among the diverse, emergent cell types of the developing brain in 3D (Trujillo et al., 2019, Tambalo and Lodato, 2020). However, the generation

of these structures is subject to variability (Qian et al., 2019) and complete maturation of the cells type requires long period.

Instead of having brain organoid we propose an integrated 3-dimensional complex bio-artificial system (i.e., Neural Systems-on-a-Chip – NSC) in which electronic devices and 3D networks are integrated with sensors/actuators that allow the monitoring/interaction of/with the model system under study (i.e. MEAs).

In this work we adapted a protocol for the fast generation of human neurons to build 3D neuronal networks with controlled structure and cell composition suitable for systematic electrophysiological investigations. We used biocompatible chitosan microbeads as scaffold to build 3D networks and to ensure nutrients-medium exchange from the core of the structure to the external environment. We used excitatory neurons derived from h-iPSCs co-cultured with astrocytes. By adapting the well-established *NgN2* differentiation protocol, we obtained 3D engineered networks with good control over cell density, volume and cell composition. We coupled the 3D neuronal networks to 60-channel micro electrode arrays (MEAs) to monitor and characterize their electrophysiological development. In parallel, we generated two-dimensional neuronal networks cultured on chitosan to compare the results of the two models. We sustained samples until 60 d *in-vitro* (DIV) and 3D cultures were healthy and functional. From the structural point of view, the h-iPSC derived neurons were able to adhere to chitosan microbeads and to form a stable 3D assembly thanks to the connections among cells. From a functional point of view, neuronal networks showed spontaneous activity after a couple of weeks. We presented a particular method to generate 3D engineered cultures for the first time with human-derived neurons coupled to MEAs, overcoming some of the limitations related to 2D and 3D neuronal networks and thus increasing the therapeutic target potential of these models for biomedical applications.

.

Materials and Methods

Human induced pluripotent stem cells generation and maintenance

We used an already characterized rtTa/*Ngn2* positive h-iPSC line (Frega et al 2017) kindly provided by Frega et al (2019) in frozen vials (Passage 10). H-iPSCs were reprogrammed via episomal reprogramming from fibroblast of an healthy donor (30 year-old female, Coriell Institute for Medical Research, GM25256). Afterword, rtTA/*Ngn2*-positive lentiviral vectors are used to stably integrate the transgenes into the genome of the h-iPSCs. By using these transfer vectors, the h-iPSC line can

be created for which the expression of murine neurogenin-2 can be induced by supplementing the medium with doxycycline. Detailed information about the protocol can be found (Frega et al 2017). After rapid thawing, 6 × 106 cells were equally distributed on three wells of a six well-plate pre coated with Matrigel (Corning, #356237) and cultured in Essential 8 Flex Medium (Thermo Fisher Scientific) supplemented with 1% pen/strep (Thermo Fisher Scientific), 50 μg ml−1 G418 (Sigma Aldrich) and 0.5 μg ml−1 puromycin (Sigma Aldrich) (in the following we will refer to this supplemented medium simply as E8F). Medium was refreshed every 2 d. Cells were split twice a week (when reaching 70% confluence) using ReleSR (Stem Cell Technologies). During the 24 h after splitting, the medium was also supplemented with 100x Revitacell (Thermo Fisher Scientific). Well-plates were kept in incubator at 37 ◦C, 5.5% CO2. The detailed protocol can be found (Frega et al 2017).

Rat astrocytes

To obtain astrocytic feeder, brain cortices were collected from E18 Sprague-Dawley rat embryos (Charles River). Briefly, cortices were enzymatically dissociated and single-cell suspension was then plated in T-75 flasks. Cells were propagated once 80% of confluence was reached and frozen after the first passage. More detail can be found (Aprile et al., 2019). Cells were shipped in frozen vials. Astrocytes were thawed and seeded in T-75 flask with DMEM high glucose (Invitrogen, Thermo Fisher Scientific) supplemented with 10% fetal bovine serum (FBS, Sigma Aldrich) and 1% pen/strep. Cells were kept in incubator to grow and proliferate. After 7–10 d, astrocytes reached confluence and were split in two flasks using trypsin-EDTA 0.05% (Thermo Fisher Scientific). Cells were finally maintained in incubator and used in the following 14 d when confluence is reached again.

Chitosan microbeads

Microbeads were fabricated following the protocol described in detail (Tedesco et al., 2018) using chitosan (low molecular weight 50–190 kDa, 77% deacetylation degree, viscosity 92 cP at c =1% w/v in 1% acetic acid, Sigma-Aldrich). Briefly, chitosan was dissolved in 0.1 M acetic acid solution (2%, w/v). Chitosan microbeads were produced two days before seeding by air-assisted jetting technique, using a microencapsulation unit (Nisco Encapsulation Unit VAR J30, conical nozzle, 0.25 mm diameter). Chitosan solution was sprayed under controlled pressure (120 mbar) and flow rate (0.6 ml min−1) into a gelling solution (2%, w/v, NaOH solution in 60%, w/v, EtOH) and left overnight to complete the gelling step. The obtained microbeads were centrifuged (1200 rpm for 5 min) to remove gelling solution, rinsed with 10 ml of ultrapure water four times and resuspended in 70% ethanol for sterilization. On the seeding day, ethanol was removed by centrifugation, the microbeads were

washed three times with sterile water (time between washing steps of 5 min) and finally resuspended in cell culture medium. The production yield was evaluated using optical microscopy and diameter of beads was 120 μm ± 30.

PDMS structure and chitosan coating on MEAs

One day before cell seeding, MEAs were washed and sterilized in the oven (120 ◦C for 2 h). The polydimethylsiloxane (PDMS) confinement structures were fabricated with a standard 1:10 ratio between curing agent and elastomer. After mixing the components, we deposited a thin layer of PDMS onto a petri dish. Consequently, we started the curing treatment by placing the dish in the oven at 70 ◦C for 40 min. Therefore, we obtained a stick layer of PDMS (height ≈ 1 mm) from which we obtained several PDMS rings. We used two different punchers to cut the PDMS into rings (inner diameter = 5 mm; thickness = 1 mm) and we used a cutter to manually remove a slice of the ring (figure 4.1 b—left) to let the reference electrode of the MEAs uncovered. All these rings were washed, sterilized in 70% ethanol, dried and placed onto sterile and dried MEAs. We used sterile tweezer to place the ring in the correct position and adhesion was achieved thanks to the stickiness of the cured PDMS. For each MEA we stacked six PDMS structures to create an inner small chamber (height of about 6 mm) on the electrode area (figure 4.1 b -right). More detailed information about the assembly of the PDMS structure on the MEA are shown in the supplementary figure 1 (available online at stacks.iop.org/ JNE/18/066030/mmedia). One day before seeding, the active area delimited by the PDMS structure was coated with a 60 μl drop of 1% (w/v) chitosan solution. Chitosan solution was previously prepared by dissolving chitosan powder in 1% of acetic acid, filtering it through 0.5 μm PTFE syringe filter (Corning) and sterilizing it (120 ◦C for 20 min in autoclave) and stored at 4 ◦C until usage. After coating, the devices were then placed in incubator at 37 ◦C and 5.5% CO2 overnight. Before plating, MEAs (with PDMS structure placed in it) were washed three times with Dulbecco's phosphate-buffered saline (DPBS, Thermo Fisher Scientific, time between washing steps of 5 min) and left to dry for 30 min under the laminar flow hood.

Neuronal differentiation and 3D neuronal network assembly

We directly induced the differentiation of h-iPSCs into excitatory cortical Layer 2/3 neurons by overexpressing the neuronal determinant Neurogenin 2 (*NgN2*) factor upon doxycycline treatment (Frega et al 2017). Figure 4.1 *a* summarizes the main steps to create neuronal network on MEA from h-iPSCs. H-iPSCs were detached from a well after reaching confluence (6 × 106 cells) using ReleSR (Stem Cell Technologies) and were redistributed equally as single cells in E8F medium with 4 μg ml−1 Doxycycline (Sigma Aldrich) on two wells of a 6-wells plate. We will refer to this step as day

after differentiation (DAD) 0 (figure 4.1 a — DAD0). The day after, the medium was entirely replaced with DMEM/F12 (ThermoFisher Scientific) supplemented with 100x N2-supplement (Thermo Fisher Scientific), MEM non-essential amino acid solution 100x (Sigma Aldrich), 10 ng ml−1 human- NT-3 (BioConnect), 10 ng ml−1 human-BDNF (BioConnect), 4 µg ml−1 Doxycycline and 1% pen/strep (figure 4.1 a—DAD1).

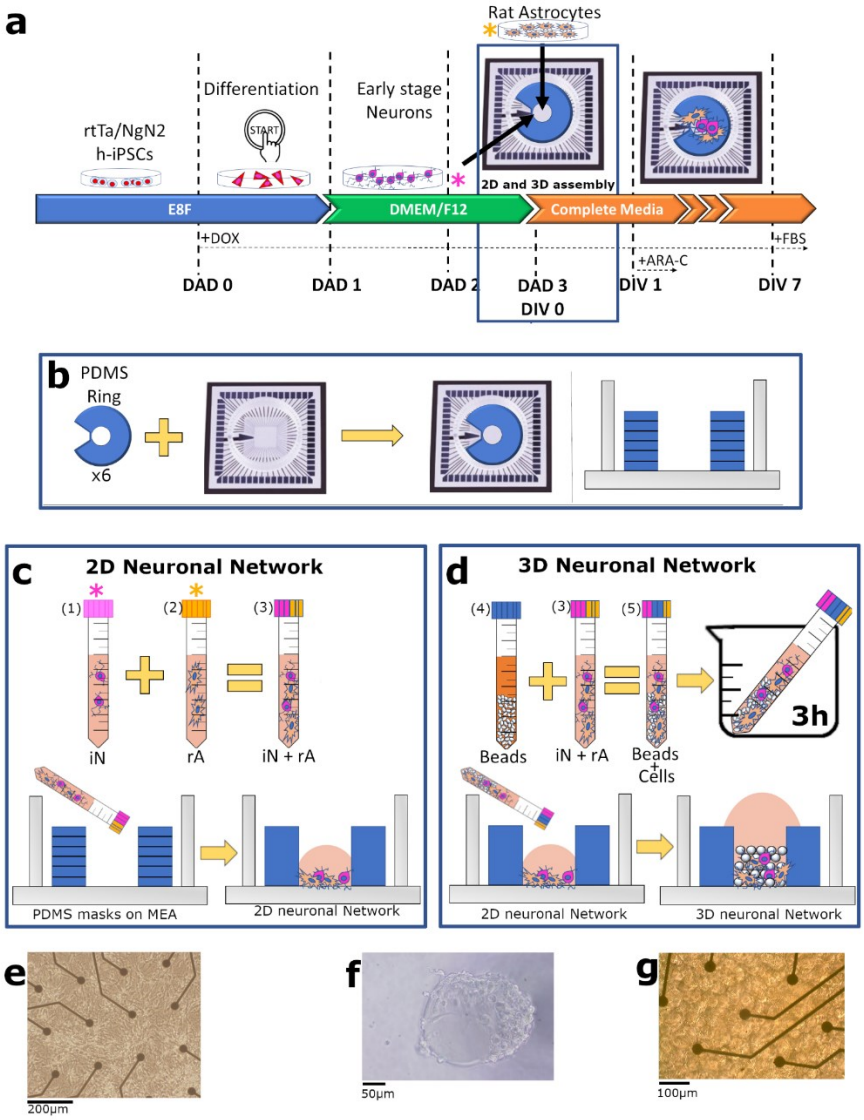

Figure 4.1. Main steps to build 3D networks, from differentiation protocol to assembly. **a)** H-iPSCs were maintained in E8F medium. Differentiation was initiated at DAD0 by supplementing Doxycycline in the medium. At DAD1, medium was changed in DMEM/F12 and cells lost their pluripotency. By DAD3, cells were used for the construction of 3D neuronal networks in neurobasal supplemented medium. **b)** PDMS structure assembly over the MEA60 devices. Six PDMS structures were stacked on top of the MEA to constrain the 3D network. **c)** Bidimensional cultures were generated by mixing iN detached from a well (Tube 1) and astrocytes detached from a flask (Tube 2) in a 1:1 ratio (Tube 3). **d)** Sketch representing the fundamental final steps for the assembly of the 3D culture. Chitosan microbeads were mixed with the cells in Tube 3 in a ratio 1:5 between beads and cells (Tube 4). We left the originated tube inclined in the incubator for 3 hours; during this time every 20 minutes we gently shaked the tube to guaratee homogenous distribution of the cells and adherence with beads. Finally we deposited a drop of beads-cells solution on top of the MEA. **e)** Image showing iNeurons grown on MEAs the day after the monolayer deposition. **f)** Image showing a microbead covered with cells withdrawed from Tube 4 during 3D assembly. **g)** Image showing

iNeurons and beads on the electrode plane 6 days after the deposition on the MEA PDMS's delimited area.

Cells will proliferate and reach confluence in both wells therefore, during DAD2 (figure 4.1 a—DAD2) medium needs to be replaced only if cells death/detachment is observed. On DAD3, the medium was changed in Neurobasal (Thermo Fisher Scientific) supplemented with B-27 supplement (Thermo Fisher Scientific), GlutaMAX (Thermo Fisher Scientific), human-BDNF, human- NT-3, 4 µg ml−1 doxycycline and 1% pen/strep. From now on we will refer to this medium composition as 'complete medium'. At this day (DAD3/DIV0), early stage induced neurons (iN) were detached from the well and were used in combination with rA, previously stored in a flask in the incubator, to create both 2D and 3D models (figure 4.1 a —DAD3/DIV0). In particular, iN and rA were detached by using Accutase (Sigma Aldrich) and trypsin-EDTA 0.05% respectively and, were collected in two separate 15 ml Falcon tubes (Corning) (figure 4.1 c). We then prepared a solution containing a total of ∼800 000 cells ml−1 where iN and rA were in 1:1 ratio. Consequently, we seeded a 60 µl drop of solution containing 50 000 cells in the active electrodes area of the MEAs delimited by the PDMS structure to achieve a final cell density of ∼2500 cells mm−2 (figures 4.1 c–e). After the monolayer deposition, we left the MEAs in the incubator for 3 h to allow cells adhesion. In parallel, we moved ∼150 000 beads from the tube containing chitosan microbeads to a new 15 ml falcon tube. Therefore, 3 h before 3D assembly, DPBS was replaced with complete medium by applying three washing steps, each composed of centrifugation, aspiration of the supernatant and resuspension in 2 ml of complete medium. Then, iN and rA (from an 1:1 solution previously prepared) were added in the chitosan-beads tube to obtain a 1:5 ratio between beads and cells (figure 4.1 d). Consequently, this tube was kept tilted in the incubator and gently shacked every 20 min to ensure adhesion between cell and beads. After 3 h, the tube was put in vertical position for at least 30 min. Finally, the supernatant was removed, and the cell-bead mix was re-suspended in 400 µl of complete medium. At this point, we started the assembly of the 3D neuronal network on the MEA previously plated with the monolayer culture of iN and rA. First, 40 µl of medium were removed from the MEAs and were replaced with a 40 µl drop of the cell-bead solution, to obtain a scaffold of cells and beads on top of the monolayer culture (figure 4.1 g). Each 3D structure was composed by 15,000 beads and 75,000 cells. Cultures were then kept in the incubator for 2 h and, after this time 100 µl of complete medium was added to avoid evaporation during the night. The next day (DIV1), the entire medium was replaced with complete medium supplemented with Ara-C (2 µM, Sigma Aldrich) (figure 4.1 a—DIV1). MEAs were then stored in the incubator and checked daily. At DIV3, 50% of the remaining medium was removed and new complete medium was added to fulfill the small chamber created by the PDMS

insert (~200 µl). From this DIV on, half of the medium was changed every two days and from DIV 7, complete medium was supplemented with 2.5% of FBS (figure 4.1 a—DIV7).

Data acquisition and analysis

We used MEA60 from MultiChannel System (MCS) to record the network activity of 2D and 3D neuronal populations. These devices present 60 electrodes (TiN/SiN, 30 µm electrode diameter, 200 µm spaced) arranged in an 8 × 8 square grid without the four corners. The electrophysiological activity was acquired with the 2100 System (MEA 2100-System, MCS) and signals were sampled at 10 kHz. Sterility was maintained using an autoclavable cap on top of the MEA chamber while normal conditions were maintained by pre-heating the head stage at 37 ◦C and by delivering humidified air with 5.5% CO2 over the MEA thanks to a plastic box placed on top of the recording system. Recordings lasted 15 min and data were analyzed offline using MATLAB (The Mathworks) scripts. Raw data were first subjected to high-pass filtering (cutoff frequency = 200 Hz) then to spike detection and finally analyzed as point processes. For each channel, noise was estimated by dividing the whole recording in 60 s bins and the noise with the lowest standard deviation was chosen among the bins. We implemented Precise Time Spike Detection algorithm as detailed (Maccione et al 2009). Spike were extracted if the peak was five times higher than the noise's standard deviation and the peak-to-peak amplitude was six times the noise's standard deviation, considering 1 ms of Peak Lifetime and refractory period. For the analysis we considered as active electrodes the ones that showed at least 0.1 spikes s−1. For each recording we quantified the array wide firing rate (AWFR) by dividing the recording in 100 ms bin and counting all the spikes detected in each bin, the mean firing rate (MFR) as the sum of all spikes recorded in one electrode divided by the recording time, averaged across only active electrodes. Inter spike interval (ISI) was obtained for each active electrode and calculated in bin of 10 ms for 10 s as probability to have an event after a certain amount of time. Burst detection algorithm was applied to each channel. We considered burst as a series of at least five spikes in which the ISI among them was not longer than 100 ms. Therefore, we quantified the array wide firing burst and the mean burst rate as we described for the spikes analysis. Inter burst interval (IBI) was obtained as the ISI but considering the time between the end of a burst and the start of the next one. Burst duration (BD) was obtained by calculating the duration (ms) of each burst. We evaluated the percentage of random spikes (PRS) as the total number of spikes in the culture that does not belong to a burst. We defined network burst (NB) as synchronous burst activity among channels. We detected a NB whenever we observed bursts in 20% of the active channel with an IBI $\leqslant$ 100 ms (Bologna et al 2010). We implemented an algorithm for the network synchronous activation (NSA) detection. We first evaluated the AWFR of a culture in 200 ms bins, then we detected the peaks higher

than the mean AWFR plus two times the standard deviation. Afterwards, for each peak we verified that in the peak bin there were synchronous activation between electrodes. We imposed the condition that at least 20% of the active electrode must fire with an ISI ⩽ 100 ms. If the condition is met, the algorithm searches for the starting point of the NSA. Therefore, we searched for the first point in the AWFR that was below threshold before the detected peak. We then divided the time between the two points in 25 ms bin and we choose the starting point as the first bin in which at least 20% of the electrodes were firing. If no bins met the criteria, peak were discarded from the NSA detection. For the ending point of the synchronous activation, we used the first point below the AWFR mean after the peak, we divided the time between these points in 25 ms bins. Consequently, we looked for four consecutive bins without activity and we assigned the end of the NSA to the first active bin preceding that silent period. Finally, we merged the NSAs that were less than 200 ms apart. We extracted and aligned the NSA of each culture by grouping all the spikes detected within NSA in chronological order. Mean shape was obtained by calculating the occurrences of spikes detected in 50 ms bins in a 5 s window. We defined an ignition site as the electrode correspondent to the first spike in at least 5% of detected NSA in a defined culture. To estimate signal propagation from the ignition sites to the rest of the electrodes we considered the latency from the first spike of the NSA to the first occurrence in the other electrodes. Distances were then evaluated considering the Euclidean distance between electrodes. Furthermore, we evaluated mean intra-latency and mean intra-distance for each detected NSA. Intra latency was evaluated by considering all the interspike- intervals within the NSA and averaging across the total number of spikes. Mean Intra-distance was evaluated in the same way but considering the distance between electrodes of consecutive spikes.

Statistical analysis

We used rank-sum MATLAB function to perform non parametrical Mann–Whitney U-test since data do not follow a normal distribution. Significance differences were considered when $p < 0.05$. 2.7.

Immunofluorescence

Sample were washed with sterile PBS solution and fixed in 4% para-formaldehyde (PFA, Sigma-Aldrich) solution for 15 min at room temperature. Then we used 0.2% of Triton X-100 (Thermo Fisher Scientific) for 10 min to permeabilize the cells and non-specific binding antibodies were blocked by adding to the sample a blocking buffer solution (BBS, composed of 5% normal goat serum (Sigma Aldrich), 1% bovine serum albumin (Sigma Aldrich, 0.2% Triton X-100 in phosphate-buffered saline) for 45 min. Primary antibodies were diluted in BBS and left overnight at 4 ◦C. After that, samples were rinsed three times with PBS and stained with secondary antibody for 1 h at room

temperature. Finally, DAPI (1:10 000, nuclei, Sigma Aldrich) was added at the end for 10 min and cells were stored in dark condition at 4 ◦C in PBS solution. GFAP (1:500, glial fibrillary acidic protein, monoclonal or polyclonal antibodies, Sigma Aldrich) and MAP-2 (1:500, dendritic microtubule associated protein, Chemicon Millipore) were used as primary antibodies to label glia and neurons, respectively. Alexa Fluor 488 and Alexa Fluor 549 Goat anti mouse or Goat anti rabbit (diluted 1:700 and 1:1000; Thermo Fisher Scientific) were used as secondary antibodies. We acquired pictures with the upright microscope Olympus BX51M equipped with the fluorescent lamp Olympus U-RFL-T and Hamamatsu ORCA-ER digital camera.

Results

Human neurons form 3D neuronal networks

To build a human 3D excitatory neuronal network on MEAs we optimized the original h-iPSCs differentiation protocol introduced (Frega et al., 2017). To achieve a controlled cell density and composition, we prepared independent solutions containing iN, rA and microbeads with known concentrations (figures 4.1 c,d—tubes 1-2-4, respectively). To create 2D neuronal networks and as a first step of the 3D network construction, we deposited a monolayer of iN and rA (i.e. 1:1 ratio, figure 4.1 c—tube 3) on top of the active area of a MEA. Figure 4.1 *e* shows a picture of the seeded cells homogeneously sparse over the entire electrode area. The iN solution was obtained by using h-iPSCs at the third day of differentiation, period necessary to allow the cells to lose their proliferative ability and thus enabling us to control final density. After 42 DIV, by immunocytochemistry we found a ratio between iN and rA of 1:1.2, confirming that the implemented methodology offers a good control over cell density (supplementary figure 2). Right after the monolayer deposition, we built the 3D engineered neuronal network. First, we combined iN, rA and microbeads to obtain a 1:1:0.2 ratio (figure 4.1 d—tube 5). Then, we kept the tube containing cells and beads tilted in the incubator for 3 h and we gently shook it every 20 min. This step was essential to ensure a homogeneous deposition of iN and rA on the beads and to enhance reciprocal adhesion. After 3 h, we observed that cells were attached to the microbeads taken from the tube, showing that cells and beads were ready to be assembled to form a 3D network (figure 4.1 f). Thus, we let the preparation precipitate by simply leaving the tube in a vertical position, avoiding centrifugation which could lead to the detachment of the cells from the beads. Finally, we placed cells and microbeads on the monolayer of iN and rA formed on the active area of MEAs delimited by the PDMS structure. The PDMS structure we created was essential to confine cells and beads, ensuring a controlled 3D network formation (figure 4.1 g). During the first week of development, the 3D structure was still weak since small mechanical

perturbations (i.e. change of culture medium) leaded to flickering of the beads, increasing the probability of creating damage to the network. During time, we observed that the diameter of the beads decreased leading to an increase in the solidity of the structure (i.e. average diameter of about 100 µm by DIV 42, figures 4.2 *a,*b). Furthermore, we investigated how the 3D structure influenced the cellular distribution in the cell monolayer. While in 2D neuronal networks a homogenous distribution of cells was present (figure 4.2 d), cells were sparser and unevenly distributed on the electrode area when the 3D structure was plated on top (figure 4.2 c). Finally, we acquired images at different height of the 3D structure to investigate neuronal organization in 3D late in development (supplementary figure 4). It is possible to observe neurons adhering to the beads that are interconnected to each other, forming a network. In addition, the presence of micro-spaces between the beads can be seen, which should ensure exchange of metabolites. These results show that also within the 3D structure neurons are present and connected.

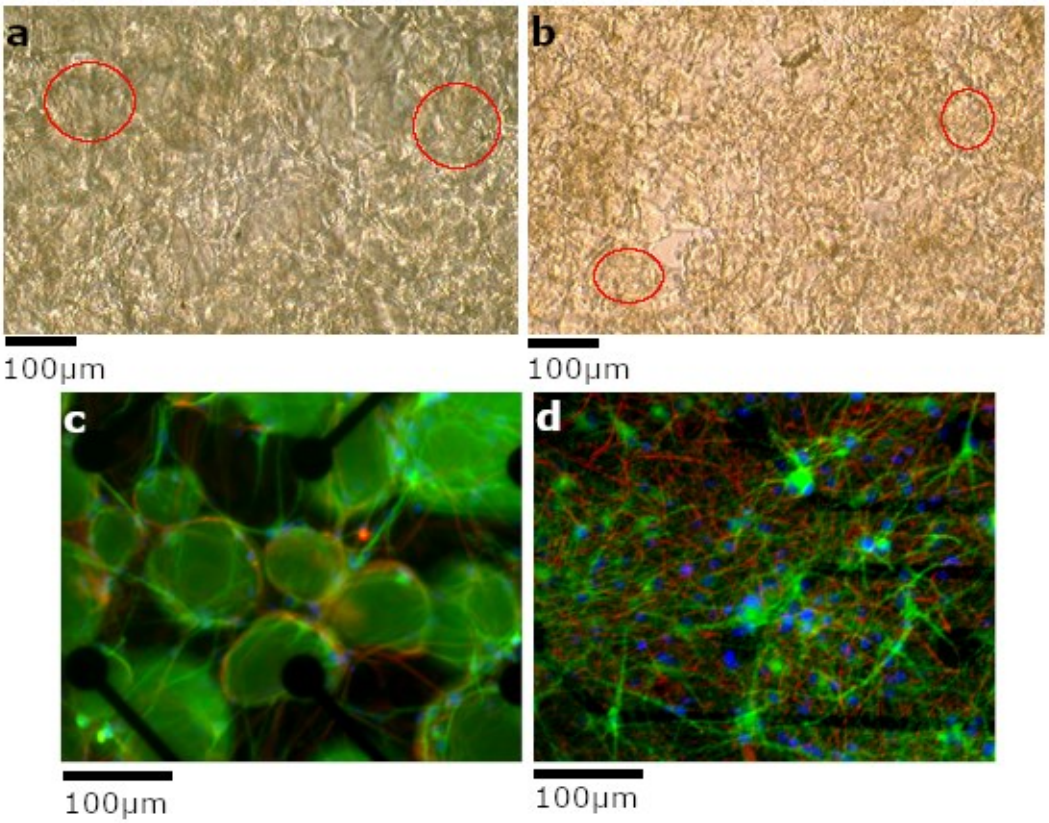

Figure 4.2. Microscope pictures during development. **a-b)** Images showing the 3D structure at DIV1 and DIV10. A reduction in beads dimension can be observed, as indicated by the red circles. Pictures were acquired with a 10x objective using an inverted microscope. Scale bar 100 µm. **c-d)** Fluorescent images showing the elctrode plane of **c)** 3D and **d)** 2D network at DIV42. A different cell organizations at the electrode plane is visible. Pictures were acquired with a 20x objective. Green: MAP-2, Red: GFAP, Blue: DAPI. Scale bar 100µm

Electrophysiological development of 2D and 3D neuronal networks coupled to MEAs

We seeded 3D neuronal networks (n = 5) on MEAs and we evaluated their electrophysiological activity during development (17–42 DIV). To investigate whether human neurons formed 3D structure functionally connected exhibiting developmental trajectories indicative of proper maturation and patterns of activity that in principle, better recapitulate the activity in the *in-vivo* brain area as compared to golden standard 2D models, we characterized 2D sister cultures (n = 8). All 2D networks showed spontaneous activity starting from DIV 17, which was mainly composed by isolated spikes and burst (figure 4.3 a). During development, the general level of activity of the network as well as the number of electrodes involved increased. As shown by the peaks present in the AWFR (figure 4.3 a), the activity increased over time and organized itself in synchronized network events (i.e. NB, NSA). 3D networks showed spontaneous activity from DIV17 composed only by sparse spikes (figure 4.3 b). As observed for 2D populations, the level of activity and the number of electrodes involved increased during time, together with the appearance of synchronous patterns (i.e. NSA, figure 4.3 b—DIV 42). These results indicate that both 2D and 3D cultures developed into functional interconnected neuronal networks. To investigate and compare the development of 2D and 3D neuronal networks, we evaluated six different features, averaged across the same experimental conditions, and we plotted their normalized trend using the maximum value reached during the development of the cultures (figure 4.3 c).

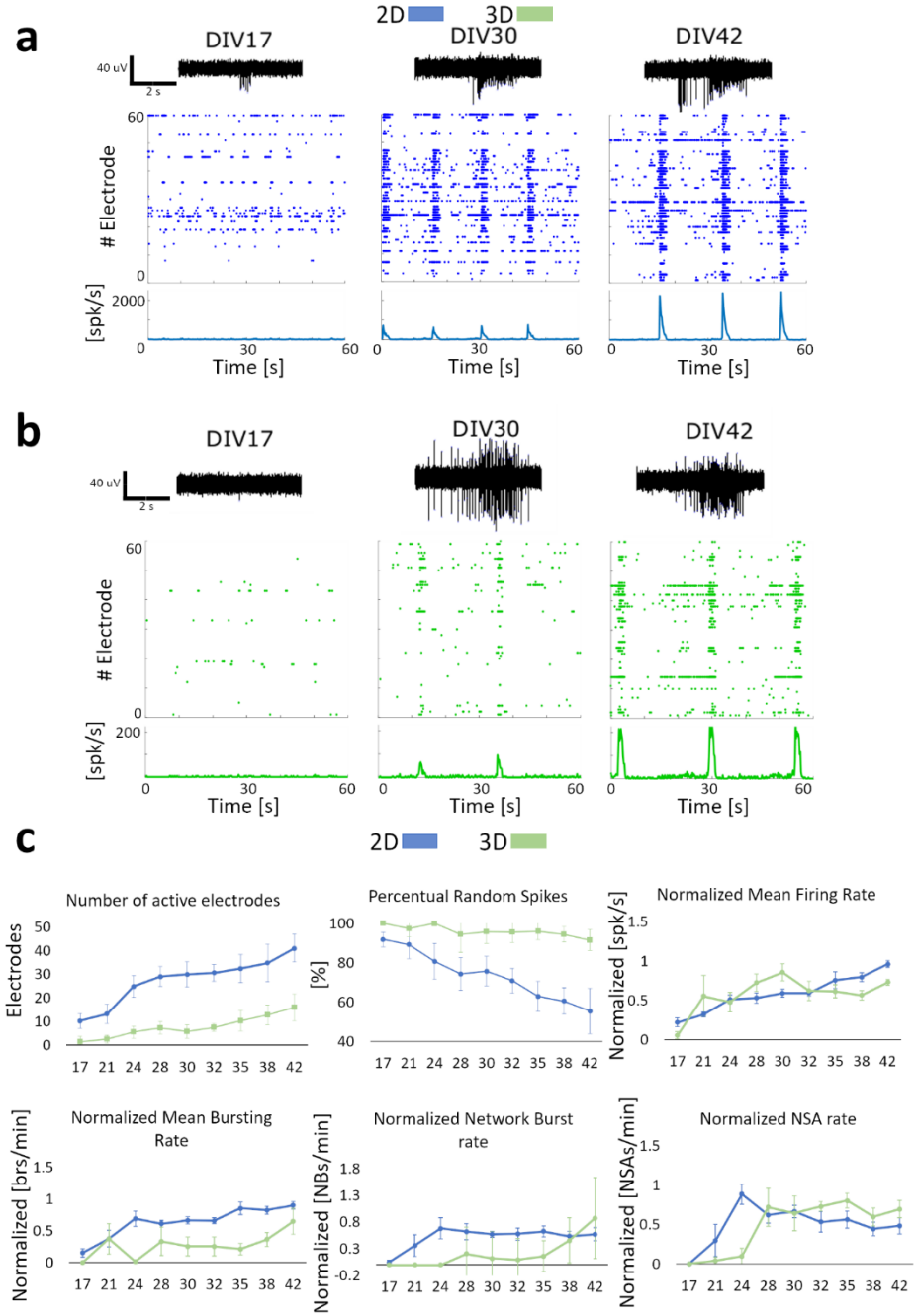

Figure 4.3. Electrophysiological activity of 2D vs 3D cultures. **a-b)** Raw data recorded from one electrode (6 s), rasterplots and AWFR exhibiting 1 minute of spontaneous activity during development. The rasterplot y-axis represents electrodes and each blu dot indicates a detected spikes in the given electrode. The AWFR quantifies the level of activity showed in the rasterplots and highlight the emergences of synchronous network event. **c)** Comparison between 2D and 3D culture during development. All Data points represents mean values across sample with same experimental conditions and errorbars represents standar deviation. Data from each sample were normalized regarding the maximun value reached during development and then averaged. Number of active electrodes and Percentual Random Spikes (PRS) are represented without normalization. 3D data are represented in blue (n=5), 2D data are represented in green (n=8).

Considering the 2D networks, we found that spikes started organizing into burst by DIV 17, while network bursts and synchronous activation emerged by DIV 24. Overall, during development the firing and (network) bursting frequencies increased, together with an involvement of more recording

electrodes and a reduction of the PRS. From DIV 32 to 35 onwards, all these parameters tended to stabilize, as shown in figure 4.3 c. We found that the dynamic exhibited by 2D and 3D cultures during development was similar, although 3D networks exhibited different changes of the observed parameters compared to 2D cultures. Firing activity was detected starting from DIV 17 while single channel bursting activity appeared around DIV 28. Network bursts were not detected in all samples until DIV 38. However, NSAs were present from DIV 28 and their frequency remains almost unchanged during development.

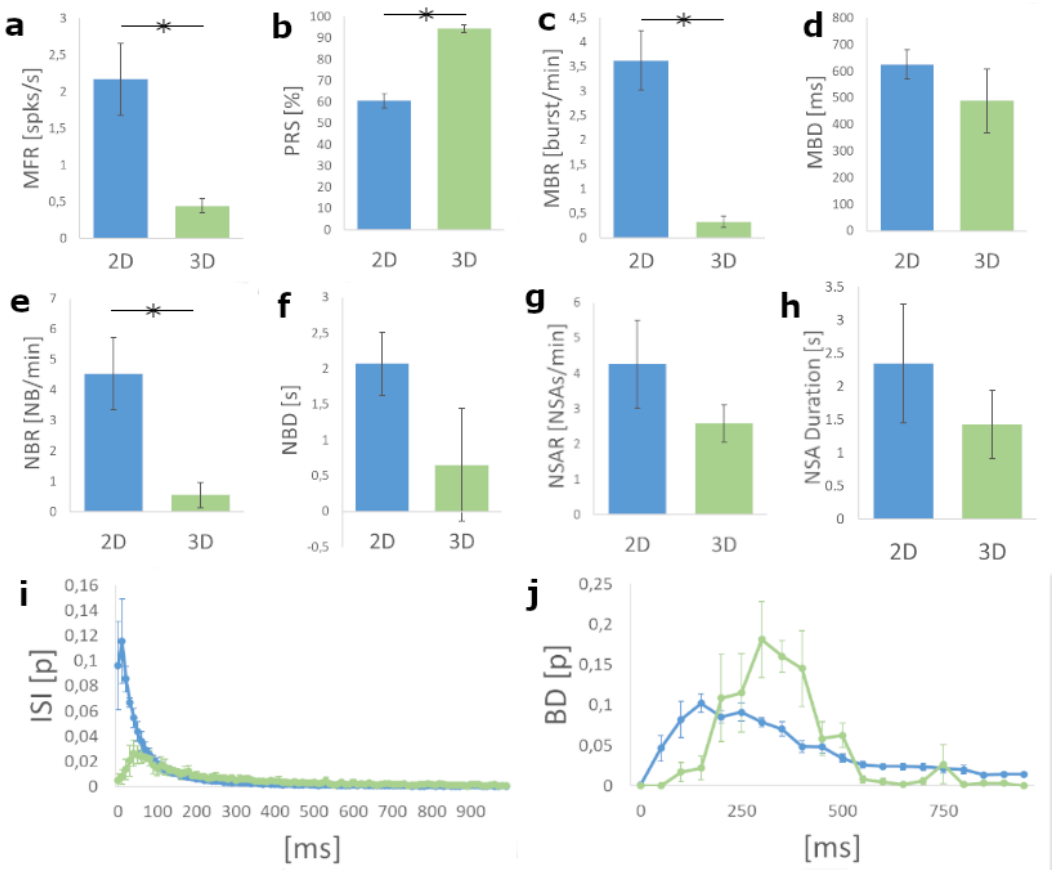

Figure 4.4. Electrophysiological comparison of 2D and 3D cultures at DIV38. **a-h)** Graphs showing the **a)** Mean firing rate (MFR), **b)** percentage of random spikes (PRS), **c)** Mean burst rate (MBR), **d)** Mean burst duration (MBD), **e)** network burst rate (NBR), **f)** network burst duration (NBD), **g)** network sychronous activation rate (NSAR), **h)** network synchronous activation duration (NSAD) in 2D and 3D neuronal networks at DIV 38. **i-j)** Graphs showing the **i)** Inter spike intervals (ISI) (10 ms bin) and **j)** burst duration (BD) (50 ms bin). Data shows the mean obtained across sample with same experimental condition and errorbars shows standard deviation. * $p<0.05$. 2D data are represented in blue (n=5), 3D data are represented in green (n=8).

Excitatory 3D neuronal networks exhibit different electrophysiological activity as compared to 2D

We have found that 3D neuronal networks exhibited similar developmental behavior as compared to 2D, although with different dynamics. To better compare 2D and 3D neuronal network activities measured by MEAs, we further analyzed the network activity at a late and stable developmental stage, when the NSA rate showed a plateau phase (i.e. DIV 38).

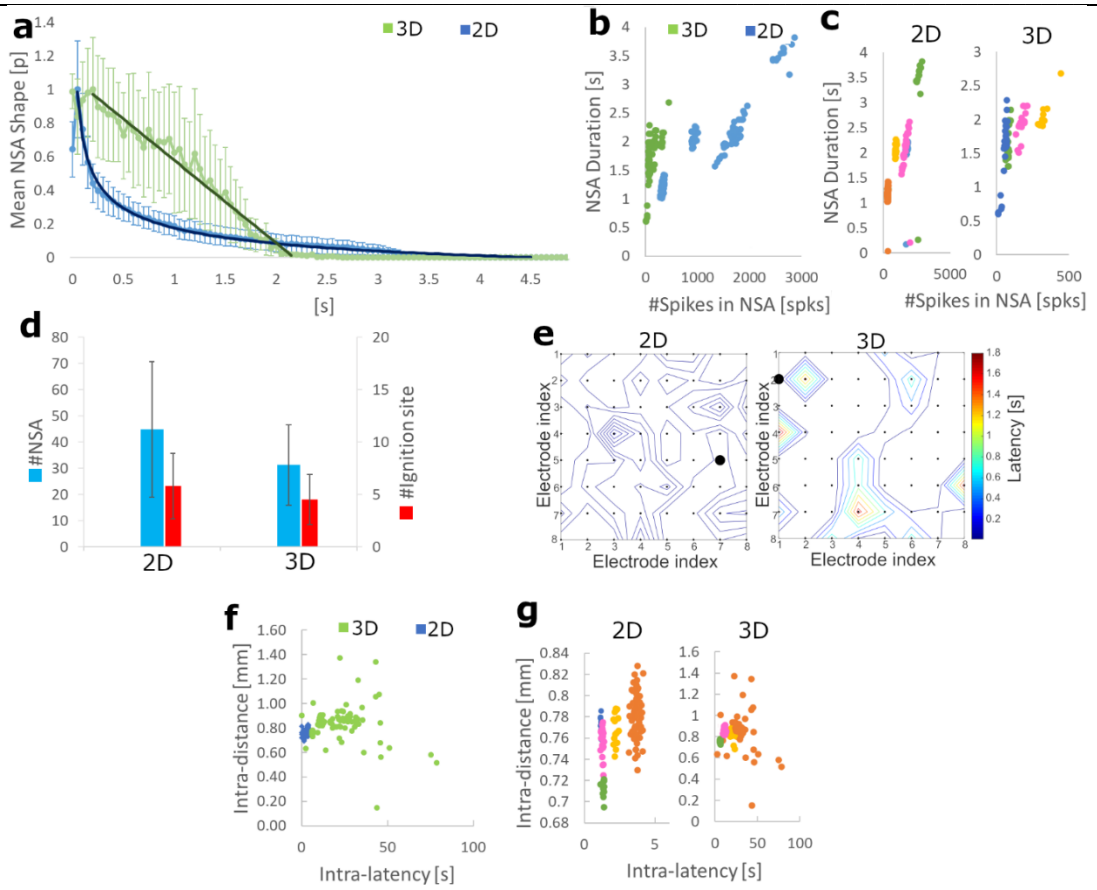

Figure 4.5. Networks synchronous activation characteristics. **a)** Mean NSA shape of the two experimental conditions (50 ms bin). Data points represents mean value and errorbars represent standard deviation. Darker lines represent the fitting for the decay phase of the NSAs. For the 2D evaluation we used a power model (R^2=0.9931), for the 3D we used a linear model (R^2 = 0.9708). **b-)** Graph showing the total number of spikes in a NSA and relative duration in 2D and 3D cultures. Each point represents a single NSA. **c)** Zoom-in of the previous panel for each experimental condition in which each color represents a different culture for 2D (left) and 3D (right) structures. **d)** Graph showing the mean total number of NSAs during recording and the mean number of ignition sites detected for each culture. **e)** Representative isochrones showing how the signal spreads from the ignition electrodes toward other channels in NSAs recorded in 2D and 3D cultures. **f)** Intra-distance / intra-latency relationship of the signal propagation within NSAs. Each point represents a single NSA. Values were evaluated by considering the NSA as a unique spikes train and then averaging the intra-distance and intra-latency of consecutive spikes. **g)** Zoom-in of the previous panel for each experimental condition in which each color represents a different culture in 2D cultures (left) and 3D cultures (right).

At this time point, we found significantly lower MFR and mean bursting rate in 3D networks as compared to 2D sister cultures, together with an increased PRS (figures 4.4 a,c, $p < 0.02$). The mean BD was also lower in 3D neuronal networks as compared to 2D, though with no statistical significance. Regarding the network burst analysis, we found significantly lower rate in 3D compared to 2D, while the duration of the NBs was not statistically different (figures 4.4 e,f). Finally, we observed a reduced NSA rate and duration in 3D neuronal networks, although not significant (figures 4.4(g) and (h)). Furthermore, from the evaluation of the ISI graph it was evident that 2D cultures fired closer spikes (ISI < 100 ms) more frequently, while in 3D networks spikes appeared spread at

different intervals, including ISIs greater than 100 ms (figure 4.4 i). Finally, by analyzing the distribution of the BDs we found that 3D neuronal networks showed mainly burst lasting between 250 and 500 ms, while in 2D a wider range of BDs was present (figure 4.4 j). Additionally, we kept alive two cultures from both experimental paradigm until DIV60 and we recorded the activity. Supplementary figure 3 shows how the network firing proprieties remained almost unchanged from DIV38, confirming that networks reached a stable developmental stage between the 5th and 6th weeks *in-vitro*. Even if no statistical difference was observed in the NSA frequency, we found a specific NSA dynamic in 2D and 3D neuronal networks (figure 4.5). By evaluating the mean NSA shape (figure 4.5 a), we found differences in the recruiting part of the NSA (initial phase) and in the NSA decay. In 2D neuronal networks, the maximal activity was reached after about 100 ms from the ignition of the event. The decay phase was fitted with a power model ($R2 = 0.9931$). Activity decreased to 20% in about 700 ms and finally ceased after about 3 s. Instead, in 3D neuronal networks the maximal activity was reached almost immediately after the ignition (<50 ms) and persisted for about 200 ms. The decay phase was fitted with a linear model ($R2 = 0.9708$) and the NSA lasted about 2 s. Furthermore, for each NSA we plotted the NSA duration versus total number of spikes observing differences in 2D and 3D neuronal networks (figure 4.5 b). In particular, we noticed distinct NSAs clusters from different cultures (figure 4.5 c different colors). In 3D, the number of spikes per NSA was smaller compared to 2D and NSAs were shorter. We then evaluated the number of NSAs and ignition sites (i.e. the electrodes from which the NSA is initiated) and we investigated the propagation of the signal during the NSAs in 2D and 3D neuronal networks. Even if no significant difference in the number of NSA and ignition sites was found (figure 4.5 d), we found a clear difference in signal propagation and latency. In particular, while 2D neuronal networks exhibited a fast and continuous propagation of the signal, in 3D we found a discontinuous propagation characterized by longer latencies (up to 1.8 s), as shown by the representative isochrones (figure 4.5 e). Finally, we analyzed the characteristics between intra-distance and intra-latency during NSAs. We noticed that 3D NSAs are sparser than 2D (figure 4.5 f)) and, more specifically, we observed that for 2D networks each cluster is bounded in a certain region in the latency-distance plane and these regions are culture specific (figure 4.5 g). In the 3D samples, we noticed a wider range of both intra-latency and distance, indicating a propagation developing in a 3D space and only partly captured in the read-out layers of neurons coupled to the planar MEA.

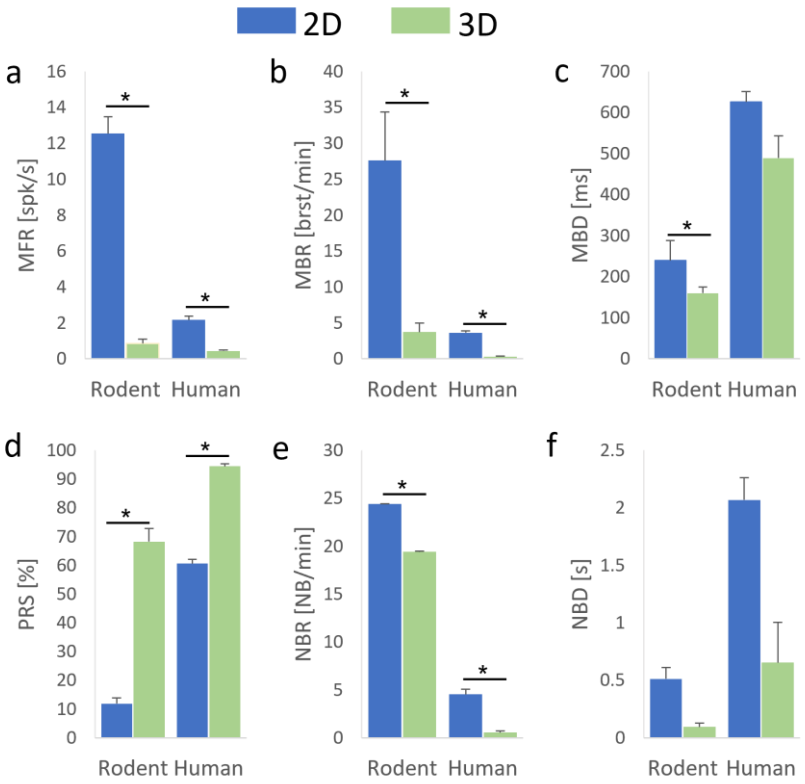

Figure 4.6.. Graphs showing the quantification of electrophysiological activity exhibited by 2D ad 3D rodent and human neuronal networks. Data regarding the rodent model were taken from (Tedesco et al., 2017). **a)** Mean firing rate (MFR), **b)** Mean burst rate (MBR), **c)** Mean burst duration (MBD), **d)** percentage of random spikes (PRS) **e)** network burst rate (NBR), **f)** network burst duration (NBD). * $p<0.05$. In blue we presented 2D models (rodent n = 3, human n=8), in green the 3D (rodent n=3, human n=5)

All these evidences can be considered as indirect proofs of signal propagation in the upper layers of the 3D structure. Finally, we investigated whether changes in activity observed when moving from 2D to 3D structures were similar in rodent and human neuronal models. We found that human neurons in a 3D environment differ from the related 2D model on the same parameters observed in rodent (figure 4.6) (Frega et al 2014, 2019, Tedesco et al 2018). In particular, when embedded in a 3D structure, neuronal networks show a lower firing and (network) burst rate, a higher PRS and a lower (network) BD as compared to 2D cultures with the same neuronal origin.

Discussion

We specifically optimized a widely used differentiation protocol (i.e. *Ngn2* induction) to be suitable for the construction of a 3D assembly onto MEAs using microbeads as scaffold. This protocol induced the fast conversion of h-iPSCs into a homogeneous population of cortical excitatory neurons, that organize into a functional network in three weeks (Frega et al., 2017). To ensure proper functional development, the protocol required co-culture with rat astrocytes. Different differentiation protocols have been developed to obtain astrocytes from h-iPSCs, however they are extremely long-time and

expensive (Krencik et al., 2011, Santos et al., 2017, Li et al., 2018). In the original protocol, h-iPSCs differentiation was initiated directly on MEA and astrocytes were added on top of the differentiating cells 3 d after *Ngn2* induction. Since integration of neurons and astrocytes in 3D is required, we plated neurons, astrocytes and microbeads at a desired ratio on MEA at the same time. To ensure proper control over cell ratio and to allow neuronal network integration, we used neurons in which *Ngn2* induction was initiated three days before. At this stage of differentiation h-iPSCs have lost their proliferative capacity, ensuring control over the number of seeded cells. Furthermore, h-iPSCs morphologically started to resemble neurons, small processes were formed although mature arborization and structural connections between neurons were still not present, thus enabling neuronal network formation. The success ratio of the protocol depends on the user's experience and working conditions. Indeed, a proper cell-beads coupling should be established before plating and mechanical perturbations should be minimal to avoid damage of the structure. Once the protocol is properly established, the success rate (i.e. 3D neuronal networks coupled to MEA showing mature electrophysiological activity) is about 80%. The cultures originated by using the last drops of cell-beads mix solution might not survive, probably because they contain cells precipitated at the bottom of the vial (i.e. dead cells or cells not adhered to beads) and a higher percentage of larger beads. These conditions do not allow a healthy/homogeneous development of the network, leading to cell death and breakdown of the construct. This success rate can be therefore increased by plating only about 80% of the solution containing beads and cells. The bead scaffold-based method has been already validated by us with the use of rodent cells (Frega et al., 2014, Tedesco et al., 2018). In particular, we have already shown network responses from stimuli delivered both from top layer of the structure proving that neurons grown in 3D with this scaffolding procedure were functionally connected. Furthermore, axonal reconstruction showed neurites propagation in different layers. The choice of chitosan microbeads as scaffold was based on several considerations. First, it has been described that the softness of the microbeads allowed to obtain a 3D tissue with mechanical properties similar to the *in-vivo* brain (Tedesco et al., 2018). Furthermore, chitosan is easily available at low cost, and the extreme biocompatibility and degradability (mediated by hydrolytic enzymes) makes it a good candidate for future *in-vivo* applications. Moreover, the inter-porosity formed by beads assembly allows the flow of nutrients and waste metabolites from the center of the tissue to the outside, thus resulting in a less dense structure than a scaffold free organoid and probably preventing long-term cell death in the core of the structure. The use of such microbeads as scaffold offers the possibility to create engineered neuronal networks. In fact, by varying the ratio between microbeads and cells, the density of the assembly can be tuned. Furthermore, making the assumption that beads were spherical and follows the cubic close packing the final dimension of the construct can be tailored by varying

the total number of microbeads and/or changing the dimension of the constrain (i.e. PDMS ring). Greater control over the bead size/shape variability would certainly lead to greater replicability of the experiments and higher control of different parameters of the resulting structure. Pre-treatment with adhesion factors or encapsulation of molecules can be performed on the microbeads to confer additional features to the structure (i.e. guidance of axonal growth, controlled release of drugs) (Arnaldi et al., 2020b, Arnaldi et al., 2020a). Finally, the possibility to integrate different h-iPSCs differentiation protocols generating homogeneous population of cells (i.e. excitatory neurons, inhibitory neurons (Mossink et al., 2021a) (Mossink et al 2021b), astrocytes) will allow to build a 3D neuronal network with controlled cell density and composition, which is not currently possible. Through imaging we monitored the development of the 3D neuronal networks. During the first week, microbeads were covered with cells not connected to each other. After the first week, we observed that microbeads decreased in diameter and the structure become more stable. In a previous work (Tedesco et al., 2018), we showed that neuronal processes were able to grow passing through the beads and that perineural net-like structures were formed. Thus, the decrease in diameter might be caused by the extension of cellular processes that—both enveloping and penetrating chitosan microbeads and connecting them to each other—sustain the formation of a complex and stable network and apply force to the beads that start to slowly shrink. Then, we investigated the functional properties of 3D human neuronal networks grown on MEAs. We found that h-iPSCs-derived neurons formed 3D functionally active neuronal networks. Our analysis revealed that the activity exhibited by 3D neuronal networks was different as compared to 2D. Since the 3D assembly was deposited on top of a 2D neuronal network, the comparison of the activities exhibited by the two structures allowed us to investigate how the 3D layers modulate the network dynamics. 3D networks exhibited lower spiking and bursting activities as compared to 2D (figure 4.3). While in 2D the activity was observed in all electrodes, a reduced number of electrodes were active in 3D (figure 4.4 a). This is in line with the lower cell density observed in the electrode plane under the 3D cultures. Considering that we assembled the 3D network on top of a 2D network, the low cell density suggests that a migration of cells in the upper layers of the structure occurred. We have already observed this behavior in our previous work (Tedesco et al., 2018) where neurons were partially transferred onto the surface of the overhanging 3D assembly because of the higher biomimeticity of 3D chitosan-beads scaffold than the 2D MEA surfaces. Low firing and bursting activity could be also indicative of poor viability. However, we showed that neurons adhering to beads connected through arborizations were present in the inner layers of the 3D structure (supplementary figure 4), indicating that complex neuronal networks are formed in the core of the structure. Moreover, we have presented chronic and protracted physiological activity (up to 60 DIV) and we have shown that activity exhibited by 3D neuronal

network at DIV60 did not differ from the one at DIV38 (figure 4.4 and supplementary figure 3) indicating that good viability was present. Indeed, in the case of cell death, the toxic signals of the dying cells (i.e. in the core of the structure) would cause damage to the surrounding area, resulting in a decrease or loss of activity later in development. Finally, since changes in activity patterns observed in 3D as compared to 2D rodent models (figure 4.6) were associated with proper 3D neuronal network formation (Frega et al., 2014, Tedesco et al., 2018), the fact that the same trend is observed when moving from a 2D to a 3D human model indicates that a 3D neuronal network was properly formed. The synchronous network bursting activity (i.e. NB) characterizing 2D neuronal networks dynamic in absence of external inputs was not maintained in 3D cultures. The absence of NBs in 3D neuronal networks might indirectly indicate that neurons on the electrode plane received inputs from neurons of the upper layers of the structure, thus giving rise to a more heterogeneous network dynamic. In both 2D and 3D networks an oscillatory dynamic based on the quasi-synchronous activation of neurons on different electrodes (i.e. NSA) was observed, although with different characteristics (i.e. shape, composition, propagation). In particular, we found that NSAs propagated uniformly over the entire surface of the MEA in 2D neuronal networks, while in 3D the propagation was apparently discontinuous (as it propagates in the 3D space). Additionally, we found specific cluster of NSAs in the intralatency/ intra-distance plane in 2D networks. The fact that these clusters were cultures specific, suggests that NSAs characteristic are influenced by intrinsic proprieties of the network. We were able to record and describe an NSA event in all 2D culture, because these events were generated and propagated in the electrodes plane. In 3D neuronal networks, instead no specific clusters were present and longer propagation latencies of the signals (and intra-latencies in NSAs) have been observed. This is an indirect proof that signals propagate in the upper layers and indicates the formation of a functionally connected network. Indeed, we have already shown in a rodent model using the same scaffolding methodology (Frega et al., 2014) that longer propagation latencies and variable spontaneous activity were a convincing hallmark of the inherent contribution of the 3D structure to the network dynamics. As a whole, in this work we have shown a microbeads-based method for the generation of engineered h-iPSC-derived 3D excitatory neuronal networks coupled to planar MEAs for chronical evaluation of electrophysiological recording. Although the methodology to build 3D neuronal networks using microbeads as scaffold has been already presented (Pautot et al., 2008) (Frega et al., 2014, Tedesco et al., 2018) protocol adaptation for h-iPSCs-derived neurons is new, as it is novel the chronical electrophysiological analysis of these particular biological samples carried out with standard MEAs (i.e. MEA with 60 planar electrodes). Electrophysiological recordings of 3D structures have been already successfully performed with MEA devices. In particular, Trujillo and coworkers have shown that h-iPSCs-derived organoids exhibit activity with

features similar to the neonatal EEG (Trujillo et al., 2019). However, the combination of h-iPSCs-derived neurons and microbeads scaffolding allows to generate engineered neuronal networks with control over several culturing variables (i.e. cell type, density and ratio, volume, good reproducibility) which is still not possible with brain organoids. Unfortunately, the electrophysiological activity exhibited by neurons belonging to the inner layers of the structure is still a hurdle. However, new technologies allowing recordings at different heights are emerging. The most recent example is shown in (Shin et al., 2021) where a device capable of recording and stimulating different sites at different heights within their 3D hydrogel-based culture is presented. The use of such a device will allow to characterize the complex electrophysiological dynamics occurring in the core of the structure. The integration with our protocol would result in a more versatile system, since the inter porosity of the beads-method could guarantee the insertion of the 3D electrodes afterwards, without forcing the construction of the culture around the electrodes. The use of h-iPSCs has opened new perspectives to study neuronal disease *in-vitro*, allowing to obtain a human model system maintaining the genetic background of the donor. It has been shown that rodent neurons show functional divergences as compared to human neurons and that genes expressed in human neurons are not present in rodent (Napoli and Obeid, 2016), making it questionable the validity of such model system for human disease investigation. In our study, we also observed differences in activity when comparing human and rodent neurons organized in both 2D and 3D networks. In particular, human neuronal networks show a lower firing and (network) burst rate, a higher PRS and a longer (network) burst as compared to rodent cultures (figure 4.6). These results might indicate a slower human neuronal network maturation, as previously shown, and thus might be indicative of species-specific differences. However, the patterns observed can be associated with other aspects (i.e. different cellular composition and developmental stages), making a proper comparison of the two system not possible.

Conclusion

In this Chapter we presented a new experimental *in-vitro* platform constituted by 3D engineered neuronal cultures derived from h-iPSCs and coupled to MEAs. This experimental model offers control over cell type, cell ratio, and total volume of the network, allows good replicability and ensures chronical functional assessment of the electrophysiological activity. Although the use of chitosan microbeads as scaffolds had already been investigated, in this work we have integrated a neuronal differentiation protocol from iPSC, showing the possibility of creating a tissue that can be engineered from various points of view. Further and deeper characterization of these construct are needed to validate the model as possible valid approach for future brain-on-a-chip.

CHAPTER 5

V. THERMOGELLING BIOMIMETIC HYDROGEL SUPPORTING 3D NEURONAL NETWORKS

Data and images are an integration of the poster abstract presented by me at the TERMIS 2021 conference entitled "*Thermogelling biomimetic hydrogel supporting 3D neuronal networks"* submitted from Di Lisa et al.

Thanks to the strong collaboration with Bio3DMatrix it was possible for me to help develop a chitosan-based gel capable of supporting the correct development of a 3D neuronal network. Chitosan is a widely used biomaterial, well known for its good properties and in combination with basic compounds, becomes thermosensitive in diluted acids and can undergo gelation around body temperature. This thermogel was developed as an artificial matrix, to encapsulate neuronal cells and to support neuronal network development for *in-vitro* studies and as an injectable-hydrogel for the *in-vivo* applications or innovative ink. In this thesis some results regarding the characterization of the material performed by Bio3DMatrix will also be illustrated for completeness, but many details will be reserved as the formulation is patented. I contributed to the creation of neuronal networks and to the recording of their spontaneous electrical activity. The results, although preliminary, show excellent potential for this material to be used successfully in the field of tissue engineering.

Concept and rationale

Engineered natural biomaterials, able to perform the sol-gel transition in the presence of cells under specific external stimuli, have gained great attention in the field of tissue engineering and regenerative medicine (DeVolder and Kong, 2012), despite of this, for the encapsulation of neurons and the development of 3D neuronal networks, are still limited. In order to study neuronal (dys)functions and particularly neuronal connectivity, *in-vitro* human brain models need to include not only a chemically and physically relevant microenvironment, but also structural network complexity (Bastiaens et al., 2019). To mimic the brain ECM environment, a porous and soft structure is preferred in the design of an artificial neural network. The goal of this study was to demonstrate the versatility of thermosensitive chitosan-based scaffold as an artificial matrix for 3D neuronal networks for *in-vitro* studies and as an injectable-hydrogel for the *in-vivo* applications or innovative ink for 3D bioprinter. Chitosan is a widely used biomaterial, well known for its biocompatibility, biodegradability, muco-adhesiveness as well as its antibacterial activity (Kim et al., 2008). It is already demonstrated that

chitosan is able to sustain the development of 3D scaffold for neuronal networks (Muzzi et al., 2021a, Tedesco et al., 2018). In this work, chitosan thermogels were fabricated and characterized by different techniques. The scaffold was used to encapsulate primary rat neurons and human-induced neurons cultures to carry out morphological characterization by immunofluorescence techniques and a preliminary electrophysiological characterization of spontaneous activity by Micro-Electrode Arrays.

Materials and Methods

h-iPSCs and differentiation protocol

We used rtTa/*NgN2* positive h-iPCSs line. Cells weremaintained by culturing and expanding colonies of h-iPCSs in different wells of a 6 multi-well plate pre coated with Matrigel (Corning). We used Essential 8 Flex Medium (Thermo Fisher scientific) supplemented with 1% pen/strep (Sigma-Aldrich) and 50µg/ml G418 (Sigma-Aldrich) and 0.5 µg/ml puromycin (Sigma-Aldrich) to preserve the integrity of the cell line (Frega et al., 2017) (we will refer to this media composition as E8F maintaining media). Whenever a well reached confluency, we detached the cells maintaining the colonies using ReleSR (Stem Cell Technologies) and redistributing the harvested cells in other 3 wells. Cells were kept in incubator at 37°C 5.5% CO2 The specific h-iPSCs line allowed us to obtain excitatory cortical neurons thanks to the rtTa/*NgN2* alteration, by overexpressing the *NgN2* factor upon doxycycline treatment (4µg/ml). On the differentiation day (Day *in-vitro* = DIV 0), we chose a confluent well of h-iPSCs, we detached all the cell using ReleSR and we redistributed equally in other 2 well precoated with Matrigel. To ignite differentiation, we supplemented 4µg/ml doxycycline to the E8F maintaining media. The next day (DIV1) we replaced the medium with DMEM/F12 (Thermo Fisher Scientific) supplemented with 1% pen/strep, MEM non-essential amino acid solution 100x (Sigma Aldrich), 100x N2-supplement (Invitrogen), 10ng/ml human-NT-3 (BioConnect), 10ng/ml human-BDNF (BioConnect). During DIV2 medium is not changed unless cell death/detachment is observed. On DIV 3 we changed the medium formulation, using Neurobasal (thermo fisher scientific) supplemented with B-27 supplement (Invitrogen), 1% pen/strep, 4µg/ml Doxycycline, GlutaMAX (Invitrogen), 10ng/ml h-BDNF, 10ng/ml h-NT-3. We refer to this media composition as ‘complete neurobasal’. At this stage, cells are not proliferating anymore and, they can be considered as an early stage of neurons in which arborization starts to sprout. Consequently, we detached the early-stage neurons from wells using Accutase (Sigma Aldrich) and we collected the harvested neurons in a 15ml tubes containing 2ml of complete neurobasal. Cells were ready to be counted and to be used in co-colture with Astrocytes. We will refer to this tube as early neurons tube (eN tube).

Astrocytes cultures

To support fully functional maturation of early neurons we used cortical rat astrocytes obtained from embryos at 18 days (E18). Cells were supplied in frozen vials. Prior to the coculture with neurons, we thawed the vial and plated the astrocytes in t-75 flask using DMEM High Glucose (Invitrogen, Thermo Fisher Scientific) supplemented with 1% pen/strep and 10% Fetal Bovine Serum (FBS). After 7 to 10 days astrocytes should reach confluency. From that moment astrocytes can be harvested using trypsin-EDTA 0.05% (Invitrogen, Thermo Fisher Scientific) and collected in 2ml of complete neurobasal in a 15ml tube. Cells were ready to be counted and used in co-colture. We refer to this tube as astrocytes tube (As tube).

Thermogel preparation and Cells encapsulation

Chitosan (CHI) was purified following the method described by Qian and Glanville. CHI solutions of 2.5% (w/v) was prepared by dissolving purified CHI powder in 0.1 M acetic acid. The stirring was kept at room temperature overnight, and then the solutions were sterilized by autoclave at 120°C for 20 min and stored at 4°C. Consequently, the CHI solution was first mixed with βGP (Figure 5.1 a) to give to the gel the ability to reticulate at 37°C. In parallel, we took 1'250'000 neurons from the eN tube (previously described) and 1'250'000 astrocytes from the As tube, originating a new solution of cells in a 1:1 ratio. Thus, we centrifugate the cell solution (1200 rpm, 5 minutes) and we discarded the supernatant. Consequently, we resuspended the cells by adding 300µl of the CHI/ βGP solution to the cell pellet (figure 5.1 b) originating a thermogel solution of ~8'300'000 cell ml^{-1}. Finally, we deposited a 30ul drop of the cells-CHI/βGP solution on the PDMS mask previously attached on the active area of the MEA (Figure 5.1 d). MEAs were then stored in the incubator to ignite the thermogelling process and after 20 minutes we added 1ml of complete neurobasal medium. For the maintaince of the cultures, half of the medium was changed every two days and from DIV 7, complete medium was supplemented with 2.5% of FBS.

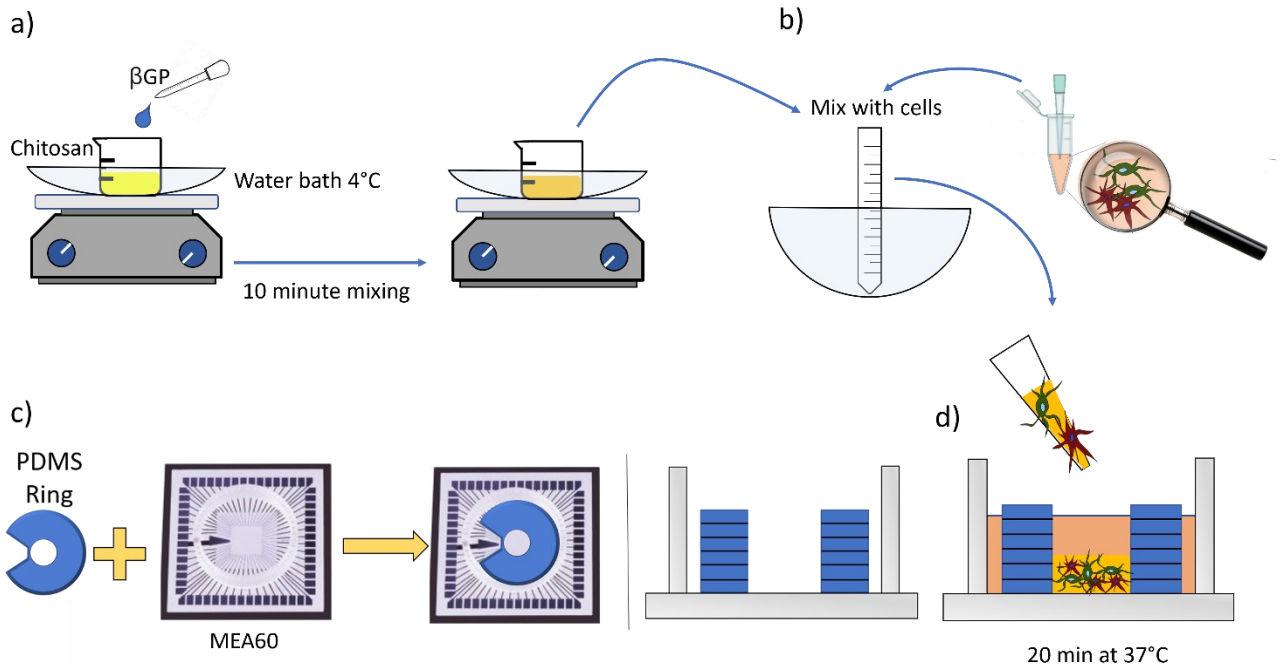

Figure 5.1. Overview of the main steps to generate 3D structure on MEA using a chitosan thermogel. **a)** We added βGP to the chitosan solution in a cold bath to avoid premature gelling. **b)** we mixed cells with the CHI/ βGP to originate our mother solution for the 3D network. **c)** Represent the shape of the PDMS mask previously attached on the MEA that is used to confine the d) 30uL drops of the cells- CHI/βGP solution that will start the reticulation at 37°C.

Mechanical characterization

The dynamic mechanical compressive analysis (DMA) was performed with home-made apparatus with frequency range between 1-100 Hz with pre strain of 10 % at room temperature. The tests were carried out on samples with cells. Injectability tests was performed by using load cell of 500 N and speed 200 mm/min in a physiological solution at 37° C.1 ml syringe with a needle (Ø 1mm) was loaded with gel prewarmed at 37°C for 5 min.

SEM characterization

The hydrogels were then kept in liquid nitrogen overnight and freeze-dried under vacuum for 24 h. Each sample was coated with gold layer before analysis. The analysis was performed with SEM Hitachi S-2005 in SE.

Electrophysiological recordings and data analysis

Standard MEA-60 and 3D MEA60 (MultiChannel System) were used to record the electrophysiological activity of neuronal network. The MEA60 are glass devices in which 60 titaniun nitride electrodes are embedded at the center of the culture well. They are arranged in a 8x8 grid without electrodes at the corner, spaced 200µm among them with 30µm diameter, generating an

active area of 1,6mm x 1,6mm (Figure 5.1 c). The 3D MEA60 have the same spatial organization of the electrodes, with the difference that electrodes are 250µm spaced among them and the electrodes are pyramidal with 100µm height and 12um diameter tip (Figure 5.1 c). Devices were sterilized in the hoven at 120°C for 2h. Therefore, we applied PDMS mask on the MEA to confine the 3D neuronal network. Confinement structures were fabricated with a standard 1:10 ratio between curing agent and elastomer. After mixing the components, we deposited a thin layer of PDMS onto a petri dish. Consequently, we started the curing treatment by placing the dish in the oven at 70 ◦C for 40 min. Therefore, we obtained a stick layer of PDMS (height ≈ 1 mm) from which we obtained several PDMS rings. We used two different punchers to cut the PDMS into rings (inner diameter = 3 mm; thickness = 1 mm) and we used a cutter to manually remove a slice of the ring (figure 5.1c) to let the reference electrode of the MEAs uncovered. All these rings were washed, sterilized in 70% ethanol, dried and placed onto sterile and dried MEAs. We used sterile tweezer to place the ring in the correct position and adhesion was achieved thanks to the stickiness of the cured PDMS. Consequently devices were coated with a solution containing a mixture of 100ug/ml PLO and 20ug/ml human laminin.

The electrophysiological activity was acquired with the 2100 System (MEA 2100-System, MCS) and signals were sampled at 10 kHz at different DIVs. During the recording, sterility was maintained using an autoclavable cap on top of the MEA chamber while normal conditions were maintained by pre-heating the head stage at 37 ◦C and by delivering humidified air with 5.5% CO2 over the MEA thanks to a plastic box placed on top of the recording system. Recordings lasted 15 min and data were analyzed offline using MATLAB (The Mathworks) scripts.

Immunofluorescence

The immunocytochemistry characterization was carried out to assess the expression of specific neuronal markers, MAP-2 for neuronal cells and DAPI for nucleus. An Olympus BX-51 upright microscope was used for immunofluorescence evaluation of the biological samples.

Results

Mechanical characterization

CHI thermogelling solution was mixed with the cell suspension and let to gel in round PDMS molds with 5 mm of diameter and 1 mm of height (Figure 5.2 b). The Elastic Modulus measured by DMA at DIV20 were found to be 12.7 kPa CHI thermogel with cells and 12 kPa without (Figure 5.2 a), which are comparable with the elastic modulus values of brain tissue. Before cell encapsulation, thermogels were morphological characterized by SEM measurements in

order to check their porosity. Figure 5.2 shows an adequate and homogenous porosity for cell seeding and penetration for both thermogels, which was found to have an average pore diameter of 20 μm. We then monitored the gelation time after the mixing of the CHI solution with the proper amount of βGP. We found a complete gelation after 13 minutes of incubation.

a)

E'(kPa)	w/o cells		with cells	
2.5%	DIV1	DIV20	DIV1	DIV20
	5,3± 2,3	12,7±2,5	3,7±0,8	12 ±1,5

b)

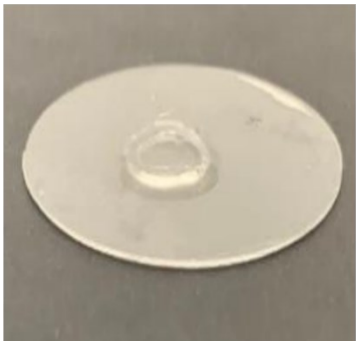

c)

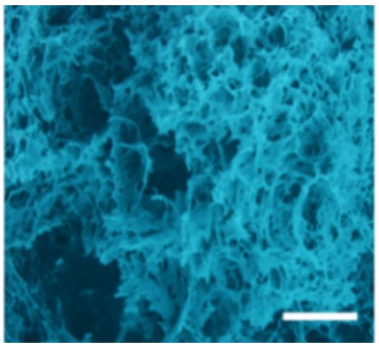

Figure 5.2. a) table showing the result of the elastic modulus evaluated thanks to dynamic compressive analysis of the gel at different DIVs carried with and without cells. **b)** shape of the gel after gelation in the PDMS mold. **c)** SEM image of the gel, scale bar represent 50um.

Chitosan thermogel promote the development of functional 3D neuronal network

The immunocytochemistry and confocal microscopy characterization allowed us to gain information on the morphology of the 3D structure of mature neuronal networks after 42 days of culture. We can see in figure 5.3 that neurons (in green) and astrocytes (in red) were homogeneously distributed onto the thermogel and they created a very 3D dense networks. Regarding cell morphology, the neuronal somata were found to be round, like the ones observed in the brain tissue. The astrocyte glial fraction also proliferates its morphology was again similar to the one found in brain tissue (i.e., having a thin morphology and expression in GFAP).

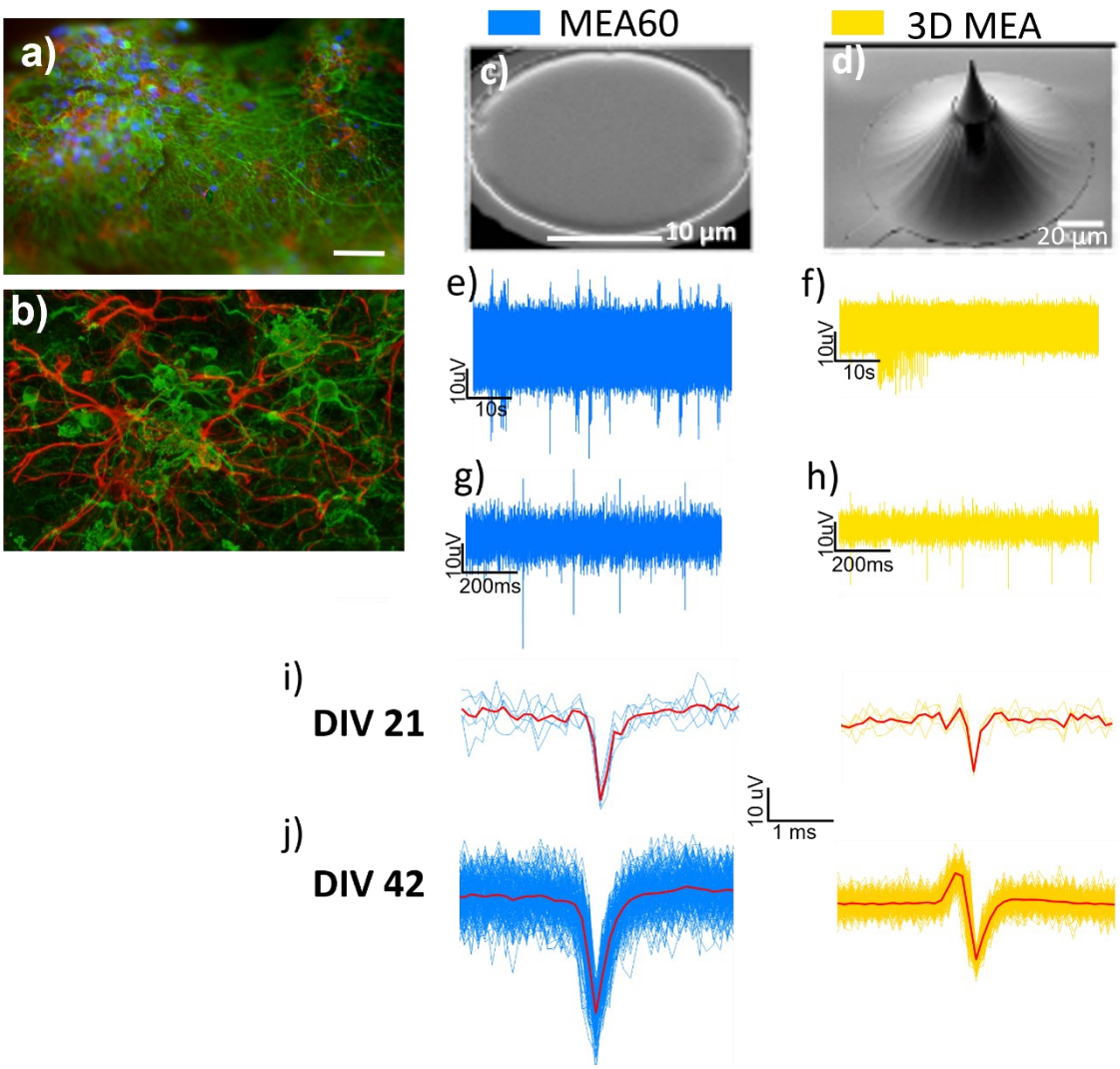

Figure 5.3 a,b) Picture acquired at DIV 42 showing the network formed on a) the surface of the gel and b) inner part. In green we have the neurons (MAP-2) and in red we have astrocytes (GFAP). Scale bar represent 100um. **C,d)** Shows SEM images of the electrodes shape for respectively MEA60 and 3D MEA. e-f) Represent 1 minute of spontaneous activity from MEA60 (in blue) and 3D MEA (in yellow), while **g,h)** are a zoom in of 1s of the same raw activity. **I,j)** Shows all the action potentials recorded from the same electrodes and they mean shape (red line), respectively at DIV21 and DIV42.

Cultures grown on MEA devices expressed spontaneous electrophysiological activity from DIV 24. Unfortunately, the number of active electrodes was extremely low throughout the observation period. Figure 5.3 report the raw signal recorded by an electrode of MEA60 and MEA3D at DIV42, where we can see the presence of bursts. In the i-j panels of the same figure we have reported the waveforms recorded by the same electrodes at DIV24 and DIV42. It can be seen how the number of spikes increases as the width of the peak of the average shape increases.

Discussion

Biomaterials are being utilized to develop biomimetic, pro-regenerative constructs in the form of 3D scaffolds to augment functional neural tissue (brain tissue) repair and regeneration. In particular,

engineered natural biomaterials, able to perform the sol-gel transition in the presence of cells under specific external stimuli, have been proposed. The great interest in these stimuli responsive hydrogels relays in the possibility to encapsulate cells, in their application as inks in 3D bioprinting and in them *in-vivo* injectability for repair or regeneration. In this work, thermogel was developed as an artificial matrix, to encapsulate neuronal cells and to support neuronal network development for *in-vitro* studies and as an injectable-hydrogel for the *in-vivo* applications or innovative ink. CHI is a widely used biomaterial, well known for its good properties. This polysaccharide in combination with basic compounds, such as β-glycerol phosphate (βGP), becomes thermosensitive in diluted acids and can undergo gelation around body temperature. In particular, their temperature-dependent gelation mechanism was found to involve the heat-induced transfer of protons from CHI to glycerol phosphate, which reduces the repulsive forces among positively charged ammonium groups and allows interaction of CHI chains. After CHI purification and sterilization, CHI/ βGP thermogels were prepared at 4°C by mixing sterilized CHI solutions with sterilized βGP gelling agent solutions added drop by drop. All the hydrogels had a final concentration of 2.5% (w/v) chitosan. 3D neuronal cultures were obtained by adding iNeurons mixed with cortical astrocytes (ratio 1:1) CHI/βGP solution. Through the rheological characterization, we obtain that gel start the gelation process at 32° C and the complete gelation was observed after 20 minutes. The mechanical characterization of the gels with and without cells was carried out one day after the sample preparation and after 21 days *in-vitro*. The obtained results show an increase of the elastic modulus over time both with and without cells. We note how the presence of cells tends to decrease the average of the elastic modulus of the gel, especially in the initial phases during network formation. In fact, at DIV1 E 'with cells measures 3.7 kPa while without cells it measures 5.3kPa. At DIV21, on the other hand, a smaller difference in the mean of the elastic modulus is observed, but we have detected a greater variability of measurement in gels without cells. This can be explained by the fact that the cells as they grow interconnect with each other creating a dense network that passes through the micropores of the gel, changing its mechanical properties. However, the results obtained relating to the elastic modulus are in line with the values obtained from the brain *in-vivo*. Thanks to the SEM analysis we reported an internal microporosity with pores having an average diameter of 20um. This allows the correct encapsulation of the cells and ensures proper development of the arborizations within the scaffold. Indeed, the images acquired using the immunofluorescence technique show us how a dense network composed of neurons and astrocytes homogeneously distributed throughout the gel. We can also note how the body of the cells actually appears spherical and the neuronal and astrocytic arborizations branch out in all directions, creating a full-fledged 3D network. Functional analysis using MEA devices led to few results as the number of active electrodes per device was less than 2 for all the monitoring of the

experiments. We think that the low number of electrodes is merely due to a probabilistic discourse that a correct cell / electrode contact is formed. In fact, as regards the MEA60, the electrodes are all planar and at the bottom level of the culture chamber. It is therefore difficult to have cells that adhere to the electrode plane and that are part of the network encapsulated in the gel. In fact at the time of plating, cells do not immediately precipitate to the bottom but remain suspended at different heights due the viscous nature of the gel, guaranteeing the formation of a 3D network. The same goes for 3D electrodes. Although these are internal to the gel once solidified, they do not necessarily come into contact with a cell that produces action potentials. Furthermore, in order to record spontaneous activity, not only the electrode must come into contact with the cell, but it must also adhere and develop synapses on it. A possible solution to better investigate the electrophysiological activity would be to use high-density 3D electrodes, or try to create gels with a much higher cell density. Although we did not find enough spontaneous activity to give a characterization at the level of firing parameters, it was possible to follow the development of the shape of the action potential where it was recorded. Figure 5.3 in fact shows how from both devices it was possible to record action potentials and from panels g-h) we can see the presence of bursting phenomena, a signal of functional neuronal maturation. We also wanted to show all the waveforms recorded by the same electrode at DIV21 and DIV42 (figure 5.3 I,j) to highlight how over time the firing and the peak of the average form of the AP increased, a signal that the cell was able to develop functional synapses on the electrode.

These results taken together suggest a great potential for this type of thermogel, as it is extremely easy and quick to use, is suitable for neuronal cell encapsulations, being able to sustain the viability and the growth in order to obtain a very biomimetic system. In particular, the injectability (data not showed) tests confirmed that the formulation is potentially usable for minimally invasive *in-vivo* applications and may thus represents alternative ink for 3D bioprinter.

Conclusion

In this chapter I wanted to show the first results that served to characterize this particular gel formulation, now patented. We have shown the potential of this gel in the field of tissue engineering by showing how it is able to correctly support the development of a long-term neuronal network even using cells generated by h-iPSCs. In this case we were unable to fully characterize the spontaneous electrophysiological activity during development, but we were still able to record functional activity protracted over time, sign of the vitality of the culture. Future experiments will be aimed to develop a protocol that is able to guarantee a multi-electrode recording of spontaneous activity, trying to use probes normally used for *in-vivo* or, if technology allows, high-density array of 3D electrodes. Thanks

to its mechanical properties, the gel is also suitable as a bio-ink, increasing the usability in tissue engineering.

CHAPTER 6

VI. HUMAN EXCITATORY CORTICAL NEUROSPHEROID ON MEA: A VALID PLATFORM FOR FUNCTIONAL TEST

All the data and images are taken from: "*Human excitatory cortical neurospheroid on MEA: a valid platform for functional test*" currently submitted to '*iScience*' journal.

After two approaches that involved the use of scaffolds to support the growth of a three-dimensional tissue, I investigated a type of approach that did not involve the use of synthetic ECM. In the literature there are different methodologies to produce 'organoids' *in-vitro* and the vast majority use the ability of stem cells (i.e. pluripotent or multipotent) to self-aggregate into spheroidal structures and then inducing the neuronal differentiation. This is useful for studying the developmental trajectories of the neurodevelopment, but the big drawbacks are related to the variability that affect the generation of these structures. As widely described in the introduction, protocol are usually time consuming, it is difficult to control the final cell composition and they suffers from inner necrosis. So, to obtain a model that was more easily controllable and decrease the variability of the final results, I exploited the adaptation of the rapid differentiation protocol to generate spheroidal cultures starting from already differentiated cells. I chose to use the hanging drop technique because it can be easily implemented in any laboratory as it does not require special instruments. Then I studied the development of their electrophysiological activity over time and for the first time I show results using three different types of MEA: with passive 3D electrode (3D MEA60), with planar electrodes (MEA60) and with C-MOS electrodes (HD-MEA). Additionally I investigated the effect of particular neuromodulators and electrical stimulation.

Concept and Rationale

The study of neuronal electrophysiological activity *in-vitro* proved to be fundamental for understanding the functioning of brain. Numerous studies have used monolayer neuronal cultures growing on micro-electrode arrays (MEA) to study how neuronal electrical activity is correlated to biological phenomena. Although these models are widely accepted, they are certainly an extreme simplification of the *in-vivo* situation. With the advent of human-induced pluripotent stem cells (h-iPSCs) and their differentiation protocols, methods to create human-derived 3D neuronal networks have been developed. In particular, neurospheroids and brain-organoids are becoming increasingly used for *in-vitro* disease modeling. Unfortunately, achieving control over the final cell composition of these structures and investigating the exhibited electrophysiological activity is still a challenge.

Here, we propose a method to generate neurospheroids of human origin in short time and with control over cell composition, and that can be used for functional investigations. We characterize the electrophysiological activity exhibited by the neurospheroids over time by using MEA with different spatial resolution and geometry. Finally, we investigated the effect of neuromodulators and electrical stimulation on neuronal activity. Our results showed that neurospheroids could be successfully grown in free culture and transferred on MEA and exhibited functional activity, indicating that this model holds great potential for different applications, ranging from in-depth study of signal transmission to drug screening and disease modeling.

Materials and Methods

Human induced pluripotent stem cells generation, maintenance and neuronal differentiation

We used a characterized rtTA/*NgN2* positive h-iPSC line generated from fibroblast of an healthy subject (30 year-old female) kindly provided in frozen vials by Frega *et al*.(Frega et al., 2017). This line was reprogrammed via episomal reprogramming (Coriell Institute for medical research, GM25256). Afterwards, rtTA/Ngn2-positive lentiviral vectors have been used to stably integrate the transgenes into the genome of the h-iPSCs. After rapid thawing, cells were plated on 6 well plate pre-coated with Matrigel (Corning) solution (1:15 in cold Dulbecco's Modified Eagle Medium (DMEM, Gibco, Thermofisher scientific inc.)) and cultured in Essential 8 Flex (E8F) Medium (Thermo Fisher scientific) supplemented with Essential 8 Flex supplement and 1% pen/strep (Thermofisher Scientific). The medium was also supplemented with 50 µg/ml G418 (Sigma-Aldrich) and 0.5 µg/ml puromycin (Sigma-Aldrich), selective antibiotic to preserve the purity of the cell line. Medium was refreshed every 2–3 days and cells were passaged twice per week using an enzyme-free reagent (ReLeSR, Stem Cell Technologies).

Neuronal differentiation and neurospheroid generation

Human iPSCs were directly derived into excitatory cortical Layer 2/3 neurons by overexpressing the neuronal determinant Neurogenin 2 (*NgN2*) upon doxycycline treatment as described previously (Frega et al., 2017). In particular, h-iPSCs were detached from a well after reaching confluence (6×10^6 cells) using ReleSR and a single-cell solution was obtained by collecting the colonies in 2 ml of "E8F+dox" medium (i.e. E8F medium supplemented with Essential 8 Flex supplement, 1% pen/strep, 50 µg/ml G418, 0.5 µg/ml puromycin and 4 µg/m doxycycline (Sigma-Aldrich)). Consequently, we added 1 ml of single-cell solution to Matrigel pre-coated wells in which 1 ml of "E8F+dox" medium was previously plated and we stored the plate into the incubator (Figure 6.1 a, Day 0). The next day (Figure 6.1 a, Day 1) we replaced the "E8F+dox" medium with DMEM/F12 (Gibco) supplemented

with MEM non-essential amino acid solution 100x (Sigma Aldrich), 100x N2-supplement (Invitrogen), 100x pens/strep, 10 ng/ml human-NT-3 (BioConnect), 10 ng/ml human-BDNF (BioConnect) and 1% pen/strep. At Day 3 cells (early-stage neurons) have reached confluence and are ready to be detached and used in co-culture with astrocytes. In particular, early-stage neurons were detached using Accutase (5 minutes at 37°C, StemPro) and cells were transferred into a 15 ml flacon tube containing 8 ml of Neurobasal medium (Gibco) supplemented with B-27 Supplement 50x (Gibco), GlutaMax 100x (Invitrogen), 5 µg/ml Doxycycline, 10 ng/ml h-BDNF 10 ng/ml h-NT-3, 100x pen/strep. After centrifugation (1200 rpm for 5 min), the supernatant was removed and the early-stage neurons were suspended in 2 ml of medium. Early-stage neurons are now ready to be counted and used in co-culture for the neurospheroid generation (Figure 6.1 b).

Neurospheroid were composed by 80'0000 early-stage neurons and astrocytes in 1:1 ratio. Astrocytes were obtained from brain cortices of day 18 embryos as described in Aprile et al. (Aprile et al., 2019) and are needed to support neuronal maturation. We choose to exploit the hanging drop method to generate spherical aggregates of cells and we used a 5 cm petri dish as 'moisture chamber' for the neurospheroid. We half-filled the petri dish with DPBS and we used the inner part of the lid as sustain for the drops of medium used as scaffold-free culture. In detail, we inverted the lid and we placed eight 15 µl drops of neurobasal medium into the inner part of the lid. Thereafter, we added 15 µl of the mixed-cells solution (i.e. solution of 5'330'000 cell/ml composed by 500'000 early neurons and 500'000 astrocytes) to each medium drops previously placed. Consequently, we placed the lid back on the petri dish with a gentle but rapid movement to avoid sliding of the drops. We then stored the dish into the incubator at 37°C and 5,5 $C0_2$. We consider this day as Day *in-vitro* (DIV 0) of the neurospheroid. On DIV 1 we added Ara-C (Sigma-Aldrich) to each drop to a final concentration of 2 µM (Figure 6.1 a, day 4). During the first week *in-vitro*, we added medium if evaporation occurred. From DIV 7 on, we replaced 10 µl of medium for each drop, paying attention to avoid damaging the forming neurospheroid. At DIV 10, neurospheroid were moved into 24 well-plates pre-coated with 1% w/v Alginate solution to avoid cell attachment and preserve the free-culture. From this moment on, medium was supplement with 2,5% of FBS and 30% of the medium was refreshed three times a week. At DIV 35, neurospheroid were moved into MEAs.

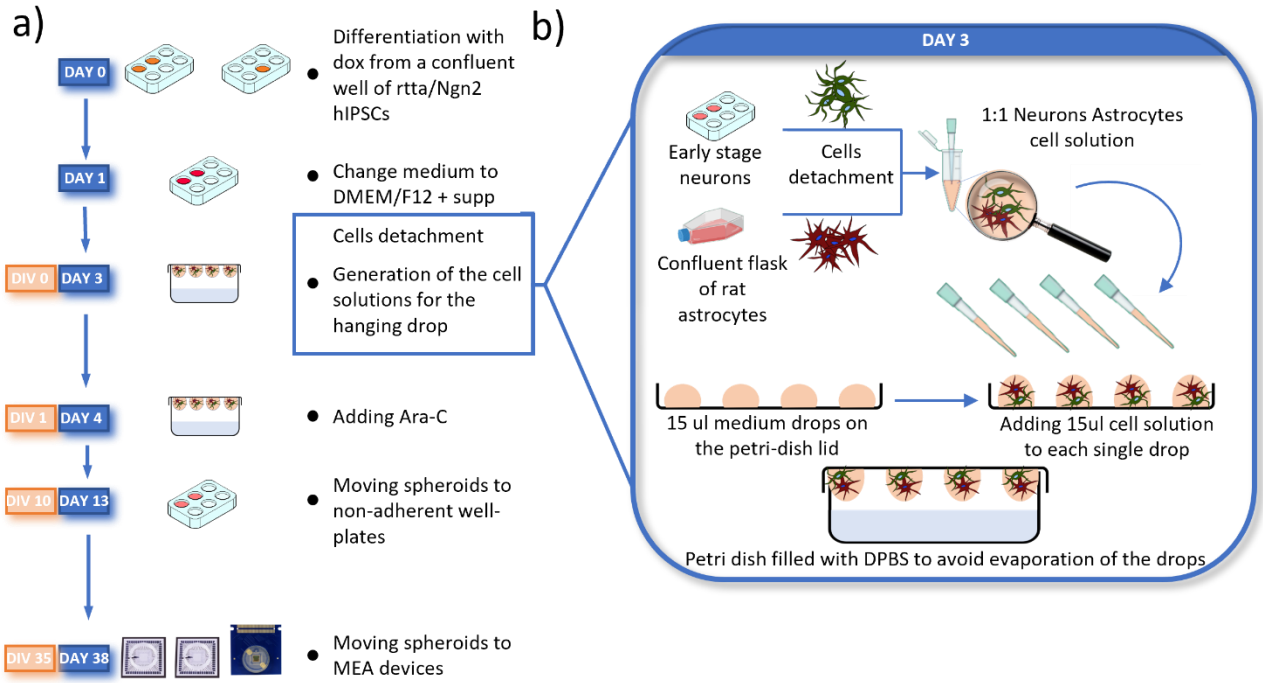

Figure 6.1. Overview of the differentiation steps and detail on neurospheroid generation. **a)** Timeline from the differentiation process to transfer to the MEAs. **b)** Focus on day 3/DIV 0 main steps, collection of cells and hanging drop technique. Early-stage neurons and astrocytes are harvested the same day in two separate tubes. Consequently, cells are counted and mixed in a 1:1 ratio in a 1 ml vial at a final concentration of 5'330'000 cell/ml. Therefore, we plated 15 µl of the cell suspension on the 15 µl medium drops in the lid of a petri-dish. Finally, we gently placed back the lid on the petri-dish bottom part half-filled with DPBS and then we stored everything in the incubator.

MEA devices

To evaluate the functional activity of the neurospheroids, we used MEA60 (Multi Channel System, MCS , GmbH), 3D MEA60 (Multi Channel System, MCS , GmbH) and Accura HD-MEA (3Brain AG, Switzerland). The MEA60 are glass devices in which 60 titaniun nitride electrodes are embedded at the center of the culture well. They are arranged in a 8x8 grid without electrodes at the corner, spaced 200 µm among them with 30 µm diameter, generating an active area of 1,6 mm x 1,6 mm. The 3D MEA60 have the same spatial organization of the electrodes, with the difference that electrodes are 250 µm spaced among them and are pyramidal with 100 µm height and 12 µm diameter tip. The HD-MEA (Accura model, 3Brain AG) devices present an active area of 3,8 mm x 3,8 mm in which 4096 C-MOS electrodes are allocated. Each microelectrode has a dimension of 21 µm x 21 µm with a 60 µm pitch, arranged in a 64x64 grid. Prior to the use, each device was cleaned and sterilized. In particular, MEA60 and 3D MEA60 were sterilized in the hoven at 120°C for 2h. The HD-MEA were cleaned with DPBS and the culture chamber was filled with 70% EtOH for 20 min for sterilization. After ethanol, the chambers were washed tree times with DPBS. Consequently, we left 2 ml of DPBS in each chamber and the devices were then stored in the incubator for 2 nights, to

improve hydrophilicity of the substrate (conditioning phase). After this phase, all the devices were coated with a bi-layer composed of poly-L-ornithine (PLO, Sigma-Aldrich) and human-laminin (BioConnect). More specifically, we deposited a 100 µl drop in the active area from a fresh solution of 50 µg/ml PLO in DBPS and we incubated the devices at 4°C overnight. The day after, we removed the drop containing PLO, we washed twice the chambers with DPBS, we deposited an 80 µl drop of 20 µg/ml human laminin in into the active area. Devices were then left overnight at 4°C, to be used the subsequent day.

Data acquisition and analysis

We recorded 10 minutes of full frame raw electrophysiological signals at DIV 42-49-56 using the 2100 System (MEA 2100-System,MCS) for the MEA60 and 3DMEA60 and the BioCam Duplex (3Brain AG) for the HD-MEAs. Data was sampled at 20 kHz. Incubator-like conditions were maintained during recording by keeping the culture at 37°C and 5.5% CO_2 in sterile conditions.

Spike detection. The Precise-Timing Spike Detection (PTSD) was used to detect the spikes (Maccione et al., 2009) Standard deviation factor (TH_{sd}) of 6 or 8 for passive MEAs and HD-MEA respectively, peak-lifetime period of 1ms, refractory period of 1ms and spike (spk) assigned to the higher peak were used as detection settings.

Mean firing rate. The Mean Firing Rate (MFR) was evaluated the for each electrode as the ratio between all the detected spikes and the recording time. We considered into the analysis only the 'active' electrodes exhibiting a MFR>0,1 spike/s.

Burst detection. we considered a burst as a series of 3 consecutive spikes firing no more than 50 ms apart from each other. The Mean Burst Rate (MBR) was evaluated as the sum of all the detected burst occurred in an active channel divided the recording time, and we considered bursting electrodes those having a MBR>0,2 burst/min. Mean Burst Duration (MBD) was evaluated by averaging all the burst duration detected in the whole culture. Therefore, we evaluated the percentage of random spikes (PRS) as the ratio between total number of non-burst spikes and total number of spikes. Similarly, we evaluated the percentage of bursting channels (PBC) as the ratio between bursting electrodes and active electrodes.

Raster plots. We generated rasterplots to show an overview of the total activity being recorded from each electrodes of the MEA. We represent the activity (i.e. dots indicating a spike detected) recorded from each included recording electrode (i.e. single line on the y-axis) during time (i.e. x-axis).

Network burst detection. Synchronous events occurring within the network, defined as *Network Bursts* (NBs) were detected as previously reported in (Muzzi et al., 2021a).

Post-Stimulus Time Histogram. To evaluate the electrical response, we computed the Post-Stimulus Time Histogram (PSTH) by counting all the detected spikes occurring after each stimulation in 10 ms bin. We then quantified the Fast response by counting all the evocated spikes occurring in the first 100 ms, the late response as the spikes occurred between 100 ms and 1000 ms and the peak latency as the time of the maximum activation. To normalize the PSTH, we obtained the Pre-stimulus time histograms by counting the detected spikes occurred 200 ms before each stimulation in 10 ms bins. We choose the mean value across bins in the Pre-stimulus time Histogram to obtain a normalization factor for each PSTH. Each normalized PSTH was then averaged across the 50-stimulation delivered in that culture and average across neurospheroid cultured on same MEAs.

Cross-Correlation. To evaluate possible functional connections between electrodes, we implemented a Cross-Correlation (CC) script in Matlab using a common normalization factor (Eytan et al., 2004). The cross correlation expresses the probability $Cxy(\tau)$ of observing a spike in one electrode y at time $(t + \tau)$, given that there was a spike in a reference electrode x at time t. We calculated the connectivity matrices by analyzing the correlograms obtained in a time window of 300 ms centered at time 0 and using a 0.2 ms bin. In order to eliminate the contribution of spurious connections we have applied a threshold to filter the connections based on their weight. The threshold was calculated as the average of the weights of the total connections plus 2 times the value of the standard deviation. Consequently, for each matrix we calculated the total number of links, their average weight and the average connection time τ (i.e. time lag). To reduce computational time we applied the CC algorithm to 144 electrodes arranged in a 12 x 12 square grid placed under the neurospheroid.

Signal propagation. To visualize the propagation of an action potential, we applied an avarage on the raw data of all the electrodes. First, we selected electrodes that have waveforms at least 300 μV peak, these will act as a reference (i.e. reference electrode). Then, we applied a spike sorting algorithm based on PCA and k-means clustering by defining units of different shape and width within the chosen channel. Consequently, for each unit, we obtained the timestamp (TS) corresponding to the highest peak and we aligned the shapes on TS, taking into consideration a time window of 10 ms. Similarly, for each other electrode we grouped and aligned the raw data on TS with the same time window. At this point we averaged all raw signals for each channel. The data obtained was then converted into *.brw* format to be displayed with BrainWave to search for proper action potential propagation. Whereas we correctly detected the propagation, we calculated the traveled distance of each propagation. To do this we identified the electrodes involved and we calculated the total distance traveled evaluated as the sum of the distances between consecutive electrodes in the propagation. Consequently, we calculated the average speed by taking the time difference between the first and last spike of the propagation divided by the total distance calculated as explained above. Data

recorded from MEA60 (and 3D MEA60) were analyzed using custom Matlab scripts, prior conversion to *hdf5* format using MultiChannel DataManager (MCS). Regarding the HD-MEA, BrainWave software (v.4.4, 3Brain AG) was used to high-pass filter the signal at 200 Hz using a 2nd order Butterworth filter and for the PTSD. Consequently, we used custom Matlab scripts to read results from the PTSD and the analysis proceed with Matlab script.

Electrical stimulation and neuromodulation

After the recordings performed during development (DIV 42—49 – 56), at DIV 57 functional tests on the neurospheroids were performed. We evaluated the effect of 3 neuromodulators, both in terms of spontaneous activity and in response to an electrical stimulation. The protocol we used includes 10 minutes of recording in spontaneous basal conditions, followed by a current stimulation protocol. Consequently, the cultures were treated with one of the neuromodulators and placed in the incubator for 30 minutes. After this time, we recorded 10 minutes the modulated spontaneous activity and then we applied the stimulation protocol again. Finally, we removed the neuromodulator from the sample by 3 consecutive washing steps in a previously conditioned medium and left the cultures to rest for at least 12 hours before testing the new drug. The neuromodulators used are 6-cyano-7-nitroquinoxaline-2,3-dione (CNQX, Sigma-Aldrich) 50 µM, D-(–)-2-Amino-5-phosphonopentanoic Acid (D-APV, Sigma-Aldrich) 80 µM, Kainic Acid (KA, Sigma-Aldrich) 5 µM. Stimulation protocol consist of injecting 50 bipolar pulses of current of 60 µA peak-to-peak amplitude, half-width of 100 µs, at 0,1 Hz from a pair of electrodes under the neurospheroid.

Immunofluorescence

After recording during development and characterization of neuronal response to neuromodulators and stimulation, samples were fixed directly on the HD-MEA at DIV 60 and we acquired fluorescence pictures. Samples were fixated for 20 min in 4% paraformaldehyde (PFA, Sigma-Aldrich) at room temperature and after 3 washing steps in Phosphate-buffered saline (PBS, Sigma-Aldrich) solution. Samples were permeabilized with 0,2% triton X-100 (Thermo Fisher Scientific) for 15 min. To block non-specific binding antibodies, we added a Blocking Buffer Solution (BBS, composed with 5% normal goat serum (Sigma-Aldrich), 1% bovine serum albumin (Sigma-Aldrich) in PBS) for 45 minutes at room temperature. We used GFAP (diluted 1:500, Sigma Aldrich) and MAP-2 (diluted 1:500, Chemicon Millipore) as primary antibodies to mark glial and neuronal cells, respectively. We used Alexa Fluor 488 (diluted 1:700, Thermo Fisher Scientific) and Alexa Fluor 546 (diluted 1:1000, Invitrogen) Goat anti mouse or Goat anti rabbit as secondary antibodies.

Statistical analysis

In this work we show data obtained from n=2 MEA60, n=2 3D MEA, n=2 3D HD-MEA. Statistical analysis was performed regard data obtained from active electrodes.After evaluation of normality test carried out with GraphPad Prism we performed non parametrical Wilcoxon signed-rank test. Differences were considered significant when $p<0.05$.

Results

Human iPSCs derived neurons aggregate into neurospheroids

First, we monitored the formation of the neurospheroids during time and we observed that h-iPSCs derived neurons started aggregating after about 10 days of culturing in the petri dish. When moved into free-cultures, the aggregates showed a spherical shape with a mean diameter of 412 ± 16 µm and 429 ± 20 µm at DIV 40 and DIV 62, respectively (Figure 6.2 a,b). Then, we investigated the formation of the neurospheroid on MEAs. Neurospheroid adhered to all MEAs and we observed that the height of the structure was lower than the mean diameter measured from the samples kept in free culture (Figure 6.2 c). In particular, we found that the highest point of the neurospheroid growing on a HD-MEA is at 180 µm from the electrode plane and that the diameter was ~550 µm (Figure 6.2 c,d). Furthermore, we observed that both neurons and astrocytes were present within the neurospheroids and that cells were viable in the inner part since nuclei were round and regular through the entire height of the structure (Figure 6.2 c,d and Supplementary videos 1).

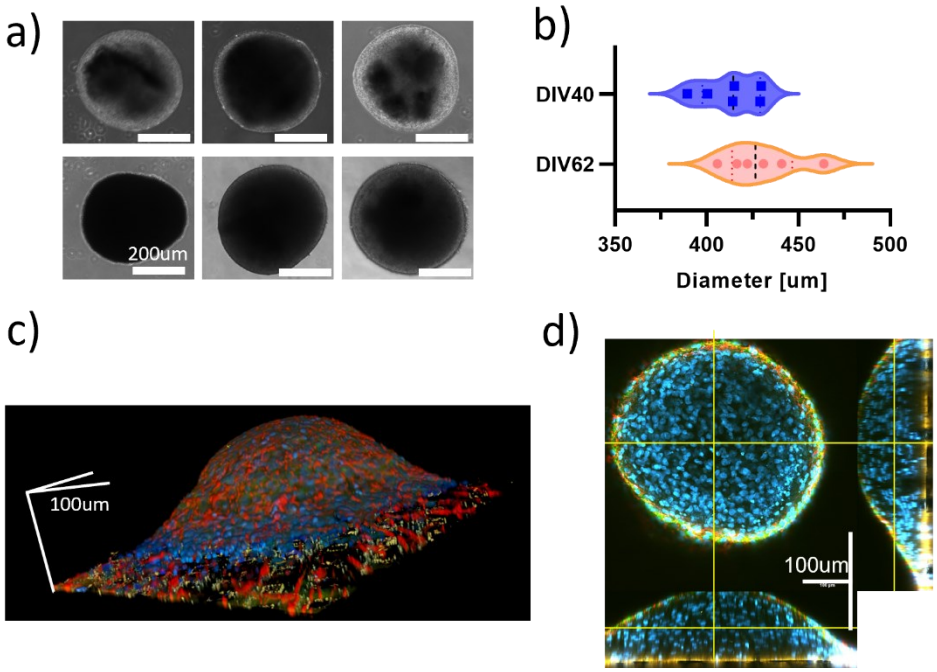

Figure 6.2. a) Images of different neurospheroids in free-culture during development. First row shows picture obtained at DIV40 and second row at DIV62. Scale bar 200 µm. **b)** Evaluation of the

mean diameter of N=6 neurospheroid at DIV40 and DIV62 in free culture. **c)** Reconstruction of the 3D volume of a spheroid plated on a HD-MEA at DIV35 and fixed at DIV62. Images were acquired with a confocal microscope using a z-stack of Scale bars represent 100 µm in each direction. **d)** Orthogonal view of the sample shown in b. Yellow lines represent the observation plane. In Blue: DAPI, Green: MAP2, red: GFAP. Scale bar represent 100 µm in each direction

Neurospheroids showed mature electrophysiological activity on MEAs

To evaluate the functionality of the neurospheroids at different resolutions, at DIV 35 we plated them into three types of MEAs having electrodes in different number and geometry (Figure 6.3 a-c). We observed that neurospheroids exhibited mature electrophysiological activity that could be detected by all devices at DIV 42. By comparing the raw data of a single electrode under the neurospheroid, we observed different levels of noise and spike amplitude. In particular, HD-MEA detects significantly larger waveforms as compared to the lower resolution devices. This fact combined with the higher resolution of the HD-MEA, allows to clearly identify the onset of network events (i.e. darker vertical bands in raster plots, Figure 6.3 g-i).

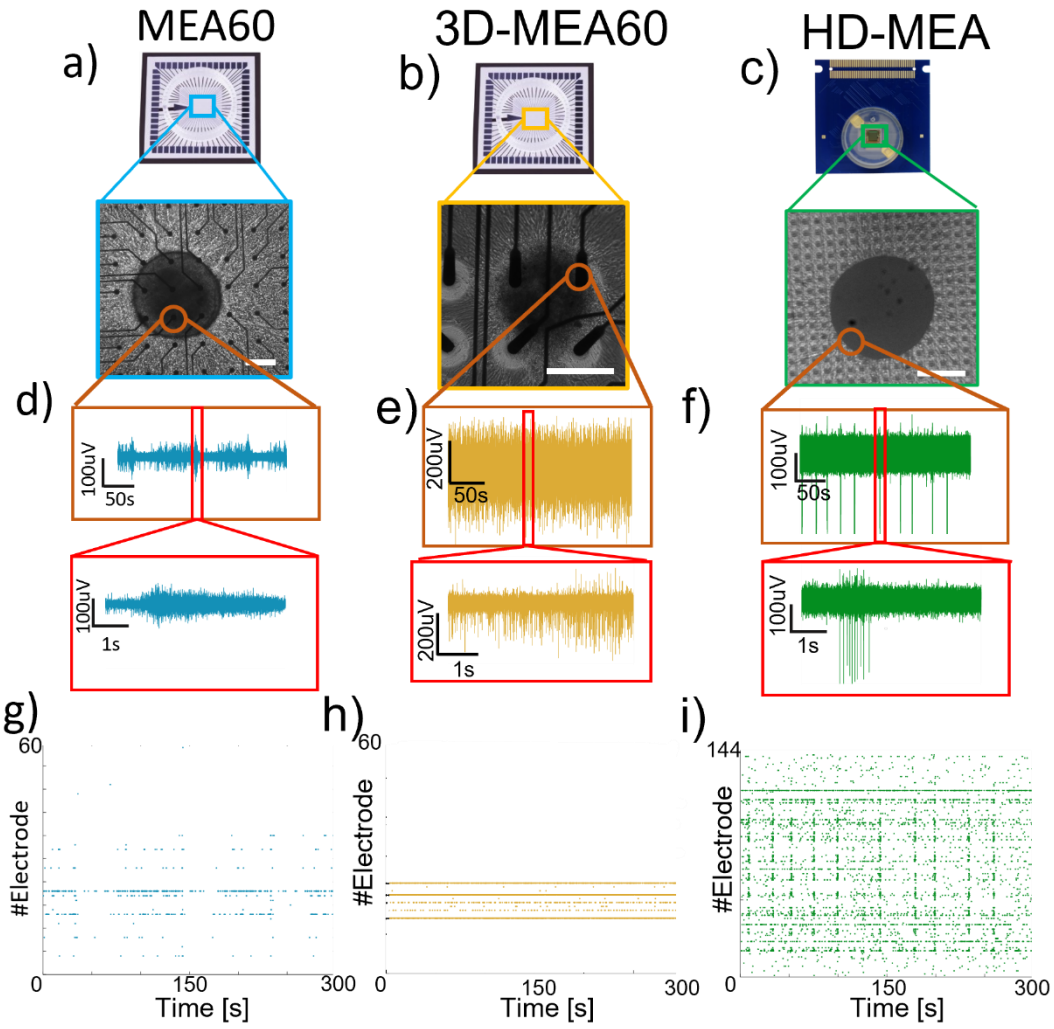

Figure 6.3. Qualitative comparison between activity recorded by MEA60, HD-MEA and 3D-MEA60. **a-c)** Picture showing a neurospheroid at DIV 49 on **a)** MEA60, **b)** 3D-MEA60, and **c)** HD-MEA. **d-f)** Raw data recorded by one electrode placed below the neurospheroid growing on **e)** MEA60, **f)** 3D-MEA60, and **g)** HD-MEA. 5 minute and 5 seconds of activity are shown in the orange and red box, respectively. **h-j)** Raster plot showing 5 minute of activity exhibited by a neurospheroid recorded by **h)** MEA60**, i)** 3D-MEA60, and **j)** HD-MEA. Each dot represents a detected spikes at the given electrode index (y axis).

We then followed the development of the neurospheroids by recording the spontaneous activity at different time point (DIV 42—49 – 56). We found that the number of active electrodes and other firing characteristics increased during time in cultures plated on HD-MEAs while they remain almost stable in the MEA60s (Figure 6.4 a-d). In all cases, we observed that activity evolved over time, moving from mainly random spiking to bursting. Indeed, percentage of random spikes (PRS) decreased over time while the percentage of active bursting channels increased (Figure 6.4 g,h). With all devices we were able to detect phenomena of synchronous network activity, although with the MEA60 and 3D-MEA60 they only emerged later in development (i.e. after DIV 42) and with a significantly lower frequency as compared to HD-MEA (Figure 6.4 e,i-k). Despite this, the duration of the NBs was comparable between the different devices (Figure 6.4 f). The average shapes of the network burst were similar for the three devices, but are very scattered in the case of the MEA60 and 3D-MEA60.

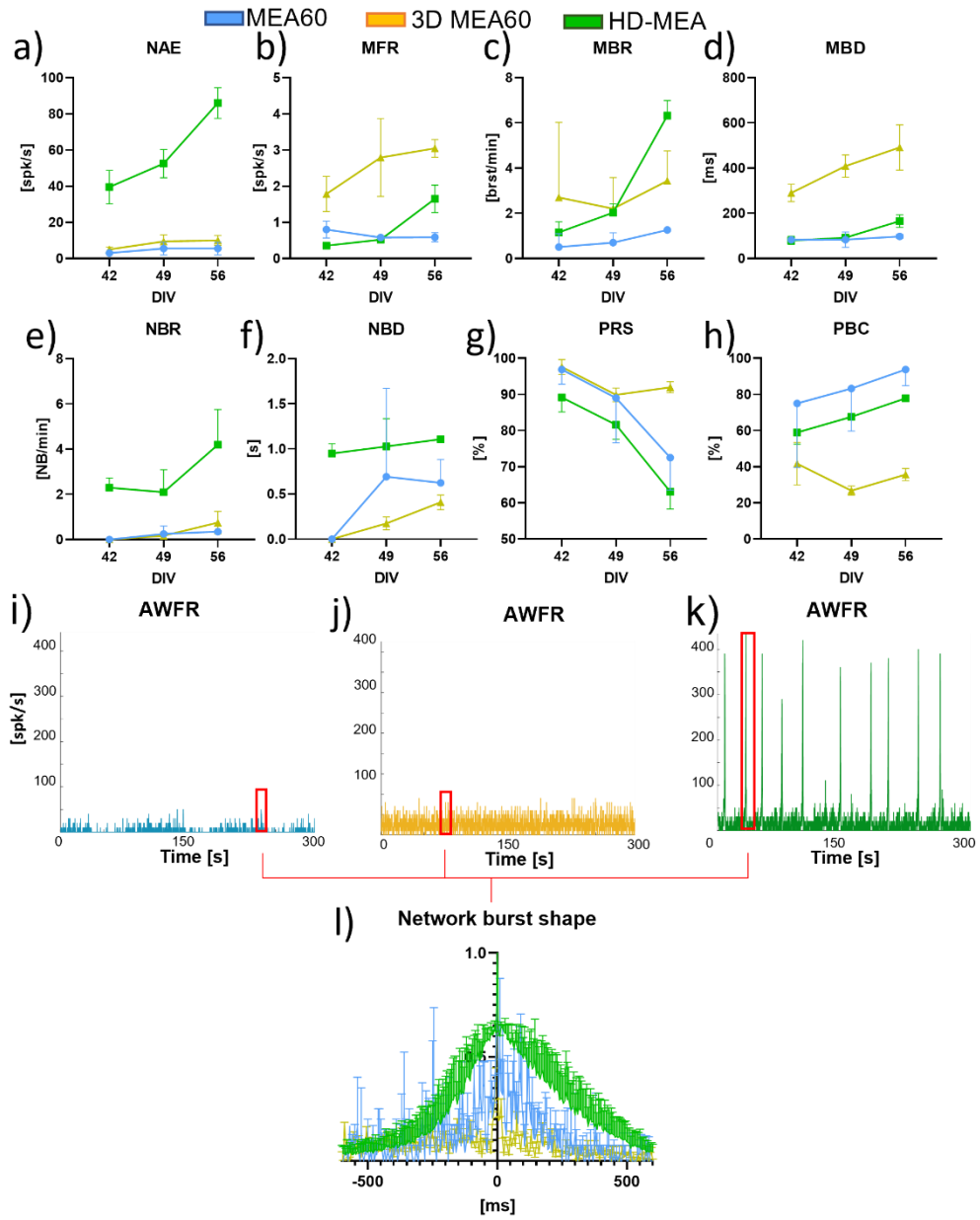

Figure 6.4. Analysis of the spontaneous activity of n=2 samples on MEA60 (data showed in blue), n=2 HD-MEA (data showed in green), n=2 3D-MEA (data showed in yellow). **a-h)** Graphs showing the **a)** number of active electrodes (NAE), **b)** Mean firing rate, **c)**, Mean bursting rate (MBR), **d)** Mean burst duration (MBD), **e)** Network burst rate (NBR), **f)** Network burst duration (NBD), **g)** Percentual random spikes (PRS), **h)** Percentual bursting channels (PBC). Data are shown as mean and standard deviation of the mean. **i-k)** Graphs showing the Array Wide Firing Rate in neurospheroids growing on **i)** MEA60, **j)** 3D-MEA60 and **k)** HD-MEA. It quantifies the level of activity as averaged firing rate of the all network evaluated in 100 ms bins. Network Burst (NB) are highlighted by red rectangles. **l)** Mean NB shape aligned and normalized by the higher peak.

Neuromodulation affects spontaneous activity and electrical induced activity

Once we verified that the samples were spontaneously active and mature (i.e. presence of network bursts), at DIV 60 we subjected the neurospheroids to stimulation conjugated with neuromodulation

protocols in order to evaluate the effects of three neuromodulators on functional activity (Figure 6.5). HD-MEAs resulted the most suited device to record electrophysiological activity thanks to the high spatial resolution and bigger signal to noise ratio acquisition. Therefore, we show results from these device but results MEA60s are available in the supplementary figure 5, while samples on 3D-MEA60 died after the first stimulation protocol. The inhibition of the AMPA receptors (CNQX 50 μM) led to a significant reduction of the mean firing rate and bursting rate (Figure 6.5 c,d). In addition, the synchronous network activity was suppressed (Figure 6.5 f,g) causing an increase in random activity and a significant decrease in active and bursting electrodes (Figure 6.5 a,h,i). As regards the effect on electrical stimulation, the response to stimuli in the presence of CNQX is slower as compared to basal condition (Figure 6.5 j, peak latency) with a significant reduction of evoked potentials in the first 100 ms following the application of the stimulus. The suppression of NMDA receptors (APV 80 μM) did not affect the number of active electrodes and did not significantly reduce the mean firing rate and mean bursting rate (Figure 6.5 c,d). The synchronous activity also remained almost unchanged while the random activity generally decreased (Figure 6.5 f,h). By evaluating the change in response to electrical stimulation, we found a significant delay in reaching the maximum response peak and a decrease in spikes evoked in the first 100 ms (figure 6.5 k). Finally, Kainic acid (5 μM) had a significant effect on the synchronous network activity, increasing its rate while maintaining a similar average duration of events (Figure 6.5 f,g). There was also a substantial decrease in active electrodes. Evaluating the response to the stimulus, the results showed an effect similar to that caused by CNQX, with an anticipation of the peak and a reduction in rapid evoked potentials, but it did not show significant differences regarding the late response phase (Figure 6.5 k).

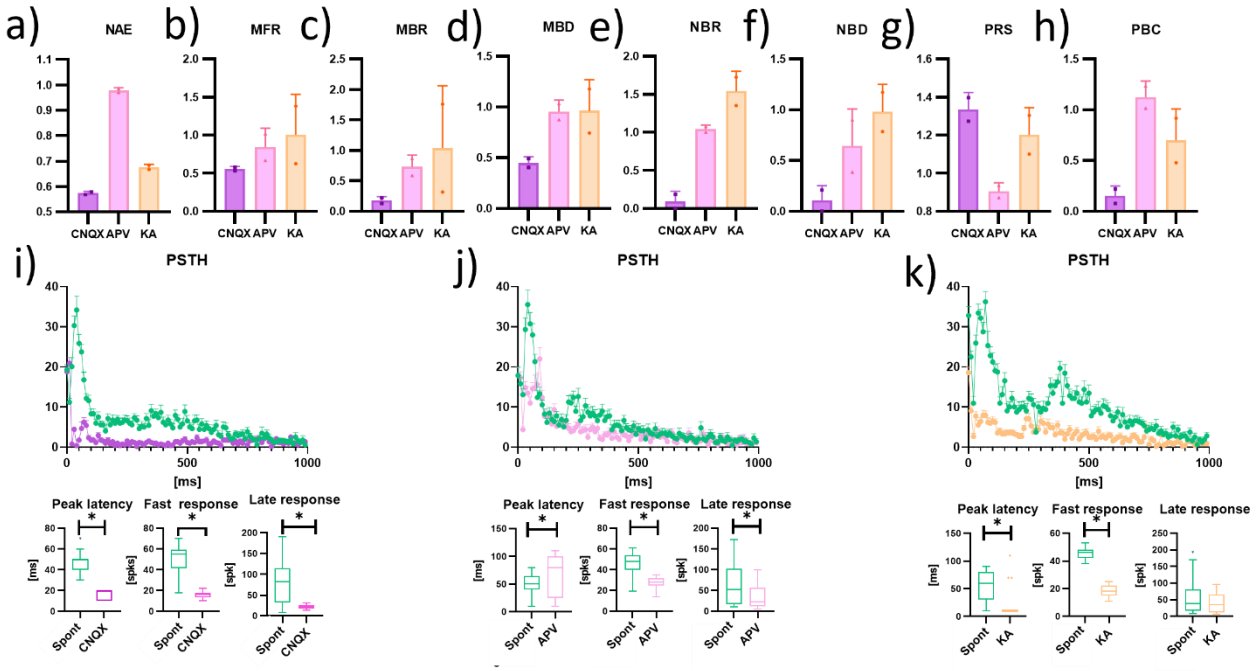

Figure 6.5. Evaluation of the electrical and chemical modulation (50 µM CNQX, 80 µM APV, and 5 µM KA). Data are obtained from experiments on HD-MEA (n = 2) and are normalized to the value detected in spontaneous conditions in the absence of drugs. Data obtained with MEA60 are reported in Supplementary Figure 1. **a-h)** Graphs showing the **a)** Number of active electrodes (NAE), **b)** Mean firing rate (MFR), **c)** Mean bursting Rate (MBR), **d)** Mean burst duration (MBD), **e)** Network burst rate (NBR), **f)** Network burst duration (NBD), **g)** Percentual random spikes (PRS), **h)** Percentual bursting channels (PBC) in neurospheroids treated with CNQX, APC and KA, represented int purple, pink and orange, respectively. Data are represented as mean and standard deviation of the mean. **i-k)** Graphs showing the effect of the modulation on the response to the electrical stimulus induced by **i)** CNQX, **j)** APV, **k)** KA. In each panel the Post-Stimulus Time Histogram (PSTH) showing the response of neurospheroids to stimulation is shown (not treated, treated with CNQX, APV and KA are represented in green, purple, pink and orange, respectively). The peak latency represent the mean latency to reach the maximum peak in the PSTHs, the fast response box plot represents the amount of evocated spikes in the first 100 ms of the PSTH while the late response box represent the amount of evocated spikes between 100 ms and 1000 ms.. Asterisk indicate $p<0.05$.

HD-MEAs allows for connectivity evaluation and action propagation tracking

To evaluate how neuromodulation and electrical stimulation affected the connectivity of the neurospheroids we performed cross-correlation analysis. We evaluate the CC of the neurospheroids under several condition. First, results indicate that inhibition of AMPA receptors with CNQX led to a decrease in the number of links and increase in the mean weight (Figure 6.6 b,c), while electrical stimulation led to an increase of the number of links and a slightly decrease in the mean weight (Figure 6.6 e,f). Comparison between electrical stimulation in spontaneous condition and CNQX stimulation led to a decrease in total number of links and increase in their mean weight (Figure 6.6 h,i The blockage of NMDA receptors with APV caused a less significative change of connectivity in the absence of stimulation. In this condition, the application of electrical stimulation leaded to a decrease of the number of links, an increase of their mean weight and a slightly reduction of the mean

lag. Comparing the stimulation under APV effect resulted in decreasing the number of link, increasing their mean weight and slightly decreasing thei mean lag (Figure 6.6 h-j). Finally, electrical stimulation after KA administration lead to a decrease in the number of links and a slight increase of their mean weight.

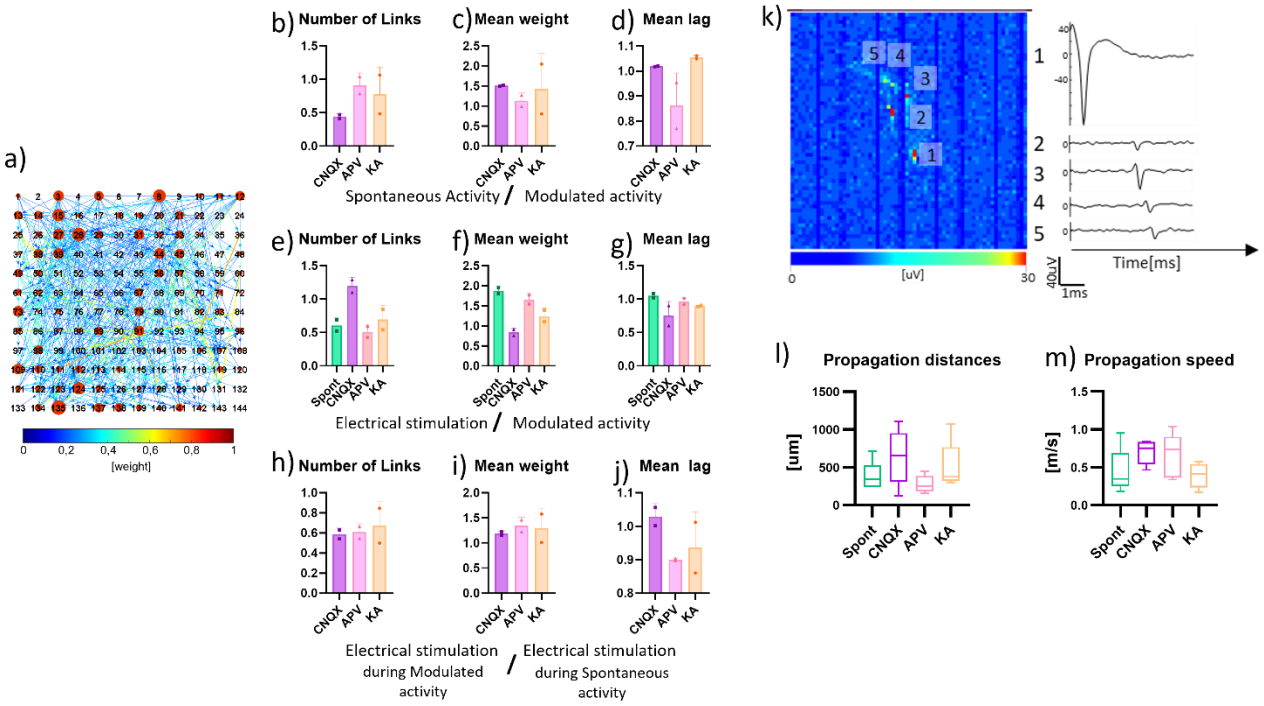

Figure 6.6. Neuronal connectivity and action propagation in neurospheroids. **a)** Connectivity matrix obtained from a neurospheroid grown on HD-MEA at DIV 57 during spontaneous basal activity. Each red circle represent an electrode, the bigger the size of the red circle the more link the electrode has. Colormap represent the weight of each link. **b-d)** Graphs showing the effect of neuromodulators on connectivity, in particular: **b)** number of links, **c)** mean weight and **d)** mean lag evaluated on 10 minutes of activity under the effects of the drugs, normalized on 10 minutes of spontaneous electrical activity without drug. **e-g)** Graphs showing the effect of electrical stimulation during neuromodulation on connectivity, in particular: **e)** number of links, **f)** mean weight and **g)** mean lag evaluated on 10 minutes of recording of spontaneous activity under the effects of the drugs (or no drug for electrical stimulation, labelled as Spont), normalized with data obtained from the recording during electrical stimulation in the same conditions. **h-j)** Graphs showing the effect of neuromodulation on during neuromodulation on connectivity, in particular: **h)** number of links, **i)** mean weight and **j)** mean lag evaluated during the electrical stimulation under the effect of the neuromodulator, normalized by the data obtained from recording during electrical stimulation without drugs. Bars represent mean value, point represent single experiments and errors are expressed using standard deviation.**k)** On the left, an image showing the activity detected by all channels of the HD-MEA is shown. In particular, each pixel in the panel represent an electrode on the active area of the HD-MEA and variation in color indicates the amplitude of the signal detected. On the right, voltage traces detected in five electrodes. Scale bar represent maximum variation of voltage in a 1 ms sliding window. Numbers represent the electrode considered. **l-m)** Graphs showing the **l)** mean propagation distances and **m)** mean propagation speed. Data represent the mean obtained from 10 different propagations.

Thanks to the high spatial resolution offered by the HD-MEA devices, it was possible to highlight, trace and estimate the speed of action potentials in the various experimental phases (Figure 6.6 k).

Under spontaneous conditions we found propagations covering mean lengths of 375 ± 194 μm with mean speeds of 0.44 ± 0.30 m/s (Figure 6.6 l,m). In the presence of CNQX, we estimated higher speeds with lower variability (0.7 ± 0.15 m/s) but over wider mean distances 636 ± 362 μm. In the presence of APV, on the other hand, we found shorter propagations (278 ± 112 μm), with an average velocity more similar to that estimated with CNQX but much more variable (0.65 ± 0.29 m/s). Finally, with KA we found average propagation lengths of 510 ± 300 μm with comparable and less varied velocity than in the normal condition (0.39 ± 0.16 m/s).

Discussion

In this article we presented a combination of various culture techniques to generate functional cortical excitatory human neurospheroids suitable for *in-vitro* functional investigation through MEA devices. We decided to exploit the rtTa / NgN2 positive h-iPSCs line because it is currently the only technique that allows the generation of a homogeneous population of cortical excitatory neurons that are mature and functional after only 5 weeks (Frega et al., 2019). Furthermore, by adapting the previous protocol, we were able to obtain greater control over the plating densities (Muzzi et al., 2021a). The fact of being able to generate a single population of neurons and to be able to combine them with a given ratio of astrocytes, proves the fact that the model might be used in combination with other rapid differentiation protocols (Mossink et al., 2021a, Yang et al., 2017) offering a broad spectrum of designability for highly engineered tissue. The use of the hanging-drop technique made it possible to generate the neurospheroids without the use of bioreactors or scaffold. We have noticed that the cells needed 7 to 10 days to form a spheroidal structure inside the drop. After 10 days, all the drops in the petri dishes contained solid and regular structures so we decided to move them to non-adherent multi-well plates. The main reason is due to the difficult maintenance of the neurospheroids in the hanging-drop condition. In particular, cells have small volume of medium available, they are easily subjected to evaporation and mechanical stresses could damage the viability of the 3D network. Once the structures were transferred to the plates, their maintenance proved to be much easier, however if not stirred from time to time, neurospheroids tended to become oval. Although we did not find significant size differences between the generated samples, we did notice a slight increase in size over time (see Figure 6.2 b). We think this is due to a proliferating astrocytic part, which recovered after the initial phases of aggregation of the spheroid where we treated it with Ara-C(Sivron et al., 1993, Horner and Palmer, 2003) . The shapes of the nuclei in the core of the spheroid are round and regular (from the z-stack) indicating that cells are healthy. This is an essential point in neurospheroid generation in which the core represents the most sensitive part because it is subjected to necrosis due to the lack of nutrient exchange (Qian et al., 2019). We also noticed how the samples adhered to the MEA devices

adapted their dimensions and preferred a radial growth on the substrate rather than preserving the spherical shape. In fact, after 30 days in culture we found a maximum height of the neurospheroid of 180 µm with a diameter of about 550 µm, thus suggesting a flattening of the structure on the electrode plane, also confirmed by the increased number of active electrodes in the MEAs.

To verify the functionality of the spheroid, we decided to monitor the development of spontaneous electrophysiological activity for 5 weeks (from the moment of adhesion to the device) on 3 different MEA devices. This allows us to investigate whether coupling these structures with MEA devices could constitute a valid 3D *in-vitro* model useful for functional characterizing. We used two types of MEA with passive electrodes, one with planar (MEA60) and one with 3D electrodes penetrating the structure and recording signals internally (3D-MEAs). In addition, to achieve a high-density spatial resolution for the recording of the electrophysiological activity and a higher signal to noise ratio we used an advanced device that exploit the C-MOS technology (HD-MEA). We moved the culture to the devices at DIV 35 because at this stage of development a mature and stable network dynamic had been observed in 2D and 3D (Tedesco et al., 2018, Frega et al., 2014, Izsak et al., 2019)(Muzzi et al., 2021). During the first few days after adhesion, we were unable to record activity. This was probably caused by the fact that cells must adhere to the electrode plane and develop synapses and functional connections before a signal can be picked up. After a week, we found active electrodes in all the devices and already a quite mature network dynamic, presenting single channel activity and burst. During time, the active bursting channels increase and PRS decrease, showing trends in line with the results of others 3D cultures in the literature (Tedesco et al., 2018, Frega et al., 2014, Izsak et al., 2019). During the recording weeks, several electrodes became active even far away from the neurospheroid. Many cells moved from the neurospheroid to the electrode plane creating a peripheral 2D network from which activity can be detected (see Figure 6.2). We observed differences in levels of firing rate recorded from different MEAs. This derives from the different nature and density of the electrodes. Considering MEA60s, passive electrodes are spaced 200 µm apart and therefore the number of electrodes used to record the neurospheroid is significantly lower than the HD-MEAs. The raw signal appears noiser compared to HD-MEAs making difficult to detect close spikes in moments of high synchronous activity such as network bursts. Consequently, lower electrode density with a lower Signal / Noie ratio led to a different quantification of the MBR, MBD and NBR in the passive MEAs.. Similar considerations also apply to 3D-MEAs with the difference that the active electrodes are located inside the spheroid and are therefore surrounded by cells in all directions. The presence of electrophysiological signal and the fact that we are able to detect NB is a further confirmation of the potential of these cultures to be used for functional tests (Mossink et al., 2021b). Once we verified that the neurospheroid was active and mature in electrophysiological terms, both internally and

externally, we evaluated its response to electrical stimuli in conjunction with neuromodulators. We tested three glutamate receptor modulators since the culture is composed of excitatory neurons only. Although we have performed these experiments on all the samples in each type of MEA, we have shown in the main text only the data obtained from the HD-MEAs because having a greater number of active electrodes allowed a more accurate analysis. Neurospheroid on 3D-MEAs detached after the application of the first stimulation protocol.. As stated in the 3D-MEAs manual "*due to the production process and the fine tip, there may be more variations in the electrode impedance, which is important for stimulation experiments, especially with current*". It is therefore possible that the actual stimulation current resulted higher than the set value, causing irremediable damage to the neurospherods.Since our spheroid is composed only of excitatory neurons we have used neuromodulators that interact with glutamatergic type receptors. CNQX and APV respectively inhibit AMPA and NMDA receptors which we know are the main mediators of the network activity of these culture (Frega et al., 2019).The administration of CNQX led to a radical change in the network dynamics of the neurospheroid. The spontaneous AMPA-inhibited activity showed a significant decrease in network properties compared to baseline, almost completely suppressing single-channel and network bursting activity. The inhibition of NMDA receptors alone did not affect significantly the spontaneous activity of the neruospheroids. The effect of the modulator is observed in a decrease of about 40% in the percentage of random spikes and a reduction in the average length of the Nework Bursts. This reflects the results of previous studies (Durens et al., 2020, Trujillo et al., 2019) in the literature where it was seen that NMDA and AMPA receptors are involved in the generation of single channel / network bursting and there is a balance between them that must be maintained to preserve the network dynamics (Heikkila et al., 2009, Odawara et al., 2018, Frega et al., 2019, Suresh et al., 2016).

Previous studies regarding the electrical response of dissociated cultured network (Chiappalone et al., 2008, Pan et al., 2009, Yvon et al., 2005, Eytan et al., 2003) shows that we can distinguish two phases of the electrical response. The first phase is called early response occur in the first 80 ms and it is related to the response of the subpopulation on neurons that are directly excited from the electrical stimulation. The late phase occurs after the 80 ms and was found to be mediated mainly from inhibitory connections that propagate the stimulation in all the network (Chiappalone et al., 2008, Pan et al., 2009, Yvon et al., 2005, Eytan et al., 2003). Here in our case, we have only excitatory neurons and we don't have the presence of GABAergic neurons but thanks to neuromodulation we can understand that the response to the stimulus is mainly mediated by AMPA receptors. In fact, AMPA receptors drive the fast dynamics, while on the contrary the NMDA receptors drive the slower dynamics (Rao and Finkbeiner, 2007, Yvon et al., 2005). Under the effect of CNQX the

neurospheroids modified the response to the electrical stimulus, not only by decreasing the amount of evocated spikes, but also by changing their response shape. The maximum response peak shifted below 20 ms, because only neurons in close contact with the stimulating electrodes were elicited and they were unable to communicate quickly with others, resulting in failing to mediate the response to the whole network. Following the APV treatment, response to the stimulus changes, finding a lower presence of evoked spikes in the first 100 ms and a delay in reaching the maximum peak. . The inhibition of spontaneous fast activity allows for a more precise extimation of propagation speeds and the identification of longer trajectories. This might be cause by the removal of the background noise coming from excitatory postsynaptic potentials, and therefore the average of the raw data centered on a single unit sorted into a channel was less influenced by the activity of other neurons in the surroundings (Bakkum et al., 2008).

Kainic acid is known to cause convulsions in *in-vivo* rats (Sperk, 1994) and cerebral cortex slices *in-vitro* and is it utilize to model epileptic-like events *in-vitro* (Vedunova et al., 2013) (Colombi et al., 2013) (Fisher and Alger, 1984, Odawara et al., 2016, Jimbo and Robinson, 2000, Avoli, 2014, Chai et al., 2014). Epileptic-like activity induced by KA are defined as intense initial bursts followed by repetitive after-discharges (Jimbo and Robinson, 2000, Odawara et al., 2018, Mzezewa et al., 2022). We then tested the effects of KA to verify the onset of epileptic-like events in the neurospheroid. The general effect of KA in our neurospheoid was a significant lowering of the number of active electrodes and a consistent increase in the Network Burst Rate. Furthermore, the response to the stimulus appeared flatter when compared to that in baseline conditions, and the response peak is squashed in the first 20 ms. These two aspects are in line with previous finding on 2D human-derive neuronal network even if we obtained opposite results (as regards MFR and MBR) in the two analyzed samples (Odawara et al., 2018, Mzezewa et al., 2022). The connectivity analysis revealed that the electrical stimulation during KA helped to strengthen the connections, by decreasing the number of link, increasing their weight and decreasing their lag. These results suggest that epileptic-like events can be successfully induced in our spheroid with KA but further studies are needed to confirm that this is a valid model for studying KA-induced seizures. In fact, all previous works vitro (Vedunova et al., 2013) (Colombi et al., 2013) (Fisher and Alger, 1984, Odawara et al., 2016, Jimbo and Robinson, 2000, Avoli, 2014, Chai et al., 2014) Epileptic-like activity induced by KA are defined as intense initial bursts followed by repetitive after-discharges (Jimbo and Robinson, 2000, Odawara et al., 2018, Mzezewa et al., 2022) have used KA in cultures where GABAergic neurons were present while we are describing, for the first time in our knowledge, the results deriving from a purely excitatory 3D culture (Mzezewa et al., 2022).

The study of the connectivity *in-vitro* is known to be essential to understand basic mechanism of memory and learning (Poli et al., 2016, Chiappalone et al., 2008, Sporns, 2018). HD-MEAs allowed us to evaluate for the first time the connectivity maps of neurospheroids *in-vitro*. The inhibition of AMPA receptors increased the disorganization of the network by increasing the number of connections and decreasing their weight., We noted that inhibiting fast transmission greatly decreases the number of connections and only those with heavier weights are preserved. The inhibition of NMDA receptors also led to a decrease in the number of links with an increase in the weight of the connections but in a less clear way. We also recorded a decrease in the average lag of these connections a clear sign that most connections under spontaneous conditions are fast connections mediated mainly by AMPA. The stimulation in the presence of APV instead led to a consolidation of the connections as the number of links decreased, preserving only the connections with the highest weight. This gives a further confirmation of how AMPA and NMDA receptors are also involved in the processes of plasticity and memory (Diering and Huganir, 2018, Haselmann et al., 2018, Collingridge, 1987, Li and Tsien, 2009, Rao and Finkbeiner, 2007) and makes our model usable also for this type of study(le Feber et al., 2010, Shahaf and Marom, 2001, Jimbo et al., 1998, Eytan et al., 2003).

Concluding, thanks to the combination of existing methodologies and technologies, we have shown how to generate cortical excitatory neurospheroids that can be potentially engineered at will, without the use of scaffolds or bioreactor. We showed that culture are easy to handle and suitable for the chronic recording of electrophysiological activity. We believe our work is important as we need development of rapid human-derived platforms for functional testing in order to model various biological aspects of the nervous system. This methodology allows to generate free 3D constructs that can be coupled to various tools for functional analysis (i.e. MEA) but also for gene and / or proteomic assays, without the need to use bioreactors or instruments in an incubator. the fact of generating the neurospheroid starting from differentiated cells instead of pluripotent allowed to generate structures with low variability regard dimension. Since stem cell-derived neurons often require very long maturation times, it is more convenient working with already differentiated cells. In addition development in a 3D conformation induces a morphology more similar to the *in-vivo* in the cells and neurospheroid can be handled and moved at will.

Conclusion

In this chapter we offered the first electrophysiological characterization of cortical excitatory neurospheroids. Our results showed that these structures are suitable for the study, characterization and modulation of electrophysiological activity. In addition, we established which tools are most

suitable for the collection of raw data in order to create a valid *in-vitro* model. The electrophysiological characterization of the spontaneous and modulated / stimulated activity in combination with confocal images indicated that the model presented holds great potential for different applications, ranging from in-depth study of signal transmission to drug screening and disease modeling.

VII. GENERAL CONCLUSION

Starting from an engineering background, I approached the world of neuroscience one step at a time. Already during the master's thesis, I had the opportunity to work directly with primary cortical rat cultures on MEA. I implemented an optogenetic closed-loop stimulation protocol to investigate about recovery mechanisms in an *in-vitro* model of the penumbra. These first experiments not only led me to the first publication but aroused in me the desire to start a research pathway in the neuroscience field.

During the first year of the PhD, I studied and learned the basic techniques to work with human-induced stem cell cultures correctly. The results from first experiments (i.e. adaptation of the rapid differentiation protocol for 3D cultures) gave me confidence and opened the collaboration with startups and companies such as Bio3DMatrix and 3Brain. The second year was particularly turbulent as it was characterized by the onset of the COVID-19 pandemic. Although many experiments have been postponed and / or canceled, I managed to participate to online conferences showing preliminary results while continuing to keep up to date on neuroscience. With the resumption of laboratory activities, during the third year I was able to design the final experiments that allowed me to collect the latest data to be able to publish articles in peer reviewed journals.

During these years I acquired knowledge and shown results regarding the generation of three-dimensional *in-vitro* models of human derived neuronal network. The first experiments, were focused on optimizing the rapid differentiation protocol proposed by Frega et al 2017 (Frega et al., 2017) in order to make it more suitable for the creation of three-dimensional engineered models. First results on 2D cultures, show that the modification to the differentiation protocol produces healthy and functional networks over time and we manage to have greater control over the final number of cells and the composition of the network. The modification to the protocol consisted in avoiding the seeding of h-iPSCs on the final substrate. By doing so, we had the opportunity to add astrocytic support (necessary for the long-term survival of neurons) from DIV 0, making the protocol also suitable for the construction of 3D structures.

The three approaches I presented for building 3D networks have different pros and cons and each will be more suited to modeling a particular phenomenon better than another. Considering the modular approach, the morphological architecture of the network does not properly represent a similar condition *in-vivo*. In fact, although the cell extensions extend in all directions, the cell bodies remain attached to the internal surfaces or microporosities of the beads. This model is particularly interesting from an engineering point of view. In fact, we could create very particular neuronal networks by having full control over various parameters chosen a priori by the user such as the size of the beads,

the number of cells attached to each and the total number of beads. Furthermore, the approach would also allow to functionalize the individual beads (i.e. addition of gold nano particles / barium titanate nanoparticles) offering the possibility of localized network modulation. This high degree of designability is restricted when compared to the methodology that use chitosan hydrogel but, it offer a higher ease of maintenance of the culture and a neuronal morphology more similar to that observed *in-vivo*. From a practical point of view, it is faster and easier to create 3D structures as it is only necessary to suspend cells in the hydrogel solution with the crosslinker. Contrary to the beads-method, where in the first days the network is very delicate as the single beads are not interconnected with each other, the cells in the hydrogel are encapsulated in a few minutes inside the thermogel creating a solid structure that is easier to maintain already at the DIV 0. Since this gel is extrudable from a needle, and thank to its biocompatibility, it can be considered as bioink. This property makes it an excellent candidate in the field of tissue engineering to print 2D or 3D cell patterns in order to build complex tissues. However, a limitation lies in the fact that it is necessary to have a very high number of cells in order to be able to actually use the gel and reach a cell density comparable to that *in-vivo*. This may have been the reason that led to having few active channels during electrophysiological recordings in our experiments, with both 2D and 3D electrodes. In fact, in neurospheroids we have a cell density comparable to the *in-vivo* and we had excellent recordings from all types of devices. Our neurospheroids differs from the so-called brain-organoids because our starting point are already differentiated cells. The starting point of the brain-organoids are agglomerations of stem cells from which differentiation is then initiated. This allows to observe the spatial organization trajectories of neurodevelopment, but in the long term, structures continue to increase their size over time and there is variability between batch of experiments. Our neurospheroids remain small in size and are functional for the entire duration of the observation. Although this approach compared to the other two presented in this thesis is the least 'customizable' from an engineering point of view (i.e., we can only change the initial number of cells that will make up the neurospheroid and the ratio), allows to generate structures that can be grown on normal low-adherence culture plates and move them to devices for functional tests when necessary. This constitute a versatile model especially useful for testing drugs as there will be no interactions with synthetic-ECM elements.

Each presented method offers different degrees of designability based on the type of biological phenomenon to be studied and / or reproduced *in-vitro*, allowing the generation of functional 3D neural network. The obtained results are perfectly placed in the current state of the art and show how we are successfully progressing towards the realization of human 3D brain-on-a-chip.

VIII. SUPPLEMENTARY FIGURES

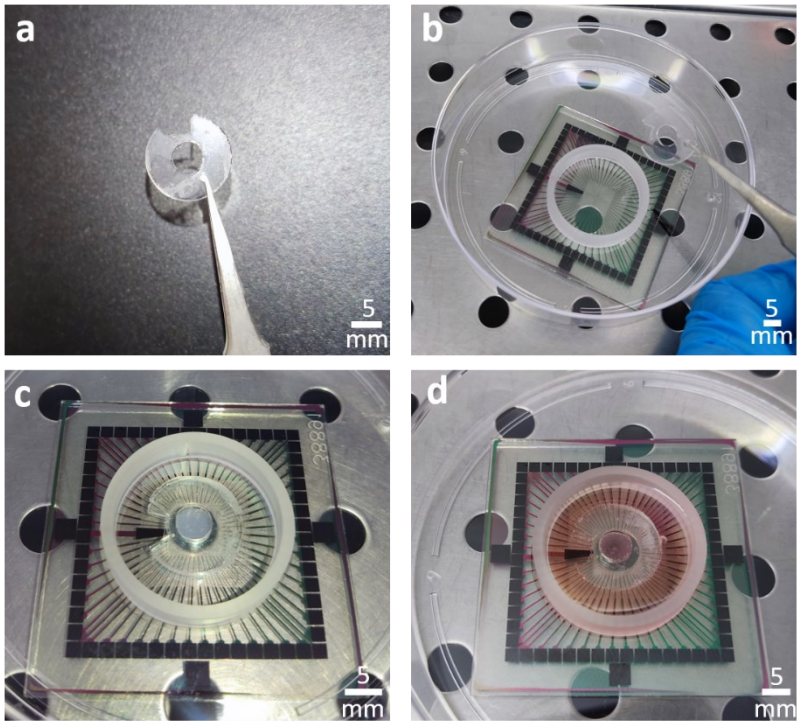

Suppl. Figure 1. PDMS and MEA structure assembly. **a)** A PDMS ring used to assembly the constraint for the chitosan microbeads. We cut a slice of the ring to avoid sealing of the reference electrode. **b)** positioning of the PDMS rings over the MEA. **c)** 40µl drops of the cells-beads solution are placed inside the assembled structure. The whitish substance in the center of the MEA are the beads. **d)** 3D culture on top of the MEA after 6 days.

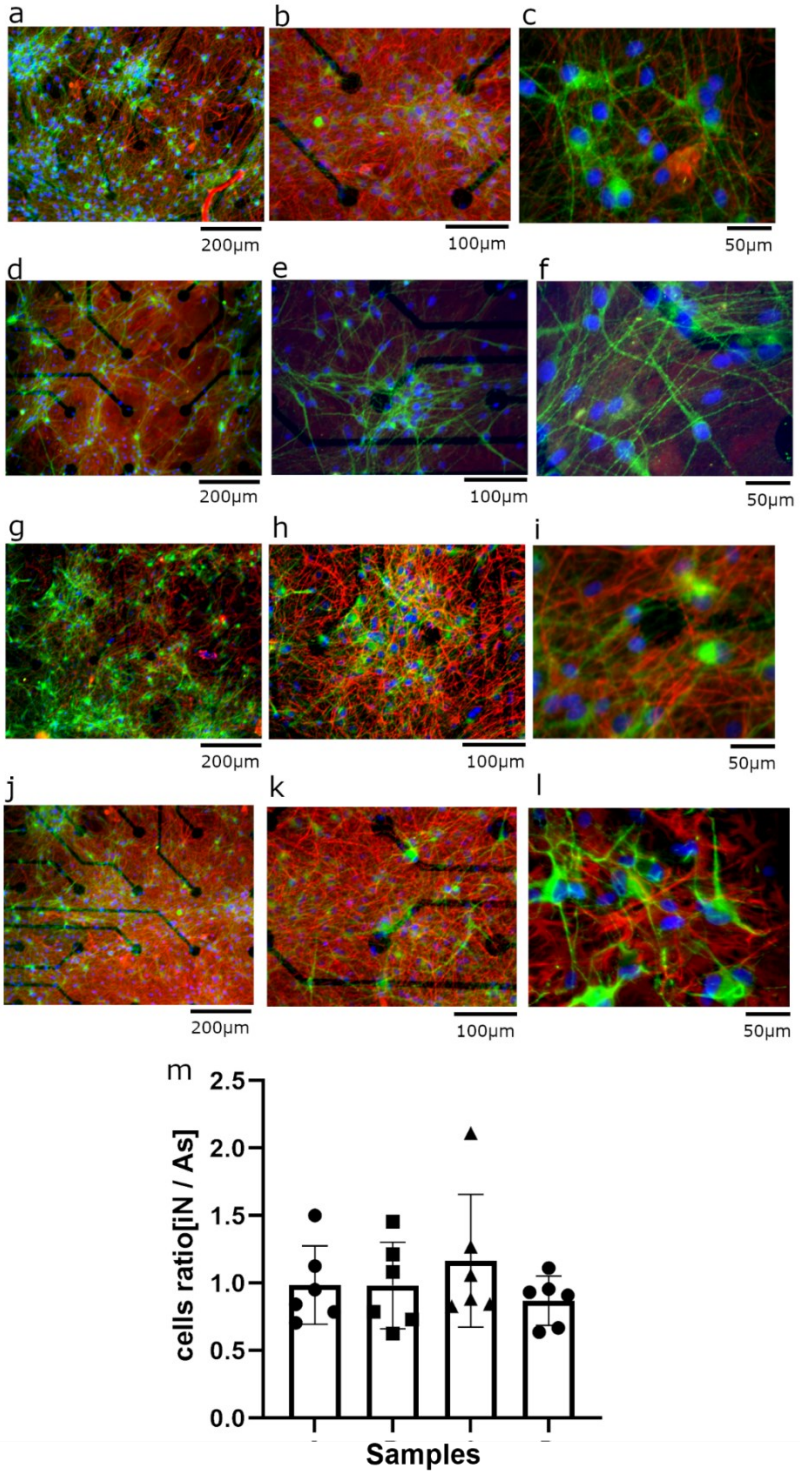

Suppl. Figure 2. Fluorescent images used for estimating the ratio between iN and rA. Each row starting from respectively panel **a-d-g-j** represent pictures of different samples. Columns shows three different magnifications of the same sample fixed at DIV42. **a-d-g-j)** Were acquired using 10x objective. Scale bars 200 µm. **b-e-h-k)** Were acquired using a 20x objective. Scale bars 100 µm. **c-f-i-l)** Were acquired using a 50x objective. Scale bars 50 µm. Green: MAP-2, Red: GFAP, Blue: DAPI. **m)** Shows the quantification of the iN:rA ratio obtained from the samples. We choose six different 0,4 mm^2 areas from the showed picture and we evaluated the iN:rA ratio by manual counting the co-localization of nuclei with either MAP-2 or GFAP. Points represent ratio in different areas, bars show mean and standard deviation.

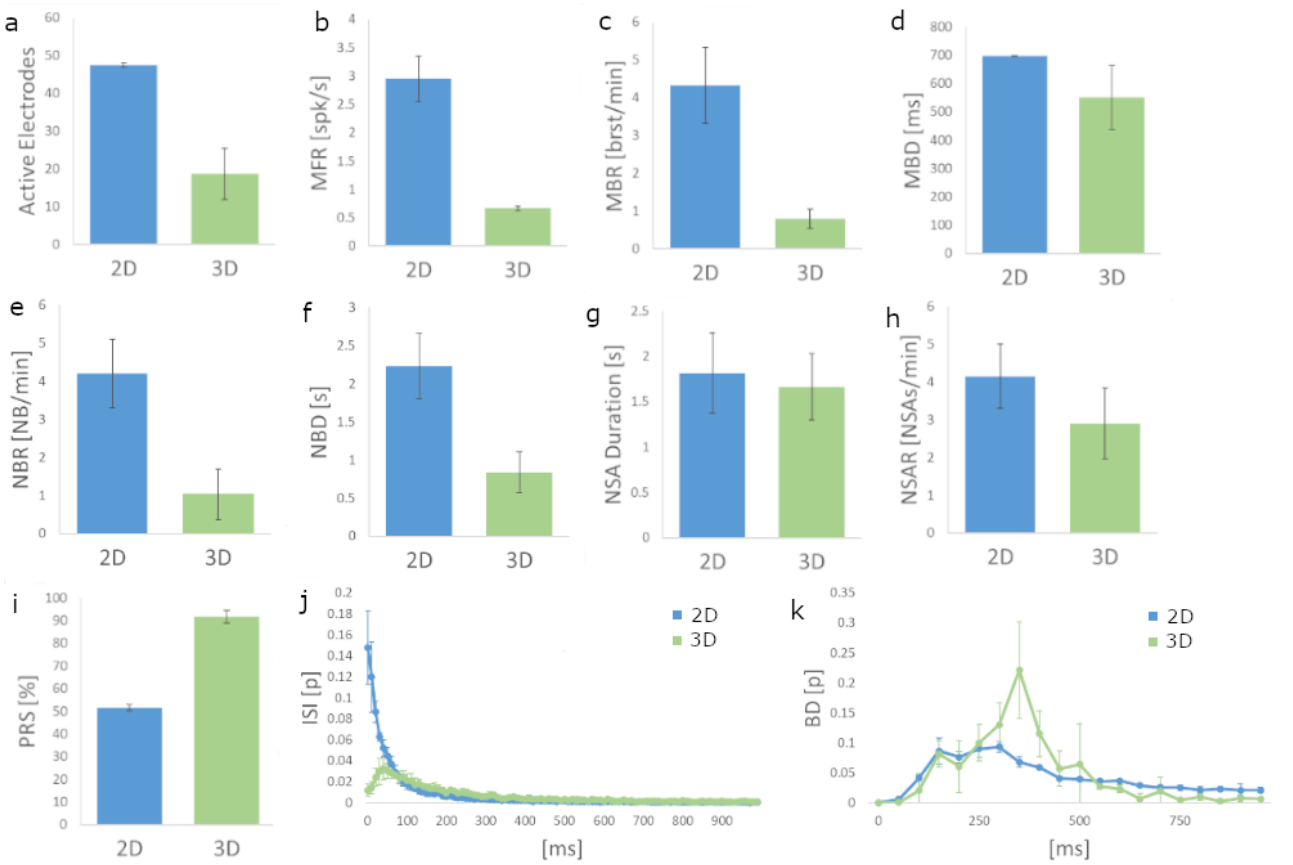

Suppl. Figure 3. Electrophysiological comparison of 2D and 3D cultures at DIV60. **a-i)** Graphs showing the **a)** Mean number of active electrodes, **b)** Mean firing rate (MFR), **c)** Mean burst rate (MBR), **d)** Mean burst duration (MBD), **e)** network burst rate (NBR), **f)** network burst duration (NBD), **g)** network sychronous activation duration (NSAD), **h)** network synchronous activation rate (NSAR), **i)** percentage of random spikes (PRS) in 2D and 3D neuronal networks at DIV 38. **i-j)** Graphs showing the **j)** Inter spike intervals (ISI) (10 ms bin) and **k)** burst duration (BD) (50 ms bin). Data shows the mean obtained across sample with same experimental condition and errorbars shows standard deviation. 2D data are represented in blue (n=2), 3D data are represented in green (n=2).

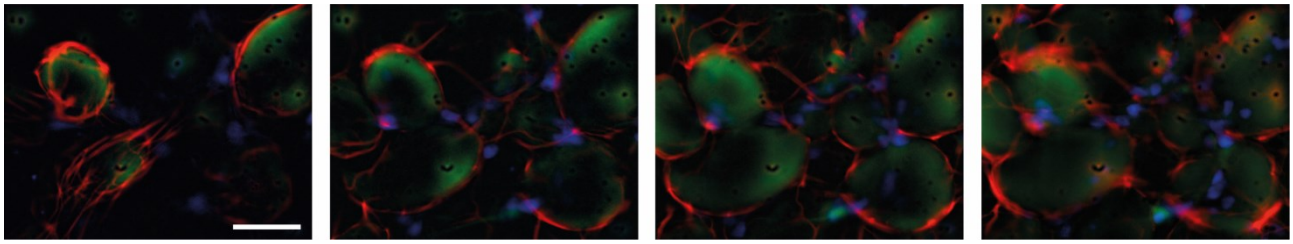

Suppl. Figure 4. Images taken from a Z-stack of a 3D neuronal network fixed at DIV56. Images were acquired at different layers with a 15µm stack and with a 20x objective using an upright microscope. Green: MAP-2, Red: GFAP, Blue: DAPI. Scale bar 100 µm.

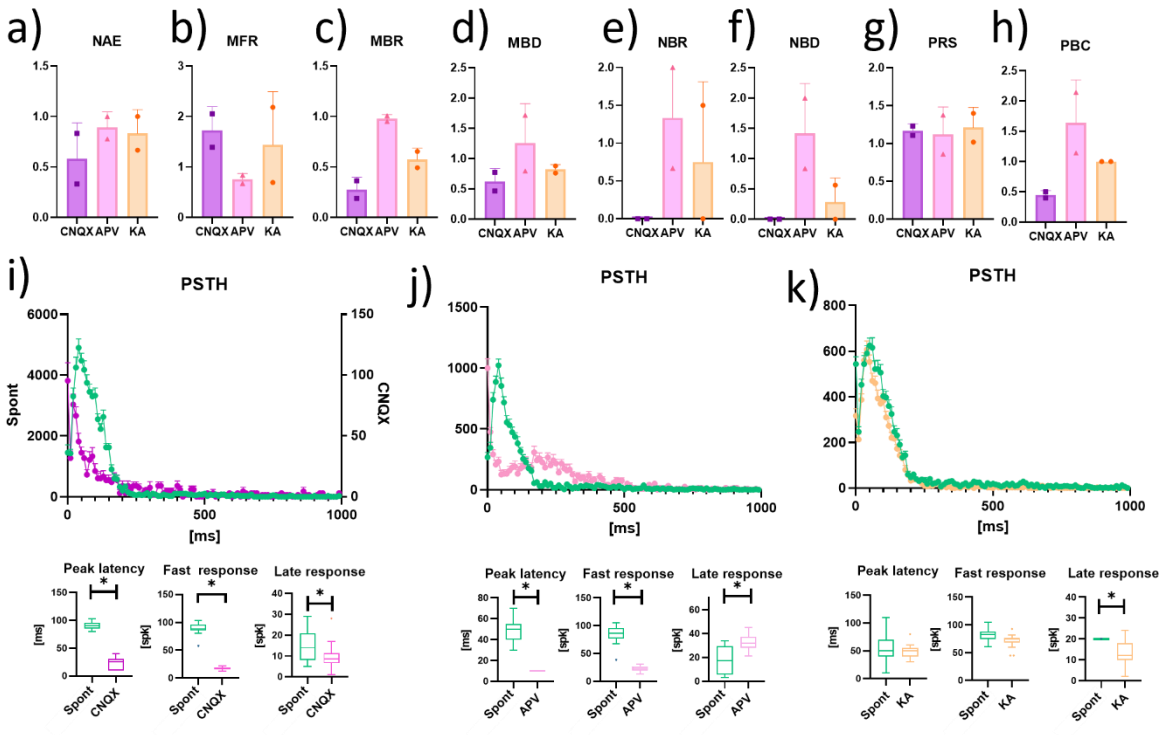

Suppl. Figure 5. Evaluation of the electrical and chemical modulation (50 µM CNQX, 80 µM APV, and 5 µM KA). Data are obtained from experiments on MEA60 (n = 2) and are normalized to the value detected in spontaneous conditions in the absence of drugs. **a-h)** Graphs showing the **a)** Number of active electrodes (NAE), **b)** Mean firing rate (MFR), **c)** Mean bursting Rate (MBR), **d)** Mean burst duration (MBD), **e)** Network burst rate (NBR), **f)** Network burst duration (NBD), **g)** Percentual random spikes (PRS), **h)** Percentual bursting channels (PBC) in neurospheroids treated with CNQX, APC and KA, represented int purple, pink and orange, respectively. Data are represented as mean and standard deviation of the mean. **i-k)** Graphs showing the effect of the modulation on the response to the electrical stimulus induced by **i)** CNQX, **j)** APV, **k)** KA. In each panel the Post-Stimulus Time Histogram (PSTH) showing the response of neurospheroids to stimulation is shown (not treated, treated with CNQX, APV and KA are represented in green, purple, pink and orange, respectively). The peak latency represent the mean latency to reach the maximum peak in the PSTHs, the fast response box plot represents the amount of evocated spikes in the first 100 ms of the PSTH while the late response box represent the amount of evocated spikes between 100 ms and 1000 ms. Asterisk indicate $p<0.05$.

IX. DISSEMINATIONS

- L.Muzzi, D. Di Lisa, P. Arnaldi, D. Aprile, L. Pastorino, S. Martinoia and M. Frega, Rapid generation of functional engineered 3D human neuronal assemblies: network dynamics evaluated by Micro-Electrodes Arrays, Accepted with substantial revision, Journal of Neural Engineering (2021)

- L. Muzzi, M. Falappa, A. Maccione, D. di Lisa, M. Frega and S. Martinoia, "Human derived cortical excitatory neurospheroids showed spontaneous activity on micro electrodes array," 2021 10th International IEEE/EMBS Conference on Neural Engineering (NER), 2021, pp. 123-127, doi: 10.1109/NER49283.2021.9441261.

- Monteiro, S. P., Voogd, E., Muzzi, L., De Vecchis, G., Mossink, B., Levers, M., ... & Frega, M. (2021). Neuroprotective effect of hypoxic preconditioning and neuronal activation in a human model of the ischemic penumbra. Journal of Neural Engineering.

- Di Lisa, D., Dellacasa, E., Muzzi, L., Lagazzo, A., Frega, M., Martinoia, S., & Pastorino, L. (2020, June). Thermosensitive hydrogels for the encapsulation of primary and human derived neuronal cells. GNB2020, June 9th-11th 2021, Trieste, Italy.

- S. Martinoia, A. Andolfi, L. Muzzi, M. Pisano, A. Spanu and R. Raiteri, "Neuro-electronic devices and nanotools to interact with neuronal networks," 2020 IEEE International Electron Devices Meeting (IEDM), 2020, pp. 14.1.1-14.1.4, doi: 10.1109/IEDM13553.2020.9372044.

- Arnaldi, P., Carosio, F., Di Lisa, D., Muzzi, L., Monticelli, O., & Pastorino, L. (2020). Assembly of chitosan-graphite oxide nanoplatelets core shell microparticles for advanced 3D scaffolds supporting neuronal networks growth. Colloids and Surfaces B: Biointerfaces, 196, 111295

- Muzzi, L., Martinoia, S., & Frega, M. (2019, January). Brain-on-a-Chip: A Human 3D Model for Clinical Application. In pHealth (pp. 274-279).

- Muzzi, L., Hassink, G., Levers, M., Jansman, M., Frega, M., Hofmeijer, J., ... & le Feber, J. (2019). Mild stimulation improves neuronal survival in an in vitro model of the ischemic penumbra. Journal of neural engineering, 17(1), 016001.

- Muzzi Lorenzo, Hassink Gerco Cornelis, Le Feber Joost. “In-vitro model of the Penumbra: closed-loop optogenetic stimulation to improve cell survival.” Frontiers in Cellular Neuroscience, N#00046, DOI=10.3389/conf.fncel.2018.38.00046

Conferences

- **ISSCR Annual Meeting 2021. Location:** Virtual. **Date:** 21-26 June. Poster presentation entitled "*Preliminar analysis of engineered functionally active human derived cortical neurospheroids for drug screening and precision medicine*" and contribution to the poster entitled "*A thermosensitive chitosan hydrogel-based 3d in vitro human neuronal culture model*"

- **10th International IEEE EMBS Conference on Neural Engineering (NER2021). Location**: Virtual. **Date:** 4-6 May 2021. Poster presentation entitled "*Human derived cortical excitatory neurospheroids showed spontaneous activity on micro electrodes array*"

- **pHealth 2019. Location:** Genoa, Italy. **Date:** 10-12 June 2019**.** Oral presentation of the work: "*Brain-on-a-chip: a human 3D model for clinical application",* published in the conference book: *pHealth 2019 proceedings of the 16th International Conference on Wearable Micro and Nano Technologies for Personalized Health*

Training activities

-Paper writing

Instructor. Mario Marchese. **Location:** Online. **Date:** October 14th –29th, 2020, 12 hours

- XL Annual School 2021 – Biofabrication: an integrated bioengineering approach for the automated fabrication of biological structures for clinical and research applications.

Location: Brixen (BZ), Italy. **Date:** September 13th-16th, 2021

- Grant Writing.

Instructor: Antonio Camurri. **Location:** Online. **Date:** 14th – 18th September 2020. 5 Credits

- Synapses, Neurons and Brains. Instructor: Idan Segev. **Location:** Coursera, Online. **Date:** July-August 2020. 3 Credits.

- Ethics and Bioethics in Bioengineering and Robotics.

Instructor: Linda Battistuzzi. **Location**: UNIGE **Date:** April 2020. 6 credits

- The 3Rs approach: Replacement, Reduction and Refinement of animal procedures in biomedical research.

Instructor: Laura Pastorino. **Location**: UNIGE **Date:** 3rd – 4th October 20. 4 Credits.

- 3rd CellFit Training School "Meet the rising stars of emerging therapies" From 3D Bioprinting to Extracellular Vesicles isolation and encapsulation for delivery

Location: Ponte di Legno (BS), UNIMONT. **Date**: 26th – 30th January 2020. 2 Credit http://cost-cellfit.eu/services/training-school-2020

- Internship at the University of Twente in Enschede, The Netherlands.

Duration: 2 months (February-March). **Objective:** training for culturing and differentiate h-iPSCs. **Tutored by:** Monica Frega.

- Theatrical techniques for Scientific Presentation. (mandatory)

Instructor: Antonio Sgorbissa. Course helded at UNIGE during march/may 2019. 4 credits. Exam passed.

- 5th NIC@IIT – Practical workshop on super resolution microscopy.

Directors: Paolo Bianchini & Alberto Diaspro, Istituto Italiano di Tecnologia, Genova, Italy. From 3rd to 7th December 2018. 3 credits

- Summer school Neural Circuit Development and Plasticity

Location: Utrecht, The Netherlands. **Organizers:** Corette Wierenga, Jeroen Pasterkamp, Lukas Kapitein, Harold MacGillavry. **Date:** 15th-19th July 2019. 4 credits. https://www.utrechtsummerschool.nl/courses/life-sciences/neural-circuit-development-and-plasticity

X. REFERENCES

ACCARDI, M. V., PUGSLEY, M. K., FORSTER, R., TRONCY, E., HUANG, H. & AUTHIER, S. 2016. The emerging role of in vitro electrophysiological methods in CNS safety pharmacology. *J Pharmacol Toxicol Methods,* 81**,** 47-59.

ALIZADEH, R., ZARRINTAJ, P., KAMRAVA, S. K., BAGHER, Z., FARHADI, M., HEIDARI, F., KOMEILI, A., GUTIERREZ, T. J. & SAEB, M. R. 2019. Conductive hydrogels based on agarose/alginate/chitosan for neural disorder therapy. *Carbohydr Polym,* 224**,** 115161.

ALTMAN, J. & DAS, G. D. 1965. Autoradiographic and histological evidence of postnatal hippocampal neurogenesis in rats. *Journal of Comparative Neurology,* 124**,** 319-335.

AMIN, H., MACCIONE, A., MARINARO, F., ZORDAN, S., NIEUS, T. & BERDONDINI, L. 2016. Electrical Responses and Spontaneous Activity of Human iPS-Derived Neuronal Networks Characterized for 3-month Culture with 4096-Electrode Arrays. *Front Neurosci,* 10**,** 121.

AMIN, H., NIEUS, T., LONARDONI, D., MACCIONE, A. & BERDONDINI, L. 2017. High-resolution bioelectrical imaging of Aβ-induced network dysfunction on CMOS-MEAs for neurotoxicity and rescue studies. *Scientific reports,* 7**,** 1-13.

APRILE, D., FRUSCIONE, F., BALDASSARI, S., FADDA, M., FERRANTE, D., FALACE, A., BUHLER, E., SARTORELLI, J., REPRESA, A., BALDELLI, P., BENFENATI, F., ZARA, F. & FASSIO, A. 2019. TBC1D24 regulates axonal outgrowth and membrane trafficking at the growth cone in rodent and human neurons. *Cell Death Differ,* 26**,** 2464-2478.

ARDHANAREESWARAN, K., MARIANI, J., COPPOLA, G., ABYZOV, A. & VACCARINO, F. M. 2017. Human induced pluripotent stem cells for modelling neurodevelopmental disorders. *Nature Reviews Neurology,* 13**,** 265-278.

ARNALDI, P., CAROSIO, F., DI LISA, D., MUZZI, L., MONTICELLI, O. & PASTORINO, L. 2020a. Assembly of chitosan-graphite oxide nanoplatelets core shell microparticles for advanced 3D scaffolds supporting neuronal networks growth. *Colloids and Surfaces B: Biointerfaces,* 196**,** 111295.

ARNALDI, P., DI LISA, D., MADDALENA, L., CAROSIO, F., FINA, A., PASTORINO, L. & MONTICELLI, O. 2021. A facile approach for the development of high mechanical strength 3D neuronal network scaffold based on chitosan and graphite nanoplatelets. *Carbohydrate Polymers*.

ARNALDI, P., PASTORINO, L. & MONTICELLI, O. 2020b. On an effective approach to improve the properties and the drug release of chitosan-based microparticles. *Int J Biol Macromol,* 163**,** 393-401.

ASHEGHALI, D., LEE, S.-J., FURCHNER, A., GRUZD, A., LARSON, S., TOKAREV, A., STAKE, S., ZHOU, X., HINRICHS, K. & ZHANG, L. G. 2020. Enhanced neuronal differentiation of neural stem cells with mechanically enhanced touch-spun nanofibrous scaffolds. *Nanomedicine: Nanotechnology, Biology and Medicine,* 24**,** 102152.

AVOLI, M. 2014. Mechanisms of epileptiform synchronization in cortical neuronal networks. *Current medicinal chemistry,* 21**,** 653-662.

BAKKUM, D. J., CHAO, Z. C. & POTTER, S. M. 2008. Spatio-temporal electrical stimuli shape behavior of an embodied cortical network in a goal-directed learning task. *Journal of neural engineering,* 5**,** 310.

BANG, S., JEONG, S., CHOI, N. & KIM, H. N. 2019. Brain-on-a-chip: A history of development and future perspective. *Biomicrofluidics,* 13**,** 051301-051301.

BANKER, G. & GOSLIN, K. 1988. Developments in neuronal cell culture. *Nature,* 336**,** 185-186.

BANKER, G. A. & COWAN, W. M. 1977. Rat hippocampal neurons in dispersed cell culture. *Brain research,* 126**,** 397-425.

BARATEIRO, A., BRITES, D. & FERNANDES, A. 2016. Oligodendrocyte development and myelination in neurodevelopment: molecular mechanisms in health and disease. *Current pharmaceutical design,* 22**,** 656-679.

BARDY, C., VAN DEN HURK, M., EAMES, T., MARCHAND, C., HERNANDEZ, R. V., KELLOGG, M., GORRIS, M., GALET, B., PALOMARES, V. & BROWN, J. 2015. Neuronal medium that supports basic synaptic functions and activity of human neurons in vitro. *Proceedings of the National Academy of Sciences,* 112**,** E2725-E2734.

BASTIAENS, A., XIE, S. & LUTTGE, R. 2019. Nanogroove-enhanced hydrogel scaffolds for 3D neuronal cell culture: An easy access brain-on-chip model. *Micromachines,* 10**,** 638.

BEDENBAUGH, P. & GERSTEIN, G. L. 1997. Multiunit normalized cross correlation differs from the average single-unit normalized correlation. *Neural computation,* 9**,** 1265-1275.

BERDONDINI, L., OVERSTOLZ, T., DE ROOIJ, N., KOUDELKA-HEP, M., WANY, M. & SEITZ, P. High-density microelectrode arrays for electrophysiological activity imaging of neuronal networks. ICECS 2001. 8th IEEE international conference on electronics, circuits and systems (Cat. No. 01EX483), 2001. IEEE, 1239-1242.

BOLAY, H., GÜRSOY-ÖZDEMIR, Y., SARA, Y., ONUR, R. S., CAN, A. & DALKARA, T. 2002. Persistent defect in transmitter release and synapsin phosphorylation in cerebral cortex after transient moderate ischemic injury. *Stroke,* 33**,** 1369-1375.

BOLOGNA, L., NIEUS, T., TEDESCO, M., CHIAPPALONE, M., BENFENATI, F. & MARTINOIA, S. 2010a. Low-frequency stimulation enhances burst activity in cortical cultures during development. *Neuroscience,* 165**,** 692-704.

BOLOGNA, L. L., PASQUALE, V., GAROFALO, M., GANDOLFO, M., BALJON, P. L., MACCIONE, A., MARTINOIA, S. & CHIAPPALONE, M. 2010b. Investigating neuronal activity by SPYCODE multi-channel data analyzer. *Neural Networks,* 23**,** 685-697.

BOUTIN, M. E., KRAMER, L. L., LIVI, L. L., BROWN, T., MOORE, C. & HOFFMAN-KIM, D. 2018. A three-dimensional neural spheroid model for capillary-like network formation. *J Neurosci Methods,* 299**,** 55-63.

BREWER, G. J. & COTMAN, C. W. 1989. Survival and growth of hippocampal neurons in defined medium at low density: advantages of a sandwich culture technique or low oxygen. *Brain research,* 494**,** 65-74.

BREWER, G. J., TORRICELLI, J., EVEGE, E. & PRICE, P. 1993. Optimized survival of hippocampal neurons in B27-supplemented neurobasal™, a new serum-free medium combination. *Journal of neuroscience research,* 35**,** 567-576.

BROSCH, M. & SCHREINER, C. E. 1999. Correlations between neural discharges are related to receptive field properties in cat primary auditory cortex. *European Journal of Neuroscience,* 11**,** 3517-3530.

BROWN, E. N., KASS, R. E. & MITRA, P. P. 2004. Multiple neural spike train data analysis: state-of-the-art and future challenges. *Nature neuroscience,* 7**,** 456-461.

CACCI, E., NEGRI, R., BIAGIONI, S. & LUPO, G. 2017. Histone methylation and microRNA-dependent regulation of epigenetic activities in neural progenitor self-renewal and differentiation. *Current topics in medicinal chemistry,* 17**,** 794-807.

CAKIR, B., XIANG, Y., TANAKA, Y., KURAL, M. H., PARENT, M., KANG, Y.-J., CHAPETON, K., PATTERSON, B., YUAN, Y. & HE, C.-S. 2019. Engineering of human brain organoids with a functional vascular-like system. *Nature methods,* 16**,** 1169-1175.

CENTENO, E. G. Z., CIMAROSTI, H. & BITHELL, A. 2018. 2D versus 3D human induced pluripotent stem cell-derived cultures for neurodegenerative disease modelling. *Mol Neurodegener,* 13**,** 27.

CHAI, X., MÜNZNER, G., ZHAO, S., TINNES, S., KOWALSKI, J., HÄUSSLER, U., YOUNG, C., HAAS, C. A. & FROTSCHER, M. 2014. Epilepsy-Induced Motility of Differentiated Neurons. *Cerebral Cortex,* 24**,** 2130-2140.

CHARKHKAR, H., MEYYAPPAN, S., MATVEEVA, E., MOLL, J. R., MCHAIL, D. G., PEIXOTO, N., CLIFF, R. O. & PANCRAZIO, J. J. 2015. Amyloid beta modulation of neuronal network activity in vitro. *Brain research,* 1629**,** 1-9.

CHEN, L., DENG, Y., LUO, W., WANG, Z. & ZENG, S. 2009. Detection of bursts in neuronal spike trains by the mean inter-spike interval method. *Progress in Natural Science,* 19**,** 229-235.

CHIAPPALONE, M., BOVE, M., VATO, A., TEDESCO, M. & MARTINOIA, S. 2006. Dissociated cortical networks show spontaneously correlated activity patterns during in vitro development. *Brain Res,* 1093**,** 41-53.

CHIAPPALONE, M., MASSOBRIO, P. & MARTINOIA, S. 2008. Network plasticity in cortical assemblies. *Eur J Neurosci,* 28**,** 221-37.

CHIAPPALONE, M., VATO, A., BERDONDINI, L., KOUDELKA-HEP, M. & MARTINOIA, S. 2007. Network dynamics and synchronous activity in cultured cortical neurons. *International journal of neural systems,* 17**,** 87-103.

CHIARADIA, I. & LANCASTER, M. A. 2020. Brain organoids for the study of human neurobiology at the interface of in vitro and in vivo. *Nature Neuroscience,* 23**,** 1496-1508.

COLLINGRIDGE, G. 1987. The role of NMDA receptors in learning and memory. *Nature,* 330**,** 604-605.

COLOMBI, I., MAHAJANI, S., FREGA, M., GASPARINI, L. & CHIAPPALONE, M. 2013. Effects of antiepileptic drugs on hippocampal neurons coupled to micro-electrode arrays. *Frontiers in neuroengineering,* 6**,** 10.

CSERCSA, R., DOMBOVÁRI, B., FABÓ, D., WITTNER, L., ERŐSS, L., ENTZ, L., SÓLYOM, A., RÁSONYI, G., SZŰCS, A. & KELEMEN, A. 2010. Laminar analysis of slow wave activity in humans. *Brain,* 133**,** 2814-2829.

CUSTÓDIO, C. A., CERQUEIRA, M., MARQUES, A., REIS, R. & MANO, J. 2015. Cell selective chitosan microparticles as injectable cell carriers for tissue regeneration. *Biomaterials,* 43**,** 23-31.

DASH, M., CHIELLINI, F., OTTENBRITE, R. M. & CHIELLINI, E. 2011. Chitosan—A versatile semi-synthetic polymer in biomedical applications. *Progress in polymer science,* 36**,** 981-1014.

DE LANGE, E. C., VAN DEN BRINK, W., YAMAMOTO, Y., DE WITTE, W. E. & WONG, Y. C. 2017. Novel CNS drug discovery and development approach: model-based integration to predict neuro-pharmacokinetics and pharmacodynamics. *Expert Opinion on Drug Discovery,* 12**,** 1207-1218.

DEVOLDER, R. & KONG, H. J. 2012. Hydrogels for in vivo-like three-dimensional cellular studies. *Wiley Interdisciplinary Reviews: Systems Biology and Medicine,* 4**,** 351-365.

DI LISA, D., DELLACASA, E., RAITERI, R., CATELANI, T., PESCE, M., MARTINOIA, S. & PASTORINO, L. 2020. Chitosan biopolymer: Alternative adhesion factor and scaffold matrix for 2D and 3D neuronal cultures. *Biomedical Science and Engineering*.

DIERING, G. H. & HUGANIR, R. L. 2018. The AMPA receptor code of synaptic plasticity. *Neuron,* 100**,** 314-329.

DOTTI, C. G., SULLIVAN, C. A. & BANKER, G. A. 1988. The establishment of polarity by hippocampal neurons in culture. *Journal of Neuroscience,* 8**,** 1454-1468.

DURENS, M., NESTOR, J., WILLIAMS, M., HEROLD, K., NIESCIER, R. F., LUNDEN, J. W., PHILLIPS, A. W., LIN, Y.-C., DYKXHOORN, D. M. & NESTOR, M. W. 2020. High-throughput screening of human induced pluripotent stem cell-derived brain organoids. *Journal of neuroscience methods,* 335**,** 108627.

DUVAL, K., GROVER, H., HAN, L. H., MOU, Y., PEGORARO, A. F., FREDBERG, J. & CHEN, Z. 2017. Modeling Physiological Events in 2D vs. 3D Cell Culture. *Physiology (Bethesda),* 32**,** 266-277.

ECKMANN, J.-P., JACOBI, S., MAROM, S., MOSES, E. & ZBINDEN, C. 2008. Leader neurons in population bursts of 2D living neural networks. *New Journal of Physics,* 10**,** 015011.

EYTAN, D., BRENNER, N. & MAROM, S. 2003. Selective Adaptation in Networks of Cortical Neurons. *The Journal of Neuroscience,* 23**,** 9349.

EYTAN, D., MINERBI, A., ZIV, N. & MAROM, S. 2004. Dopamine-Induced Dispersion of Correlations Between Action Potentials in Networks of Cortical Neurons. *Journal of Neurophysiology,* 92**,** 1817-1824.

FAIR, S. R., JULIAN, D., HARTLAUB, A. M., PUSULURI, S. T., MALIK, G., SUMMERFIED, T. L., ZHAO, G., HESTER, A. B., ACKERMAN IV, W. E. & HOLLINGSWORTH, E. W. 2020. Electrophysiological maturation of cerebral organoids correlates with dynamic morphological and cellular development. *Stem cell reports,* 15**,** 855-868.

FAN, C., LI, X., XIAO, Z., ZHAO, Y., LIANG, H., WANG, B., HAN, S., LI, X., XU, B. & WANG, N. 2017. A modified collagen scaffold facilitates endogenous neurogenesis for acute spinal cord injury repair. *Acta biomaterialia,* 51**,** 304-316.

FARDET, T., BALLANDRAS, M., BOTTANI, S., MÉTENS, S. & MONCEAU, P. 2018. Understanding the generation of network bursts by adaptive oscillatory neurons. *Frontiers in neuroscience,* 12**,** 41.

FEBER, J. L. 2019. In Vitro Models of Brain Disorders. *In Vitro Neuronal Networks***,** 19-49.

FEDOROVICH, S., HOFMEIJER, J., VAN PUTTEN, M. J. & LE FEBER, J. 2017. Reduced Synaptic Vesicle Recycling during Hypoxia in Cultured Cortical Neurons. *Front Cell Neurosci,* 11**,** 32.

FISHER, R. S. & ALGER, B. E. 1984. Electrophysiological mechanisms of kainic acid-induced epileptiform activity in the rat hippocampal slice. *The Journal of Neuroscience,* 4**,** 1312.

FREGA, M., LINDA, K., KELLER, J. M., GÜMÜŞ-AKAY, G., MOSSINK, B., VAN RHIJN, J.-R., NEGWER, M., GUNNEWIEK, T. K., FOREMAN, K. & KOMPIER, N. 2019. Neuronal network dysfunction in a model for Kleefstra syndrome mediated by enhanced NMDAR signaling. *Nature communications,* 10**,** 1-15.

FREGA, M., TEDESCO, M., MASSOBRIO, P., PESCE, M. & MARTINOIA, S. 2014. Network dynamics of 3D engineered neuronal cultures: a new experimental model for in-vitro electrophysiology. *Sci Rep,* 4**,** 5489.

FREGA, M., VAN GESTEL, S. H., LINDA, K., VAN DER RAADT, J., KELLER, J., VAN RHIJN, J.-R., SCHUBERT, D., ALBERS, C. A. & KASRI, N. N. 2017. Rapid neuronal differentiation of induced pluripotent stem cells for measuring network activity on micro-electrode arrays. *JoVE (Journal of Visualized Experiments)***,** e54900.

FRISTON, K. J. 2009. Modalities, modes, and models in functional neuroimaging. *Science,* 326**,** 399-403.

FURSHPAN, E. & POTTER, D. 1989. Seizure-like activity and cellular damage in rat hippocampal neurons in cell culture. *Neuron,* 3**,** 199-207.

GAGE, F. H. 2000. Mammalian neural stem cells. *Science,* 287**,** 1433-1438.

GANGULI, A., MOSTAFA, A., SAAVEDRA, C., KIM, Y., LE, P., FARAMARZI, V., FEATHERS, R., BERGER, J., RAMOS-CRUZ, K. & ADENIBA, O. 2021. Three-dimensional microscale hanging drop arrays with geometric control for drug screening and live tissue imaging. *Science Advances,* 7.

GERSTEIN, G. L. & PERKEL, D. H. 1969. Simultaneously recorded trains of action potentials: analysis and functional interpretation. *Science,* 164**,** 828-830.

GHATAK, S., DOLATABADI, N., GAO, R., WU, Y., SCOTT, H., TRUDLER, D., SULTAN, A., AMBASUDHAN, R., NAKAMURA, T. & MASLIAH, E. 2020. NitroSynapsin ameliorates hypersynchronous neural network activity in Alzheimer hiPSC models. *Molecular Psychiatry***,** 1-15.

GIANDOMENICO, S. L., MIERAU, S. B., GIBBONS, G. M., WENGER, L., MASULLO, L., SIT, T., SUTCLIFFE, M., BOULANGER, J., TRIPODI, M. & DERIVERY, E. 2019. Cerebral organoids at the air–liquid interface generate diverse nerve tracts with functional output. *Nature neuroscience,* 22**,** 669-679.

GORDON, J. & AMINI, S. 2021. General overview of neuronal cell culture. *neuronal cell culture***,** 1-8.

GRAY, E. G. 1959. Axo-somatic and axo-dendritic synapses of the cerebral cortex: an electron microscope study. *Journal of anatomy,* 93**,** 420.

GRAZIADEI, P. & MONTI GRAZIADEI, G. 1980. Neurogenesis and neuron regeneration in the olfactory system of mammals. III. Deafferentation and reinnervation of the olfactory bulb following section of thefila olfactoria in rat. *Journal of neurocytology,* 9**,** 145-162.

GROSS, G., RIESKE, E., KREUTZBERG, G. & MEYER, A. 1977. A new fixed-array multi-microelectrode system designed for long-term monitoring of extracellular single unit neuronal activity in vitro. *Neuroscience letters,* 6**,** 101-105.

GULLO, F., MANFREDI, I., LECCHI, M., CASARI, G., WANKE, E. & BECCHETTI, A. 2014. Multi-electrode array study of neuronal cultures expressing nicotinic β2-V287L subunits, linked to autosomal dominant nocturnal frontal lobe epilepsy. An in vitro model of spontaneous epilepsy. *Frontiers in neural circuits,* 8**,** 87.

HAN, S. S., WILLIAMS, L. A. & EGGAN, K. C. 2011. Constructing and deconstructing stem cell models of neurological disease. *Neuron,* 70**,** 626-644.

HARRISON, R. G. 1910. The outgrowth of the nerve fiber as a mode of protoplasmic movement. *Journal of Experimental Zoology,* 9**,** 787-846.

HASELMANN, H., MANNARA, F., WERNER, C., PLANAGUMÀ, J., MIGUEZ-CABELLO, F., SCHMIDL, L., GRÜNEWALD, B., PETIT-PEDROL, M., KIRMSE, K. & CLASSEN, J. 2018. Human autoantibodies against the AMPA receptor subunit GluA2 induce receptor reorganization and memory dysfunction. *Neuron,* 100**,** 91-105.

HEIKKILA, T. J., YLA-OUTINEN, L., TANSKANEN, J. M., LAPPALAINEN, R. S., SKOTTMAN, H., SUURONEN, R., MIKKONEN, J. E., HYTTINEN, J. A. & NARKILAHTI, S. 2009. Human embryonic stem cell-derived neuronal cells form spontaneously active neuronal networks in vitro. *Exp Neurol,* 218**,** 109-16.

HODGKIN, A. & HUXLEY, A. 1990. A quantitative description of membrane current and its application to conduction and excitation in nerve. *Bulletin of mathematical biology,* 52**,** 25-71.

HODGKIN, A. L. & HUXLEY, A. F. 1952. A quantitative description of membrane current and its application to conduction and excitation in nerve. *The Journal of physiology,* 117**,** 500.

HOFMEIJER, J., MULDER, A. T., FARINHA, A. C., VAN PUTTEN, M. J. & LE FEBER, J. 2014. Mild hypoxia affects synaptic connectivity in cultured neuronal networks. *Brain research,* 1557**,** 180-189.

HOFRICHTER, M., NIMTZ, L., TIGGES, J., KABIRI, Y., SCHRÖTER, F., ROYER-POKORA, B., HILDEBRANDT, B., SCHMUCK, M., EPANCHINTSEV, A. & THEISS, S. 2017. Comparative performance analysis of human iPSC-derived and primary neural progenitor cells (NPC) grown as neurospheres in vitro. *Stem cell research,* 25**,** 72-82.

HONDEBRINK, L., KASTEEL, E. E., TUKKER, A. M., WIJNOLTS, F. M., VERBOVEN, A. H. & WESTERINK, R. H. 2017. Neuropharmacological characterization of the new psychoactive substance methoxetamine. *Neuropharmacology,* 123**,** 1-9.

HORNER, P. J. & PALMER, T. D. 2003. New roles for astrocytes: the nightlife of an 'astrocyte'. La vida loca! *Trends in neurosciences,* 26**,** 597-603.

HYVÄRINEN, T., HAGMAN, S., RISTOLA, M., SUKKI, L., VEIJULA, K., KREUTZER, J., KALLIO, P. & NARKILAHTI, S. 2019a. Co-stimulation with IL-1β and TNF-α induces an inflammatory reactive astrocyte phenotype with neurosupportive characteristics in a human pluripotent stem cell model system. *Scientific reports,* 9**,** 1-15.

HYVÄRINEN, T., HYYSALO, A., KAPUCU, F. E., AARNOS, L., VINOGRADOV, A., EGLEN, S. J., YLÄ-OUTINEN, L. & NARKILAHTI, S. 2019b. Functional characterization of human pluripotent stem cell-derived cortical networks differentiated on laminin-521 substrate: comparison to rat cortical cultures. *Scientific reports,* 9**,** 1-15.

HYYSALO, A., RISTOLA, M., MÄKINEN, M. E.-L., HÄYRYNEN, S., NYKTER, M. & NARKILAHTI, S. 2017. Laminin α5 substrates promote survival, network formation and functional development of human pluripotent stem cell-derived neurons in vitro. *Stem cell research,* 24**,** 118-127.

ILLES, S., FLEISCHER, W., SIEBLER, M., HARTUNG, H.-P. & DIHNÉ, M. 2007. Development and pharmacological modulation of embryonic stem cell-derived neuronal network activity. *Experimental neurology,* 207**,** 171-176.

ISLAM, M. M., SHAHRUZZAMAN, M., BISWAS, S., SAKIB, M. N. & RASHID, T. U. 2020. Chitosan based bioactive materials in tissue engineering applications-A review. *Bioactive materials,* 5**,** 164-183.

IZSAK, J., SETH, H., ANDERSSON, M., VIZLIN-HODZIC, D., THEISS, S., HANSE, E., AGREN, H., FUNA, K. & ILLES, S. 2019. Robust Generation of Person-Specific, Synchronously Active Neuronal Networks Using Purely Isogenic Human iPSC-3D Neural Aggregate Cultures. *Front Neurosci,* 13**,** 351.

JACKSON, E. & LU, E. H. 2016. Three-dimensional models for studying development and disease: moving on from organisms to organs-on-a-chip and organoids. *Integrative Biology,* 8**,** 672-683.

JIMBO, Y. & ROBINSON, H. P. C. 2000. Propagation of spontaneous synchronized activity in cortical slice cultures recorded by planar electrode arrays. *Bioelectrochemistry,* 51**,** 107-115.

JIMBO, Y., ROBINSON, H. P. C. & KAWANA, A. 1998. Strengthening of synchronized activity by tetanic stimulation in cortical cultures: application of planar electrode arrays. *IEEE Transactions on Biomedical Engineering,* 45**,** 1297-1304.

JING, Y. & JIAN-XIONG, Y. 2011. 3-D spheroid culture of bone marrow mesenchymal stem cell of rhesus monkey with improved multi-differentiation potential to epithelial progenitors and neuron in vitro. *Clin Exp Ophthalmol,* 39**,** 808-19.

JO, J., XIAO, Y., SUN, A. X., CUKUROGLU, E., TRAN, H. D., GOKE, J., TAN, Z. Y., SAW, T. Y., TAN, C. P., LOKMAN, H., LEE, Y., KIM, D., KO, H. S., KIM, S. O., PARK, J. H., CHO, N. J., HYDE, T. M., KLEINMAN, J. E., SHIN, J. H., WEINBERGER, D. R., TAN, E. K., JE, H. S. & NG, H. H. 2016. Midbrain-like Organoids from Human Pluripotent Stem Cells Contain Functional Dopaminergic and Neuromelanin-Producing Neurons. *Cell Stem Cell,* 19**,** 248-257.

JONES, I. L., LIVI, P., LEWANDOWSKA, M. K., FISCELLA, M., ROSCIC, B. & HIERLEMANN, A. 2011. The potential of microelectrode arrays and microelectronics for biomedical research and diagnostics. *Analytical and bioanalytical chemistry,* 399**,** 2313-2329.

JORFI, M., D'AVANZO, C., KIM, D. Y. & IRIMIA, D. 2018. Three-Dimensional Models of the Human Brain Development and Diseases. *Adv Healthc Mater,* 7.

KASTEEL, E. E. & WESTERINK, R. H. 2017. Comparison of the acute inhibitory effects of Tetrodotoxin (TTX) in rat and human neuronal networks for risk assessment purposes. *Toxicology letters,* 270**,** 12-16.

KATHURIA, A., LOPEZ-LENGOWSKI, K., JAGTAP, S. S., MCPHIE, D., PERLIS, R. H., COHEN, B. M. & KARMACHARYA, R. 2020a. Transcriptomic landscape and functional characterization of induced pluripotent stem cell–derived cerebral organoids in schizophrenia. *JAMA psychiatry,* 77**,** 745-754.

KATHURIA, A., LOPEZ-LENGOWSKI, K., VATER, M., MCPHIE, D., COHEN, B. M. & KARMACHARYA, R. 2020b. Transcriptome analysis and functional characterization of cerebral organoids in bipolar disorder. *Genome medicine,* 12**,** 1-16.

KATO-NEGISHI, M., TSUDA, Y., ONOE, H. & TAKEUCHI, S. 2010. A neurospheroid network-stamping method for neural transplantation to the brain. *Biomaterials,* 31**,** 8939-45.

KAYAMA, T., SUZUKI, I., ODAWARA, A., SASAKI, T. & IKEGAYA, Y. 2018. Temporally coordinated spiking activity of human induced pluripotent stem cell-derived neurons co-cultured with astrocytes. *Biochem Biophys Res Commun,* 495**,** 1028-1033.

KELLER, J. M. & FREGA, M. 2019. Past, present, and future of neuronal models in vitro. *In Vitro Neuronal Networks***,** 3-17.

KEPECS, A. & LISMAN, J. 2003. Information encoding and computation with spikes and bursts. *Network: Computation in neural systems,* 14**,** 103.

KHAZIPOV, R., CONGAR, P. & BEN-ARI, Y. 1995. Hippocampal CA1 lacunosum-moleculare interneurons: comparison of effects of anoxia on excitatory and inhibitory postsynaptic currents. *Journal of neurophysiology,* 74**,** 2138-2149.

KIESE, K., JABLONSKI, J., HACKENBRACHT, J., WROSCH, J., GROEMER, T., KORNHUBER, J., BLÜMCKE, I. & KOBOW, K. 2017. Epigenetic control of epilepsy target genes contributes to a cellular memory of epileptogenesis in cultured rat hippocampal neurons. *Acta neuropathologica communications,* 5**,** 1-14.

KIM, I.-Y., SEO, S.-J., MOON, H.-S., YOO, M.-K., PARK, I.-Y., KIM, B.-C. & CHO, C.-S. 2008. Chitosan and its derivatives for tissue engineering applications. *Biotechnology advances,* 26**,** 1-21.

KRAHE, R. & GABBIANI, F. 2004. Burst firing in sensory systems. *Nature Reviews Neuroscience,* 5**,** 13-23.

KRENCIK, R., WEICK, J. P., LIU, Y., ZHANG, Z.-J. & ZHANG, S.-C. 2011. Specification of transplantable astroglial subtypes from human pluripotent stem cells. *Nature biotechnology,* 29**,** 528-534.

KUNZE, A., GIUGLIANO, M., VALERO, A. & RENAUD, P. 2011. Micropatterning neural cell cultures in 3D with a multi-layered scaffold. *Biomaterials,* 32**,** 2088-2098.

KUPERSTEIN, I., BROERSEN, K., BENILOVA, I., ROZENSKI, J., JONCKHEERE, W., DEBULPAEP, M., VANDERSTEEN, A., SEGERS-NOLTEN, I., VAN DER WERF, K. & SUBRAMANIAM, V. 2010. Neurotoxicity of Alzheimer's disease Aβ peptides is induced by small changes in the Aβ42 to Aβ40 ratio. *The EMBO journal,* 29**,** 3408-3420.

LAM, D., FISCHER, N. O. & ENRIGHT, H. A. 2021. Probing function in 3D neuronal cultures: A survey of 3D multielectrode array advances. *Current Opinion in Pharmacology,* 60**,** 255-260.

LAMA, N., HARGREAVES, A., STEVENS, B. & MCGINNITY, T. M. Spike Train Synchrony Analysis of Neuronal Cultures. 2018 International Joint Conference on Neural Networks (IJCNN), 2018. IEEE, 1-8.

LANCASTER, M. A., RENNER, M., MARTIN, C.-A., WENZEL, D., BICKNELL, L. S., HURLES, M. E., HOMFRAY, T., PENNINGER, J. M., JACKSON, A. P. & KNOBLICH, J. A. 2013. Cerebral organoids model human brain development and microcephaly. *Nature,* 501**,** 373-379.

LANG, E. J. & ROSENBLUTH, J. 2003. Role of myelination in the development of a uniform olivocerebellar conduction time. *Journal of neurophysiology,* 89**,** 2259-2270.

LANGER, R., VACANTI, J. P., VACANTI, C. A., ATALA, A., FREED, L. E. & VUNJAK-NOVAKOVIC, G. 1995. Tissue engineering: biomedical applications. *Tissue engineering,* 1**,** 151-161.

LAVIK, E., TENG, Y. D., SNYDER, E. & LANGER, R. 2002. Seeding neural stem cells on scaffolds of PGA, PLA, and their copolymers. *Neural stem cells: methods and protocols.* Springer.

LE FEBER, J., STEGENGA, J. & RUTTEN, W. L. 2010. The effect of slow electrical stimuli to achieve learning in cultured networks of rat cortical neurons. *PLoS One,* 5**,** e8871.

LE FEBER, J., TZAFI PAVLIDOU, S., ERKAMP, N., VAN PUTTEN, M. J. & HOFMEIJER, J. 2016. Progression of neuronal damage in an in vitro model of the ischemic penumbra. *PLoS One,* 11**,** e0147231.

LECOMTE, A., GIANTOMASI, L., RANCATI, S., BOI, F., ANGOTZI, G. N. & BERDONDINI, L. 2020. Surface-Functionalized Self-Standing Microdevices Exhibit Predictive Localization and Seamless Integration in 3D Neural Spheroids. *Adv Biosyst,* 4**,** e2000114.

LEE, K., KIM, C., YOUNG YANG, J., LEE, H., AHN, B., XU, L., YOON KANG, J. & OH, K. W. 2012. Gravity-oriented microfluidic device for uniform and massive cell spheroid formation. *Biomicrofluidics,* 6**,** 14114-141147.

LI, F. & TSIEN, J. Z. 2009. Memory and the NMDA receptors. *The New England journal of medicine,* 361**,** 302.

LI, X., TAO, Y., BRADLEY, R., DU, Z., TAO, Y., KONG, L., DONG, Y., JONES, J., YAN, Y., HARDER, C. R. K., FRIEDMAN, L. M., BILAL, M., HOFFMANN, B. & ZHANG, S. C. 2018. Fast Generation of Functional Subtype Astrocytes from Human Pluripotent Stem Cells. *Stem Cell Reports,* 11**,** 998-1008.

LISMAN, J. E. 1997. Bursts as a unit of neural information: making unreliable synapses reliable. *Trends in neurosciences,* 20**,** 38-43.

LOCHTER, A. & SCHACHNER, M. 1993. Tenascin and extracellular matrix glycoproteins: from promotion to polarization of neurite growth in vitro. *Journal of Neuroscience,* 13**,** 3986-4000.

LOUIS, E. D. & STAPF, C. 2001. Unraveling the neuron jungle: the 1879-1886 publications by Wilhelm His on the embryological development of the human brain. *Archives of neurology,* 58**,** 1932-1935.

MACCIONE, A., GANDOLFO, M., MASSOBRIO, P., NOVELLINO, A., MARTINOIA, S. & CHIAPPALONE, M. 2009. A novel algorithm for precise identification of spikes in extracellularly recorded neuronal signals. *J Neurosci Methods,* 177**,** 241-9.

MÄKINEN, M. E.-L., YLÄ-OUTINEN, L. & NARKILAHTI, S. 2018. GABA and gap junctions in the development of synchronized activity in human pluripotent stem cell-derived neural networks. *Frontiers in cellular neuroscience,* 12**,** 56.

MANSOUR, A. A., GONCALVES, J. T., BLOYD, C. W., LI, H., FERNANDES, S., QUANG, D., JOHNSTON, S., PARYLAK, S. L., JIN, X. & GAGE, F. H. 2018. An in vivo model of functional and vascularized human brain organoids. *Nat Biotechnol,* 36**,** 432-441.

MARIANI, J., COPPOLA, G., ZHANG, P., ABYZOV, A., PROVINI, L., TOMASINI, L., AMENDUNI, M., SZEKELY, A., PALEJEV, D., WILSON, M., GERSTEIN, M., GRIGORENKO, E. L., CHAWARSKA, K., PELPHREY, K. A., HOWE, J. R. & VACCARINO, F. M. 2015. FOXG1-Dependent Dysregulation of GABA/Glutamate Neuron Differentiation in Autism Spectrum Disorders. *Cell,* 162**,** 375-390.

MARIANI, J., SIMONINI, M. V., PALEJEV, D., TOMASINI, L., COPPOLA, G., SZEKELY, A. M., HORVATH, T. L. & VACCARINO, F. M. 2012. Modeling human cortical development in vitro using induced pluripotent stem cells. *Proc Natl Acad Sci U S A,* 109**,** 12770-5.

MARKRAM, H., TOLEDO-RODRIGUEZ, M., WANG, Y., GUPTA, A., SILBERBERG, G. & WU, C. 2004. Interneurons of the neocortical inhibitory system. *Nature reviews neuroscience,* 5**,** 793-807.

MAROM, S. & SHAHAF, G. 2002. Development, learning and memory in large random networks of cortical neurons: lessons beyond anatomy. *Quarterly reviews of biophysics,* 35**,** 63.

MARTON, R. M., MIURA, Y., SLOAN, S. A., LI, Q., REVAH, O., LEVY, R. J., HUGUENARD, J. R. & PAŞCA, S. P. 2019. Differentiation and maturation of oligodendrocytes in human three-dimensional neural cultures. *Nature neuroscience,* 22**,** 484-491.

MASON, J. O. & PRICE, D. J. 2016. Building brains in a dish: prospects for growing cerebral organoids from stem cells. *Neuroscience,* 334**,** 105-118.

MAYER, M., ARRIZABALAGA, O., LIEB, F., CIBA, M., RITTER, S. & THIELEMANN, C. 2018. Electrophysiological investigation of human embryonic stem cell derived neurospheres using a novel spike detection algorithm. *Biosens Bioelectron,* 100**,** 462-468.

MCCARTHY, K. D. & DE VELLIS, J. 1980. Preparation of separate astroglial and oligodendroglial cell cultures from rat cerebral tissue. *Journal of Cell Biology,* 85**,** 890-902.

MCSWEENEY, K. M., GUSSOW, A. B., BRADRICK, S. S., DUGGER, S. A., GELFMAN, S., WANG, Q., PETROVSKI, S., FRANKEL, W. N., BOLAND, M. J. & GOLDSTEIN, D. B. 2016. Inhibition of microRNA 128 promotes excitability of cultured cortical neuronal networks. *Genome research,* 26**,** 1411-1416.

MILLET, L. J. & GILLETTE, M. U. 2012. Over a century of neuron culture: from the hanging drop to microfluidic devices. *The Yale journal of biology and medicine,* 85**,** 501.

MONTEIRO, S. P., VOOGD, E., MUZZI, L., DE VECCHIS, G., MOSSINK, B., LEVERS, M., HASSINK, G., VAN PUTTEN, M., LE FEBER, J. & HOFMEIJER, J. 2021. Neuroprotective effect of hypoxic preconditioning and neuronal activation in a in vitro human model of the ischemic penumbra. *Journal of neural engineering,* 18**,** 036016.

MONZEL, A. S., SMITS, L. M., HEMMER, K., HACHI, S., MORENO, E. L., VAN WUELLEN, T., JARAZO, J., WALTER, J., BRÜGGEMANN, I. & BOUSSAAD, I. 2017. Derivation of human midbrain-specific organoids from neuroepithelial stem cells. *Stem cell reports,* 8**,** 1144-1154.

MOSSINK, B., VAN RHIJN, J.-R., WANG, S., LINDA, K., VITALE, M. R., ZÖLLER, J. E., VAN HUGTE, E. J., BAK, J., VERBOVEN, A. H. & SELTEN, M. 2021a. Cadherin-13 is a critical regulator of GABAergic modulation in human stem-cell-derived neuronal networks. *Molecular Psychiatry***,** 1-18.

MOSSINK, B., VERBOVEN, A. H., VAN HUGTE, E. J., GUNNEWIEK, T. M. K., PARODI, G., LINDA, K., SCHOENMAKER, C., KLEEFSTRA, T., KOZICZ, T. & VAN BOKHOVEN, H. 2021b. Human neuronal networks on micro-electrode arrays are a highly robust tool to study disease-specific genotype-phenotype correlations in vitro. *Stem cell reports,* 16**,** 2182-2196.

MU, M., LI, X., TONG, A. & GUO, G. 2019. Multi-functional chitosan-based smart hydrogels mediated biomedical application. *Expert opinion on drug delivery,* 16**,** 239-250.

MUKAI, T., NAGAMURA-INOUE, T., SHIMAZU, T., MORI, Y., TAKAHASHI, A., TSUNODA, H., YAMAGUCHI, S. & TOJO, A. 2016. Neurosphere formation enhances the neurogenic differentiation potential and migratory ability of umbilical cord-mesenchymal stromal cells. *Cytotherapy,* 18**,** 229-41.

MUZZI, L., DI LISA, D., ARNALDI, P., APRILE, D., PASTORINO, L., MARTINOIA, S. & FREGA, M. 2021a. Rapid generation of functional engineered 3D human neuronal assemblies: network dynamics evaluated by micro-electrodes arrays. *Journal of Neural Engineering,* 18**,** 066030.

MUZZI, L., FALAPPA, M., MACCIONE, A., DI LISA, D., FREGA, M. & MARTINOIA, S. Human derived cortical excitatory neurospheroids showed spontaneous activity on micro electrodes array. 2021 10th International IEEE/EMBS Conference on Neural Engineering (NER), 2021b. IEEE, 123-127.

MUZZI, L., HASSINK, G., LEVERS, M., JANSMAN, M., FREGA, M., HOFMEIJER, J., VAN PUTTEN, M. & LE FEBER, J. 2019. Mild stimulation improves neuronal survival in an in vitro model of the ischemic penumbra. *Journal of neural engineering,* 17**,** 016001.

MZEZEWA, R., LOTILA, J., KIISKI, H., VINOGRADOV, A., KAPUCU, E., PELTOLA, J., HAGMAN, S. & NARKILAHTI, S. 2022. A kainic acid-induced seizure model in human pluripotent stem cell-derived cortical neurons for studying the role of IL-6 in the functional activity. *Stem Cell Research***,** 102665.

NAPOLI, A. & OBEID, I. 2016. Comparative Analysis of Human and Rodent Brain Primary Neuronal Culture Spontaneous Activity Using Micro-Electrode Array Technology. *Journal of Cellular Biochemistry,* 117**,** 559-565.

NEHER, E., SAKMANN, B. & STEINBACH, J. H. 1978. The extracellular patch clamp: a method for resolving currents through individual open channels in biological membranes. *Pflügers Archiv,* 375**,** 219-228.

NICOLELIS, M. A. Dynamic and distributed somatosensory representations as the substrate for cortical and subcortical plasticity. Seminars in neuroscience, 1997. Elsevier, 24-33.

NIMTZ, L., HARTMANN, J., TIGGES, J., MASJOSTHUSMANN, S., SCHMUCK, M., KEßEL, E., THEISS, S., KÖHRER, K., PETZSCH, P. & ADJAYE, J. 2020. Characterization and application of electrically active neuronal networks established from human induced pluripotent stem cell-derived neural progenitor cells for neurotoxicity evaluation. *Stem Cell Research,* 45**,** 101761.

OBERHEIM, N. A., TAKANO, T., HAN, X., HE, W., LIN, J. H., WANG, F., XU, Q., WYATT, J. D., PILCHER, W. & OJEMANN, J. G. 2009. Uniquely hominid features of adult human astrocytes. *Journal of Neuroscience,* 29**,** 3276-3287.

OBIEN, M. E. J., DELIGKARIS, K., BULLMANN, T., BAKKUM, D. J. & FREY, U. 2015. Revealing neuronal function through microelectrode array recordings. *Frontiers in neuroscience,* 8**,** 423.

ODAWARA, A., KATOH, H., MATSUDA, N. & SUZUKI, I. 2016. Physiological maturation and drug responses of human induced pluripotent stem cell-derived cortical neuronal networks in long-term culture. *Sci Rep,* 6**,** 26181.

ODAWARA, A., MATSUDA, N., ISHIBASHI, Y., YOKOI, R. & SUZUKI, I. 2018. Toxicological evaluation of convulsant and anticonvulsant drugs in human induced pluripotent stem cell-derived cortical neuronal networks using an MEA system. *Sci Rep,* 8**,** 10416.

ODAWARA, A., SAITOH, Y., ALHEBSHI, A. H., GOTOH, M. & SUZUKI, I. 2014. Long-term electrophysiological activity and pharmacological response of a human induced pluripotent stem cell-derived neuron and astrocyte co-culture. *Biochem Biophys Res Commun,* 443**,** 1176-81.

OHARA, Y., KOGANEZAWA, N., YAMAZAKI, H., ROPPONGI, R. T., SATO, K., SEKINO, Y. & SHIRAO, T. 2015. Early-stage development of human induced pluripotent stem cell-derived neurons. *Journal of Neuroscience Research,* 93**,** 1804-1813.

OHNUKI, M., TAKAHASHI, K. & YAMANAKA, S. 2009. Generation and characterization of human induced pluripotent stem cells. *Current protocols in stem cell biology,* 9**,** 4A. 2.1-4A. 2.25.

PAMIES, D., HARTUNG, T. & HOGBERG, H. T. 2014. Biological and medical applications of a brain-on-a-chip. *Exp Biol Med (Maywood),* 239**,** 1096-1107.

PAN, L., SONG, X., XIANG, G., ZHU, J. & CHENG, J. 2009. Effects of disinhibition on spatiotemporal pattern of neuronal first recruitment in neuronal networks. *Progress in Natural Science,* 19**,** 615-621.

PANG, Z. P., YANG, N., VIERBUCHEN, T., OSTERMEIER, A., FUENTES, D. R., YANG, T. Q., CITRI, A., SEBASTIANO, V., MARRO, S. & SÜDHOF, T. C. 2011. Induction of human neuronal cells by defined transcription factors. *Nature,* 476**,** 220-223.

PASCA, A. M., SLOAN, S. A., CLARKE, L. E., TIAN, Y., MAKINSON, C. D., HUBER, N., KIM, C. H., PARK, J. Y., O'ROURKE, N. A., NGUYEN, K. D., SMITH, S. J., HUGUENARD, J. R., GESCHWIND, D. H., BARRES, B. A. & PASCA, S. P. 2015. Functional cortical neurons and astrocytes from human pluripotent stem cells in 3D culture. *Nat Methods,* 12**,** 671-8.

PASPALA, S. A. B., MURTHY, T. K., MAHABOOB, V. & HABEEB, M. 2011. Pluripotent stem cells-a review of the current status in neural regeneration. *Neurology India,* 59**,** 558.

PASQUALE, V., MASSOBRIO, P., BOLOGNA, L., CHIAPPALONE, M. & MARTINOIA, S. 2008. Self-organization and neuronal avalanches in networks of dissociated cortical neurons. *Neuroscience,* 153**,** 1354-1369.

PASTORE, V. P., MASSOBRIO, P., GODJOSKI, A. & MARTINOIA, S. 2018. Identification of excitatory-inhibitory links and network topology in large-scale neuronal assemblies from multi-electrode recordings. *PLoS Comput Biol,* 14**,** e1006381.

PAUTOT, S., WYART, C. & ISACOFF, E. Y. 2008. Colloid-guided assembly of oriented 3D neuronal networks. *Nat Methods,* 5**,** 735-40.

PELKONEN, A., PISTONO, C., KLECKI, P., GÓMEZ-BUDIA, M., DOUGALIS, A., KONTTINEN, H., STANOVÁ, I., FAGERLUND, I., LEINONEN, V. & KORHONEN, P. 2021. Functional Characterization of Human Pluripotent Stem Cell-Derived Models of the Brain with Microelectrode Arrays. *Cells,* 11**,** 106.

PEYRACHE, A., DEHGHANI, N., ESKANDAR, E. N., MADSEN, J. R., ANDERSON, W. S., DONOGHUE, J. A., HOCHBERG, L. R., HALGREN, E., CASH, S. S. & DESTEXHE, A. 2012. Spatiotemporal dynamics of neocortical excitation and inhibition during human sleep. *Proc Natl Acad Sci U S A,* 109**,** 1731-6.

PHAM, M. T., POLLOCK, K. M., ROSE, M. D., CARY, W. A., STEWART, H. R., ZHOU, P., NOLTA, J. A. & WALDAU, B. 2018. Generation of human vascularized brain organoids. *Neuroreport,* 29**,** 588.

PINE, J. 1980. Recording action potentials from cultured neurons with extracellular microcircuit electrodes. *Journal of neuroscience methods,* 2**,** 19-31.

POLI, D., PASTORE, V. P., MARTINOIA, S. & MASSOBRIO, P. 2016. From functional to structural connectivity using partial correlation in neuronal assemblies. *Journal of neural engineering,* 13**,** 026023.

POLI, D., PASTORE, V. P. & MASSOBRIO, P. 2015. Functional connectivity in in vitro neuronal assemblies. *Frontiers in neural circuits,* 9**,** 57.

POTTER, S. M. 2001. Distributed processing in cultured neuronal networks. *Progress in brain research,* 130**,** 49-62.

PYKA, M., BUSSE, C., SEIDENBECHER, C., GUNDELFINGER, E. D. & FAISSNER, A. 2011. Astrocytes are crucial for survival and maturation of embryonic hippocampal neurons in a neuron-glia cell-insert coculture assay. *Synapse,* 65**,** 41-53.

QIAN, X., NGUYEN, H. N., SONG, M. M., HADIONO, C., OGDEN, S. C., HAMMACK, C., YAO, B., HAMERSKY, G. R., JACOB, F. & ZHONG, C. 2016a. Brain-region-specific organoids using mini-bioreactors for modeling ZIKV exposure. *Cell,* 165**,** 1238-1254.

QIAN, X., NGUYEN, H. N., SONG, M. M., HADIONO, C., OGDEN, S. C., HAMMACK, C., YAO, B., HAMERSKY, G. R., JACOB, F., ZHONG, C., YOON, K. J., JEANG, W., LIN, L., LI, Y., THAKOR, J., BERG, D. A., ZHANG, C., KANG, E., CHICKERING, M., NAUEN, D., HO, C. Y., WEN, Z., CHRISTIAN, K. M., SHI, P. Y., MAHER, B. J., WU, H., JIN, P., TANG, H., SONG, H. & MING, G. L. 2016b. Brain-Region-Specific Organoids Using Mini-bioreactors for Modeling ZIKV Exposure. *Cell,* 165**,** 1238-1254.

QIAN, X., SONG, H. & MING, G.-L. 2019. Brain organoids: advances, applications and challenges. *Development,* 146**,** dev166074.

QIAN, X., SU, Y., ADAM, C. D., DEUTSCHMANN, A. U., PATHER, S. R., GOLDBERG, E. M., SU, K., LI, S., LU, L. & JACOB, F. 2020. Sliced human cortical organoids for modeling distinct cortical layer formation. *Cell Stem Cell,* 26**,** 766-781. e9.

QUADRATO, G., NGUYEN, T., MACOSKO, E. Z., SHERWOOD, J. L., MIN YANG, S., BERGER, D. R., MARIA, N., SCHOLVIN, J., GOLDMAN, M. & KINNEY, J. P. 2017. Cell diversity and network dynamics in photosensitive human brain organoids. *Nature,* 545**,** 48-53.

RAMAKERS, G., CORNER, M. & HABETS, A. 1990. Development in the absence of spontaneous bioelectric activity results in increased stereotyped burst firing in cultures of dissociated cerebral cortex. *Experimental brain research,* 79**,** 157-166.

RAMÓN, Y. & CAJAL, S. 1890. A quelle époque apparaissent les expansions des cellules nerveuses de la moelle épinière du poulet. *Anatomischer Anzeiger,* 5**,** 609-613.

RAO, V. R. & FINKBEINER, S. 2007. NMDA and AMPA receptors: old channels, new tricks. *Trends in Neurosciences,* 30**,** 284-291.

RUSSO, F. B., FREITAS, B. C., PIGNATARI, G. C., FERNANDES, I. R., SEBAT, J., MUOTRI, A. R. & BELTRÃO-BRAGA, P. C. B. 2018. Modeling the interplay between neurons and astrocytes in autism using human induced pluripotent stem cells. *Biological psychiatry,* 83**,** 569-578.

RYBACHUK, O., KOPACH, O., PIVNEVA, T. & KYRYK, V. 2019. Isolation of Neural Stem Cells from the embryonic mouse hippocampus for in vitro growth or engraftment into a host tissue. *Bio Protoc,* 9**,** e3165.

SAKAGUCHI, H., KADOSHIMA, T., SOEN, M., NARII, N., ISHIDA, Y., OHGUSHI, M., TAKAHASHI, J., EIRAKU, M. & SASAI, Y. 2015. Generation of functional hippocampal neurons from self-organizing human embryonic stem cell-derived dorsomedial telencephalic tissue. *Nat Commun,* 6**,** 8896.

SALINAS, E. & SEJNOWSKI, T. J. 2001. Correlated neuronal activity and the flow of neural information. *Nature reviews neuroscience,* 2**,** 539-550.

SANTOS, R., VADODARIA, K. C., JAEGER, B. N., MEI, A., LEFCOCHILOS-FOGELQUIST, S., MENDES, A. P. D., ERIKSON, G., SHOKHIREV, M., RANDOLPH-MOORE, L., FREDLENDER, C., DAVE, S., OEFNER, R., FITZPATRICK, C., PENA, M., BARRON, J. J., KU, M., DENLI, A. M., KERMAN, B. E., CHARNAY, P., KELSOE, J. R., MARCHETTO, M. C. & GAGE, F. H. 2017. Differentiation of Inflammation-Responsive Astrocytes from Glial Progenitors Generated from Human Induced Pluripotent Stem Cells. *Stem Cell Reports,* 8**,** 1757-1769.

SCHWARTZ, M. P., HOU, Z., PROPSON, N. E., ZHANG, J., ENGSTROM, C. J., SANTOS COSTA, V., JIANG, P., NGUYEN, B. K., BOLIN, J. M., DALY, W., WANG, Y., STEWART, R., PAGE, C. D., MURPHY, W. L. & THOMSON, J. A. 2015. Human pluripotent stem cell-derived neural constructs for predicting neural toxicity. *Proc Natl Acad Sci U S A,* 112**,** 12516-21.

SHAHAF, G. & MAROM, S. 2001. Learning in networks of cortical neurons. *Journal of Neuroscience,* 21**,** 8782-8788.

SHEW, W. L., YANG, H., YU, S., ROY, R. & PLENZ, D. 2011. Information capacity and transmission are maximized in balanced cortical networks with neuronal avalanches. *J Neurosci,* 31**,** 55-63.

SHIMBA, K., SAKAI, K., IIDA, S., KOTANI, K. & JIMBO, Y. 2019. Long-term developmental process of the human cortex revealed in vitro by axon-targeted recording using a microtunnel-augmented microelectrode array. *IEEE Transactions on Biomedical Engineering,* 66**,** 2538-2545.

SHIN, H., JEONG, S., LEE, J.-H., SUN, W., CHOI, N. & CHO, I.-J. 2021. 3D high-density microelectrode array with optical stimulation and drug delivery for investigating neural circuit dynamics. *Nature communications,* 12**,** 1-18.

SINGER, W. 1993. Synchronization of cortical activity and its putative role in information processing and learning. *Annual review of physiology,* 55**,** 349-374.

SIVRON, T., EITAN, S., SCHREYER, D. J. & SCHWARTZ, M. 1993. Astrocytes play a major role in the control of neuronal proliferation in vitro. *Brain research,* 629**,** 199-208.

SMITH, I., HAAG, M., UGBODE, C., TAMS, D., RATTRAY, M., PRZYBORSKI, S., BITHELL, A. & WHALLEY, B. J. 2015. Neuronal-glial populations form functional networks in a biocompatible 3D scaffold. *Neurosci Lett,* 609**,** 198-202.

SMITH, I., SILVEIRINHA, V., STEIN, J. L., DE LA TORRE-UBIETA, L., FARRIMOND, J. A., WILLIAMSON, E. M. & WHALLEY, B. J. 2017. Human neural stem cell-derived cultures in three-dimensional substrates form spontaneously functional neuronal networks. *J Tissue Eng Regen Med,* 11**,** 1022-1033.

SOSCIA, D. A., LAM, D., TOOKER, A. C., ENRIGHT, H. A., TRIPLETT, M., KARANDE, P., PETERS, S. K., SALES, A. P., WHEELER, E. K. & FISCHER, N. O. 2020. A flexible 3-dimensional microelectrode array for in vitro brain models. *Lab on a Chip,* 20**,** 901-911.

SPANU, A., COLISTRA, N., FARISELLO, P., FRIZ, A., ARELLANO, N., RETTNER, C. T., BONFIGLIO, A., BOZANO, L. & MARTINOIA, S. 2020. A three-dimensional micro-electrode array for in-vitro neuronal interfacing. *Journal of Neural Engineering,* 17**,** 036033.

SPERK, G. 1994. Kainic acid seizures in the rat. *Progress in Neurobiology,* 42**,** 1-32.

SPORNS, O. 2018. Graph theory methods: applications in brain networks. *Dialogues in clinical neuroscience,* 20**,** 111.

STABA, R. J., WILSON, C. L., BRAGIN, A., FRIED, I. & ENGEL, J. 2002. Sleep states differentiate single neuron activity recorded from human epileptic hippocampus, entorhinal cortex, and subiculum. *Journal of Neuroscience,* 22**,** 5694-5704.

STETT, A., EGERT, U., GUENTHER, E., HOFMANN, F., MEYER, T., NISCH, W. & HAEMMERLE, H. 2003. Biological application of microelectrode arrays in drug discovery and basic research. *Analytical and bioanalytical chemistry,* 377**,** 486-495.

STOYANOVA, I. I., HOFMEIJER, J., VAN PUTTEN, M. J. & LE FEBER, J. 2016. Acyl ghrelin improves synapse recovery in an in vitro model of postanoxic encephalopathy. *Molecular neurobiology,* 53**,** 6136-6143.

SUN, M.-K., XU, H. & ALKON, D. L. 2002. Pharmacological protection of synaptic function, spatial learning, and memory from transient hypoxia in rats. *Journal of Pharmacology and Experimental Therapeutics,* 300**,** 408-416.

SURESH, J., RADOJICIC, M., PESCE, L. L., BHANSALI, A., WANG, J., TRYBA, A. K., MARKS, J. D. & VAN DRONGELEN, W. 2016. Network burst activity in hippocampal neuronal cultures: the role of synaptic and intrinsic currents. *Journal of Neurophysiology,* 115**,** 3073-3089.

SZEBÉNYI, K., WENGER, L., SUN, Y., DUNN, A. W., LIMEGROVER, C. A., GIBBONS, G. M., CONCI, E., PAULSEN, O., MIERAU, S. B. & BALMUS, G. 2021. Human ALS/FTD brain organoid slice cultures display distinct early astrocyte and targetable neuronal pathology. *Nature neuroscience,* 24**,** 1542-1554.

TAKAHASHI, K. & YAMANAKA, S. 2006. Induction of pluripotent stem cells from mouse embryonic and adult fibroblast cultures by defined factors. *cell,* 126**,** 663-676.

TAMBALO, M. & LODATO, S. 2020. Brain organoids: Human 3D models to investigate neuronal circuits assembly, function and dysfunction. *Brain Res,* 1746**,** 147028.

TANG, M., LI, J., HE, L., GUO, R., YAN, X., LI, D., ZHANG, Y., LIAO, M., SHAO, B. & HU, Y. 2019. Transcriptomic profiling of neural stem cell differentiation on graphene substrates. *Colloids and surfaces B: Biointerfaces,* 182**,** 110324.

TANG, Z., WANG, Y., PODSIADLO, P. & KOTOV, N. A. 2006. Biomedical Applications of Layer-by-Layer Assembly: From Biomimetics to Tissue Engineering. *Advanced Materials,* 18**,** 3203-3224.

TAUPIN, P. & GAGE, F. H. 2002. Adult neurogenesis and neural stem cells of the central nervous system in mammals. *Journal of neuroscience research,* 69**,** 745-749.

TEDESCO, M. T., DI LISA, D., MASSOBRIO, P., COLISTRA, N., PESCE, M., CATELANI, T., DELLACASA, E., RAITERI, R., MARTINOIA, S. & PASTORINO, L. 2018. Soft chitosan microbeads scaffold for 3D functional neuronal networks. *Biomaterials,* 156**,** 159-171.

TERRASSO, A. P., PINTO, C., SERRA, M., FILIPE, A., ALMEIDA, S., FERREIRA, A. L., PEDROSO, P., BRITO, C. & ALVES, P. M. 2015. Novel scalable 3D cell based model for in vitro neurotoxicity testing: Combining human differentiated neurospheres with gene expression and functional endpoints. *J Biotechnol,* 205**,** 82-92.

THOMAS JR, C., SPRINGER, P., LOEB, G., BERWALD-NETTER, Y. & OKUN, L. 1972. A miniature microelectrode array to monitor the bioelectric activity of cultured cells. *Experimental cell research,* 74**,** 61-66.

THOMAS, W. E. 1985. Synthesis of acetylcholine and γ-aminobutyric acid by dissociated cerebral cortical cells in vitro. *Brain Research,* 332**,** 79-89.

TOIVONEN, S., OJALA, M., HYYSALO, A., ILMARINEN, T., RAJALA, K., PEKKANEN-MATTILA, M., ÄÄNISMAA, R., LUNDIN, K., PALGI, J. & WELTNER, J. 2013. Comparative analysis of targeted differentiation of human induced pluripotent stem cells (hiPSCs) and human embryonic stem cells reveals variability associated with incomplete transgene silencing in retrovirally derived hiPSC lines. *Stem cells translational medicine,* 2**,** 83-93.

TRUJILLO, C. A., GAO, R., NEGRAES, P. D., GU, J., BUCHANAN, J., PREISSL, S., WANG, A., WU, W., HADDAD, G. G. & CHAIM, I. A. 2019. Complex oscillatory waves emerging from cortical organoids model early human brain network development. *Cell stem cell,* 25**,** 558-569. e7.

TUKKER, A. M., WIJNOLTS, F. M., DE GROOT, A. & WESTERINK, R. H. 2018. Human iPSC-derived neuronal models for in vitro neurotoxicity assessment. *Neurotoxicology,* 67**,** 215-225.

TUNG, Y.-C., HSIAO, A. Y., ALLEN, S. G., TORISAWA, Y.-S., HO, M. & TAKAYAMA, S. 2011. High-throughput 3D spheroid culture and drug testing using a 384 hanging drop array. *Analyst,* 136**,** 473-478.

TURNBULL, L., DIAN, E. & GROSS, G. 2005. The string method of burst identification in neuronal spike trains. *Journal of neuroscience methods,* 145**,** 23-35.

VAN DER WORP, H. B., HOWELLS, D. W., SENA, E. S., PORRITT, M. J., REWELL, S., O'COLLINS, V. & MACLEOD, M. R. 2010. Can animal models of disease reliably inform human studies? *PLoS Med,* 7**,** e1000245.

VAN PELT, J., CORNER, M., WOLTERS, P., RUTTEN, W. & RAMAKERS, G. 2004. Longterm stability and developmental changes in spontaneous network burst firing patterns in dissociated rat cerebral cortex cell cultures on multielectrode arrays. *Neuroscience letters,* 361**,** 86-89.

VARGHESE, K., MOLNAR, P., DAS, M., BHARGAVA, N., LAMBERT, S., KINDY, M. S. & HICKMAN, J. J. 2010. A new target for amyloid beta toxicity validated by standard and high-throughput electrophysiology. *PLoS One,* 5**,** e8643.

VEDUNOVA, M., SAKHARNOVA, T., MITROSHINA, E., PERMINOVA, M., ZAKHAROV, Y., PIMASHKIN, A., DITYATEV, A. & MUKHINA, I. 2013. Seizure-like activity in hyaluronidase-treated dissociated hippocampal cultures. *Frontiers in Cellular Neuroscience,* 7.

VENTURA, V., CAI, C. & KASS, R. E. 2005. Statistical assessment of time-varying dependency between two neurons. *Journal of Neurophysiology,* 94**,** 2940-2947.

VOYTEK, B., KAYSER, A. S., BADRE, D., FEGEN, D., CHANG, E. F., CRONE, N. E., PARVIZI, J., KNIGHT, R. T. & D'ESPOSITO, M. 2015. Oscillatory dynamics coordinating human frontal networks in support of goal maintenance. *Nature neuroscience,* 18**,** 1318-1324.

WAGENAAR, D. A., MADHAVAN, R., PINE, J. & POTTER, S. M. 2005a. Controlling bursting in cortical cultures with closed-loop multi-electrode stimulation. *J Neurosci,* 25**,** 680-8.

WAGENAAR, D. A., MADHAVAN, R., PINE, J. & POTTER, S. M. 2005b. Controlling bursting in cortical cultures with closed-loop multi-electrode stimulation. *Journal of Neuroscience,* 25**,** 680-688.

WAGENAAR, D. A., PINE, J. & POTTER, S. M. 2006. An extremely rich repertoire of bursting patterns during the development of cortical cultures. *BMC Neurosci,* 7**,** 11.

WAINGER, B. J., KISKINIS, E., MELLIN, C., WISKOW, O., HAN, S. S., SANDOE, J., PEREZ, N. P., WILLIAMS, L. A., LEE, S. & BOULTING, G. 2014. Intrinsic membrane hyperexcitability of amyotrophic lateral sclerosis patient-derived motor neurons. *Cell reports,* 7**,** 1-11.

WILLERTH, S. M. & SAKIYAMA-ELBERT, S. E. 2007. Approaches to neural tissue engineering using scaffolds for drug delivery. *Adv Drug Deliv Rev,* 59**,** 325-38.

WILLIAMSON, A., SINGH, S., FERNEKORN, U. & SCHOBER, A. 2013. The future of the patient-specific Body-on-a-chip. *Lab on a Chip,* 13**,** 3471-3480.

WÖRSDÖRFER, P., DALDA, N., KERN, A., KRÜGER, S., WAGNER, N., KWOK, C. K., HENKE, E. & ERGÜN, S. 2019. Generation of complex human organoid models including vascular networks by incorporation of mesodermal progenitor cells. *Scientific reports,* 9**,** 1-13.

YAMAMOTO, C. 1972. Activation of hippocampal neurons by mossy fiber stimulation in thin brain sections in vitro. *Experimental Brain Research,* 14**,** 423-435.

YANG, N., CHANDA, S., MARRO, S., NG, Y.-H., JANAS, J. A., HAAG, D., ANG, C. E., TANG, Y., FLORES, Q. & MALL, M. 2017. Generation of pure GABAergic neurons by transcription factor programming. *Nature methods,* 14**,** 621-628.

YAO, H., WU, W., CERF, I., ZHAO, H. W., WANG, J., NEGRAES, P. D., MUOTRI, A. R. & HADDAD, G. G. 2020. Methadone interrupts neural growth and function in human cortical organoids. *Stem Cell Research,* 49**,** 102065.

YAO, Y., GULARI, M. N. & WISE, K. D. Microassembly techniques for a three-dimensional neural stimulating microelectrode array. 2006 International Conference of the IEEE Engineering in Medicine and Biology Society, 2006. IEEE, 4643-4646.

YIN, X., MEAD, B. E., SAFAEE, H., LANGER, R., KARP, J. M. & LEVY, O. 2016. Engineering Stem Cell Organoids. *Cell Stem Cell,* 18**,** 25-38.

YLÄ-OUTINEN, L., HEIKKILÄ, J., SKOTTMAN, H., SUURONEN, R., ÄÄNISMAA, R. & NARKILAHTI, S. 2010. Human cell-based micro electrode array platform for studying neurotoxicity. *Frontiers in neuroengineering,* 3**,** 111.

YOKOI, R., OKABE, M., MATSUDA, N., ODAWARA, A., KARASHIMA, A. & SUZUKI, I. 2019. Impact of sleep–wake-associated neuromodulators and repetitive low-frequency stimulation on human iPSC-derived neurons. *Frontiers in neuroscience,* 13**,** 554.

YOON, S. J., ELAHI, L. S., PASCA, A. M., MARTON, R. M., GORDON, A., REVAH, O., MIURA, Y., WALCZAK, E. M., HOLDGATE, G. M., FAN, H. C., HUGUENARD, J. R., GESCHWIND, D. H. & PASCA, S. P. 2019. Reliability of human cortical organoid generation. *Nat Methods,* 16**,** 75-78.

YOUNES, I. & RINAUDO, M. 2015. Chitin and chitosan preparation from marine sources. Structure, properties and applications. *Marine drugs,* 13**,** 1133-1174.

YUSTE, R. 2015. From the neuron doctrine to neural networks. *Nature reviews neuroscience,* 16**,** 487-497.

YVON, C., RUBLI, R. & STREIT, J. 2005. Patterns of spontaneous activity in unstructured and minimally structured spinal networks in culture. *Experimental Brain Research,* 165**,** 139-151.

ZHANG, Y., PAK, C., HAN, Y., AHLENIUS, H., ZHANG, Z., CHANDA, S., MARRO, S., PATZKE, C., ACUNA, C. & COVY, J. 2013. Rapid single-step induction of functional neurons from human pluripotent stem cells. *Neuron,* 78**,** 785-798.

ZHONG, S., ZHANG, S., FAN, X., WU, Q., YAN, L., DONG, J., ZHANG, H., LI, L., SUN, L. & PAN, N. 2018. A single-cell RNA-seq survey of the developmental landscape of the human prefrontal cortex. *Nature,* 555**,** 524-528.